

UC San Diego

UC San Diego Electronic Theses and Dissertations

Title

The versatile role of V-type ATPases in the physiology of marine diatoms

Permalink

<https://escholarship.org/uc/item/3t6445db>

Author

Yee, Daniel P

Publication Date

2020

Peer reviewed|Thesis/dissertation

UNIVERSITY OF CALIFORNIA SAN DIEGO

The versatile role of V-type ATPases in the physiology of marine diatoms

A dissertation submitted in partial satisfaction of the requirements for the
degree Doctor of Philosophy

in

Marine Biology

by

Daniel Patrick Yee

Committee in charge:

Professor Martin Tresguerres, Chair
Professor Andrew E. Allen
Professor Bianca Brahamsha
Professor Amro Hamdoun
Professor Julian I. Schroeder

2020

©

Daniel Patrick Yee, 2020

All rights reserved.

The dissertation of Daniel Patrick Yee is approved, and it is acceptable in quality and form for publication on microfilm and electronically:

Chair

University of California San Diego

2020

EPIGRAPH

“I think it's much more interesting to live not knowing than to have answers which might be wrong. I have approximate answers and possible beliefs and different degrees of uncertainty about different things, but I am not absolutely sure of anything and there are many things I don't know anything about, such as whether it means anything to ask why we're here. I don't have to know an answer. I don't feel frightened not knowing things, by being lost in a mysterious universe without any purpose, which is the way it really is as far as I can tell.”

-Richard P. Feynman

TABLE OF CONTENTS

Signature Page	iii
Epigraph.....	iv
Table of Contents.....	v
List of Figures	vi
List of Tables	viii
Acknowledgements.....	ix
Vita.....	xii
Abstract of the Dissertation	xiii
Chapter 1: General Introduction	1
Chapter 2: Dynamic subcellular translocation of V-type H ⁺ -ATPase is essential for biomineralization of the diatom silica cell wall	17
Chapter 3: Evolution of a V-type H ⁺ -ATPase-mediated carbon concentrating mechanism in secondary endosymbiotic phytoplankton	36
Chapter 4: The potential roles of V-type H ⁺ -ATPase in the function diatom vacuoles	63
Chapter 5: Conclusion.....	86

LIST OF FIGURES

Chapter 2

Fig. 2.1: Diagram of a diatom underdoing cell division	19
Fig. 2.2: Subcellular localization of VHA to the SDVs and vacuoles of <i>T. pseudonana</i>	21
Fig. 2.3: VHA _B protein and mRNA abundance	22
Fig. 2.4: Dynamics of VHA in the valve SDV	23
Fig. 2.5: Effect of concanamycin A on VHA localization	24
Fig. 2.6: Time-lapse of VHA translocation in the valve SDV	24
Fig. 2.7: Time-lapse of VHA translocation in the girdle band SDV	25
Fig. 2.8: Localization of SAP1 +/- concanamycin A	26
Fig. 2.9: Effect of partial VHA inhibition on valve morphology	27

Chapter 2 Supplemental

Fig. S2.1: Localization of VHA _B in <i>T. pseudonana</i>	30
Fig. S2.2: Western blots for VHA _B protein abundance in synchronized cell cultures	31
Fig. S2.3: Additional images of the effect of concanamycin A on VHA localization	32
Fig. S2.4: Additional images of localization of SAP1 +/- concanamycin A	33
Fig. S2.5: Additional images of the effect of partial VHA inhibition on valve morphology	34

Chapter 3

Fig. 3.1: VHA localized around chloroplasts of <i>T. pseudonana</i>	52
Fig. 3.2: Effect of VHA inhibition on oxygen production in marine phytoplankton	53
Fig. 3.3: Contribution of VHA to carbon fixation at different DIC and irradiance levels	54
Fig. 3.4: Model for a VHA mediated CCM in diatoms	55

Chapter 3 Supplemental

Fig. S3.1: VHA mRNA transcriptional profiles	56
Fig. S3.2: Growth and culture conditions of marine phytoplankton	57

Fig. S3.3: P-E plots for <i>T. pseudonana</i> in ambient DIC +/- concanamycin A.....	58
Fig. S3.4: P-E plots for <i>T. pseudonana</i> in modified DIC +/- concanamycin A	59
Fig. S3.5: Growth and culture conditions of <i>T. pseudonana</i> in FSW and ASW.....	60
Fig. S3.6: P-E curve fittings for <i>T. pseudonana</i> in FSW and ASW	61
 Chapter 4	
Fig. 4.1: VHA localized in vacuoles tonoplasts of <i>T. pseudonana</i>	82
Fig. 4.2: VHA localized in vacuole tonoplasts of <i>T. pseudonana</i> +/- concanamycin A	83
Fig. 4.3: Model for a VHA mediated vacuolar transport in diatoms	84
Fig. 4.4: VHA localized in vacuole tonoplasts of a <i>T. pseudonana</i> auxospore	85
 Chapter 5	
Fig. 5.1: Localization of VHA subunits c and c'	92

LIST OF TABLES

Chapter 3

Table 3.1 P-values for gross O ₂ production	62
Table 3.2 P-values for ¹⁴ C P-E curves	62

ACKNOWLEDGEMENTS

I would like to first acknowledge my advisor and the chair of my dissertation, Martin Tresguerres, for his unwavering support of my research and training by enabling opportunities to advance my skills in microscopy, and for the many hours spent editing all of my writing. I have benefited incredibly from comradery in and out of the Tresguerres lab which will serve as a model for comparison as I move forward in my career. I would also like to thank my late former co-advisor, Mark Hildebrand, who shared with me his passion for fundamental science, discovery, and an unmatched appreciation for diatoms. I would like to thank my committee members Andy Allen, Bianca Brahamsha, Amro Hamdoun, and Julian Schroeder who have provided invaluable guidance and resources during my PhD, and who have provided broad perspectives regarding my research on the biochemistry, molecular, and cell biology of the ocean's greatest photosynthesizers.

I would like to thank various members of the Tresguerres and Hildebrand lab's at SIO, and the Allen lab at the J. Craig Venter Institute for all their help in troubleshooting problems in the lab and experimental design. I would particularly like to acknowledge from the Tresguerres lab, Garfield Kwan for his friendship as both a lab and officemate, and Bethany Shimasaki for giving me the opportunity to provide mentorship and for help in experimental data collection. I would specifically like to thank from the Hildebrand lab, Roshan Shrestha for developing and sharing the tools he developed for the genetic manipulation of diatoms, and Raffaella Abbrian-Burke for analysis of diatom transcriptome data. I would like to thank Hong Zheng from the Allen lab for lending time and supplies, as well as helping me navigate the halls of JCVI.

I would like to acknowledge the following individuals for their assistance in the work presented in Chapter 3 of this dissertation. Starting with Greg Mitchell who was my master's thesis advisor and who first introduced me to the world of phytoplankton. Thank you for your continued support during my PhD through the generous donation of algal culturing equipment and incubators

for radioisotope work. I would like to thank Maria Vernet who also mentored me during my master's and who granted me access to her lab during this Covid crisis in order to carry out radioisotope work vital to my work. Lastly, I want to thank Brian Palenik for loaning the oxygen respirometer crucial to the initial discovery of this chapter, Chris Hewes for use of the fluorometer in the Holm-Hansen lab, and Orna Cook for supplying non-diatom algal cultures.

I would also like to thank the many people who helped me grow and develop into a scientist. Starting with my parents, Patrick and Lucy Yee who raised me to work hard and to always finish what I started. My sister, Joyclyn Yee-Greenbaum and her family who have been my anchor throughout most of my years in San Diego. My high-school journalism advisor, Jeorgia Moore who taught me to dream big and push the boundaries of my own understanding. My boss while working at Synthetic Genomics, Shaun Bailey, who helped me realize my potential and pushed me to leave industry in order to earn my PhD. I would like to thank all of my friends throughout life who have provided endless support and laughter, in particular, Travis Courtney for the life-talks and the much needed reminders that surfing is a way of life, Elliot Weiss for igniting my passion for climbing and gluttony for pain, Karthik Venkataraman for a lifetime of brotherly love, Cherry Duong for always listening, Joseph Sun and Andrew Chua for all the memories they were and are still to come, and Evan Shulman and Alice Chen for showing me how to live life with intention.

This research would not have been possible with financial support from the Scripps Fellowship, UCSD Frontiers in Innovation Scholars Program, Edna Bailey Sussman Foundation, UCSD Friends of the International Center, and the NIH Marine Biotechnology Training Program. I would lastly like to acknowledge the administrative and logistical support from Dejan Ristic from SIO Facilities, Gilbert Bretado and Denise Darling from the SIO Graduate Department, and Shelley Weisel and Maureen McCormack from the SIO Financial Department.

Chapter 2, in full, is a reprint of the material as it appears in Yee, D. P., Hildebrand, H., & Tresguerres, M. (2019). Dynamic subcellular translocation of V-type H⁺-ATPase is essential for diatom silica cell wall biomineralization. *New Phytologist*, 225.6, 2411-2422. The dissertation author was the primary investigator and author of this paper.

Chapter 3, in full, is in preparation for submission as Yee, D.P., Shimasaki, B.L., & Tresguerres, M. Evolution of a V-type H⁺-ATPase-mediated carbon concentrating mechanism in secondary endosymbiotic phytoplankton. The dissertation author was the primary investigator and author of this paper.

VITA

- 2008 Bachelors of Science, University of California, San Diego
- 2010 Masters of Science, University of California, San Diego
- 2020 Doctor of Philosophy, University of California, San Diego

PUBLICATIONS

- Tresguerres, M., Clifford, A.M., Harter, T.S., Roa, J.N., Thies, A.B., **Yee, D.P.**, & Brauner, C.J., (2020). Evolutionary links between intra- and extracellular acid-base regulation in fish and other aquatic animals. *Journal of Experimental Zoology Part A: Ecological and Integrative Physiology*.
- Gaidarenko, O., **Yee, D. P.**, & Hildebrand, M. (2020). Enhanced triacylglycerol (TAG) and protein accumulation in transgenic diatom *Thalassiosira pseudonana* with altered photosynthetic pigmentation. *bioRxiv*.
- Yee, D. P.**, Hildebrand, H., & Treguerres, M. (2019). Dynamic subcellular translocation of V-type H⁺-ATPase is essential for diatom silica cell wall biomineralization. *New Phytologist*, 225.6, 2411-2422.
- Abbriano, R., Vardar, N., **Yee, D.**, & Hildebrand, M. (2018). Manipulation of a glycolytic regulator alters growth and carbon partitioning in the marine diatom *Thalassiosira pseudonana*. *Algal research*, 32, 250-258.

ABSTRACT OF THE DISSERTATION

The versatile role of V-type ATPases in the physiology of marine diatoms

by

Daniel Patrick Yee

Doctor of Philosophy in Marine Biology

University of California San Diego, 2020

Professor Martin Tresguerres, Chair

Diatoms are among the most successful group of phytoplankton in the oceans and produce up to one-fifth of earth's primary production. Their high productivity and ability to form dense blooms have a proportionately large impact on the ecology and biogeochemistry of the oceans. Diatoms possess unique traits that collectively help them outcompete and out-survive other phytoplankton which include a cell wall made of biosilica called the frustule, a robust carbon

concentrating mechanism (CCM) for photosynthesis, and large vacuoles that allows them to store high amounts intracellular nutrients. While these strategies is generally recognized, the cellular and molecular mechanisms for these traits are not well understood. Leveraging modern tools in molecular biology and subcellular imaging, this study investigates the function of the evolutionarily conserved proton pump and pH regulation enzyme V-type H⁺ATPase (VHA) in the physiology of diatoms.

The VHA proton pump was found to localize in the membranes of three distinct organelles in the marine diatom *Thalassiosira pseudonana* including silica deposition vesicles (SDVs), chloroplasts, and vacuoles. In the SDV, VHA promotes silica biomineralization by maintain acidic pH and helps traffic the structural proteins which guide frustule morphology. This investigation also revealed that vacuole play a role in translocating VHA and donating membrane to the SDV. In chloroplasts, VHA was found to support a carbon concentrating mechanism (CCM) to enhance photosynthesis. The activity of VHA in the CCM was found to respond dynamically to irradiance and DIC, and was also confirmed in the coccolithophore *Emiliana huxleyi*, but not in the chlorophyte *Chlorella*. Collectively, these results suggest that a VHA mediated CCM maybe a conserved mechanism of secondary endosymbiosis of red algal symbionts. The VHA proton pump was prominently found in diatom vacuoles at various stages of the cell. Inhibition of VHA increased pH in the vacuole, suggesting it actively pumps protons to support the various functions of the vacuole including nutrient storage and generating buoyancy for the cell. In combination, these results show a vital role for pH regulation by VHA in multiple aspects of diatom biology which are key to their competitive success.

CHAPTER 1

General Introduction

1.1 Background

Evolution and ecology of diatoms. Diatoms are a major group of unicellular microalgae from the phylum heterokontophyta which evolved ~275 million years ago following the endosymbiosis of red alga by a eukaryotic host (1, 2). Fossil records suggest that diatoms gained dominance in the world's oceans ~70 million years ago during the Late Cretaceous period (3) as Pangaea began to rift and more nutrients flowed into the oceans. With over 100,000 predicted species (4) annual diatom production greatly impacts the biogeochemistry of earth's oceans and atmosphere. Inhabiting both freshwater and marine ecosystems, diatoms are responsible for up to 20% of the primary production on the planet and around 40% of the carbon fixed in the oceans (5, 6). Their high rates of growth, especially in upwelling regions of the ocean, make diatoms major biogeochemical cyclers of silica, carbon, nitrogen, phosphorous, and iron (7, 8). Diatoms are significant contributors to the biological carbon pump and marine food webs (9, 10), for example, forming the base of the short trophic chain between krill and baleen whales in the Southern Ocean (11).

In high-nitrogen low-chlorophyll (HNLC) waters phytoplankton blooms can be stimulated by iron and silica availability (12, 13). These blooms can last for several months and are often dominated by diatoms which can account for up to 75% of the primary production and over 50% of the biomass (12, 14). While diatom biomass is important for biogeochemical processes and trophic cascades, negative impacts come in the form of harmful algal blooms, especially by diatoms which produce toxins (15). The neurotoxin domoic acid is produced by several blooming species of *Pseudo-nitzschia* and is known to cause amnesic shellfish poisoning in mammals (16–18).

Molecular biology of diatoms. In the last two decades, the genomes of 8 diatom species have been sequenced (19–26) and have significantly advanced our understanding of diatom molecular biology and evolution. In addition to the plastid genome inherited from red algal endosymbiont, the nuclear genome of diatoms is composed of genes derived from green alga and bacteria (27). It is from this metropolitan gene pool that diatoms have evolved unique strategies for survival such as the use of silica as a substrate for growth, a carbon concentrating mechanism (CCM) for photosynthesis, and the ability to concentrate nutrients intracellularly and outcompete their competitors.

Diatom cell walls. A defining characteristic of diatoms is their silica cell wall called the frustule which vary in shape and size depending on species. The morphology of the frustule divide diatoms into two main groups, centric diatoms are characterized by radial symmetry while pennate diatoms have bilateral symmetry. Compared to free-living centric diatoms, some pennate diatoms can colonize substrates and glide across surfaces by excretions from a slit in the cell wall called the raphe (28). Despite the diversity in diatom morphologies, the general architecture of the frustule is conserved and consists of a hypotheca and epitheca. Each theca is composed of a valve and a series of overlapping rings of girdle bands which form a junction between the two theca (29). On the surface of valves are species-specific patterns of meso- and nanoscale structures such as ribs and pores formed through an organized amalgam of silica particles ranging from 20-200 nm in size (30). Altogether, the frustule provides several advantages including mechanical protection from grazing (31), increasing nutrient uptake through pore structures, altering incident light to promote photosynthesis (32, 33), and the use of silicic acid as an abundant substrate for growth.

Diatoms synthesize their frustule intracellularly under strict biological control. Synthesis of the frustule begins by the uptake of silicon in the form of silicic acid from the environment by

passive diffusion (34) and silicic acid transports (35, 36). Silicic acid is biomineralized into silica within the silica deposition vesicle (SDV), a subcellular compartment defined by a membrane called the silicalemma (37). Valves and girdle bands are produced in their own specific SDVs and get exocytosed out of the cell once the biomineralization process is complete. The cytoskeleton is speculated to orchestrate interactions between various silicification proteins located throughout the silicalemma (38). While transcriptomic approaches have identified hundreds of potential silicification genes (39) only a handful have been characterized so far.

Embedded within the frustule is an organic matrix of polysaccharides, proteins, and peptides which were categorized into ammonium fluoride soluble and insoluble fractions (40). The silicification proteins that have been identified in the soluble fraction are the silaffins, silacidins, as well as long-chain polyamine peptides (41–43). Meanwhile only cingulin proteins (40) have been identified from the insoluble fraction so far. A third group of silicification proteins are located in the silicalemma and include the silicanin-1 (Sin1), silicalemma associated protein (SAPs), and V-type H⁺-ATPase (VHA) which have all been shown to participate in biosynthesis of frustules (44–46).

Carbon concentrating mechanisms of diatoms. Compared to photosynthesis on land, aquatic photosynthesis is limited by the availability of dissolved CO₂. Carbon fixation is carried out by ribulose-1,5-bisphosphate carboxylase/oxygenase (RuBisCO) concentrated in the pyrenoid of chloroplasts. Enzymatic assays have shown that RuBisCO requires over 25 μM CO₂ to saturate its binding affinity for carboxylation (47). Under ideal conditions, seawater in equilibrium with the atmosphere contains about 10 μM CO₂ (48) which is below the saturation constant of RuBisCO. Therefore, many eukaryotic phytoplankton including diatoms have evolved a CCM for photosynthesis. The goal of the CCM is to concentrate CO₂ around the pyrenoid to promote fast

rates of photosynthesis, diatom plastids are surrounded by four membranes consisting of the inner and outer chloroplast envelopes, the periplastid membrane, and chloroplast endoplasmic reticulum. These last two membranes are remnants from the phagocytosis of a red algal ancestor, and are believed to provide diatoms a competitive edge in photosynthesis by trapping CO₂ (49).

Current knowledge supports two types of CCMs in diatoms, one involving the transport and interconversion of CO₂ and HCO₃⁻, and another involving the shuttling of four carbon (C4) compounds via Crassalacean acid metabolism (CAM) enzymes. For the former, carbonic anhydrases and solute carrier 4 (SLC4) bicarbonate transporters have been studied in both pennate and centric diatoms (50–52) and support a mechanism of shuttling HCO₃⁻ and promoting diffusion of CO₂ through multiple layers of the plastid to enhance photosynthesis. Meanwhile, the operation of CAM based CCM in diatoms is still debated. While diatoms possess all the necessary CAM enzymes and inhibition of one of these enzymes has been shown to reduce photosynthesis (53), localization data for several of these proteins do not support the operation of this type of CCM (54, 55).

Vacuolar function in diatoms. Diatoms possess large vacuoles which are considered to serve many functions which include providing buoyancy and storing nutrients. It has been suggested that large vacuoles in combination with their silica shells enable a strategy for diatoms to remain physically large to avoid predation while remaining metabolically small via a reduced cytosol (56). Without the vacuole to provide buoyancy, diatoms will sink under the weight of their frustules. It has been shown that diatoms can migrate through the water column by accumulating ‘light’ and ‘heavy’ osmolytes, such as ammonium or nitrate respectively (57). Diatoms have been observed to accumulate high amounts of intracellular nitrogen (58) and phosphate (59) which has long been seen as a strategy to sequester nutrients from competitors and promote fast growth rates.

So far only iron (60) and chrysolaminarin (61) have been localized within diatom vacuoles, but nitrogen and phosphate are likely to be stored there as well. While diatom genomes possess many of the enzymes to transport these various nutrients and osmolytes, few studies have been able to identify their location and even fewer have characterized their functions in diatoms.

Acid-base regulation by V-type ATPase. Control of intracellular pH is essential for facilitating many biological processes within cells. The conserved eukaryotic proton pump, VHA, is a multi-subunit protein complex consisting of a ~650 kDA cytosolic V_1 domain composed of eight subunits A-H, and a ~260 kDA membrane bound V_0 domain composed of subunits a, d, e, c, c', and c''(62). While the V_1 domain facilitates the hydrolysis of adenine triphosphate (ATP) to power the molecular machinery, the V_0 domain contains a proteolipid ring for translocating hydrogen ions across membranes. Though structurally and mechanistically similar to a family of F-type ATPases, VHA exclusively functions in the hydrolytic direction. The modification of intracellular pH by VHA can affect protein folding and enzymatic activity, while pumping H^+ can generate electrochemical gradients and proton motive forces to facilitate membrane transport, enabling VHA to serve in diverse functions in the cell.

VHA was first identified in regulating pH within neurosecretory vesicles of mammalian chromaffin granule cells (63). Since then, VHA has been shown to participate in many roles such as bone dissolution, renal acidification, tumor metastasis, enzyme secretion, blood pH homeostasis, lysosomal protein degradation, plant osmoregulation, and carbon concentrating mechanisms for photosynthesis (64–69). Studying the function of VHA across diverse organisms is aided by the availability of several highly specific inhibitors. The most common VHA inhibitors used are bafilomycin and concanamycin A which are effective at nanomolar concentrations and interfere with the mechanics of the -c subunit in the proteolipid ring of the V_0 domain (70–72).

Two other inhibitors are, FR177995 which was demonstrated on rat osteoclasts (73), and KM91104 which was shown to interfere with the association of the -a and -B subunits belonging to the V_0 and V_1 domains, respectively (74).

Because VHA is a reversibly assembled holoenzyme and is composed of different subunit isoforms, its activity can be regulated in several ways. In yeast, the pump was shown to be switched on and off by the reversible attachment of the hydrolytic V_1 domain to the pumping activity of the V_0 domain (75). The composition of subunit isoforms has shown to impart differential targeting of VHA to different tissues and subcellular compartments. In plants, it was shown that several VHA c subunits are differentially localized between roots and shoots (76). These spatial and activation related regulatory mechanisms enables multilevel control of VHA in the cell.

Role of acid-base regulation in the physiology of diatoms. Within the diatom cell, there are several subcellular compartments which can host the proton pump, including the SDV, chloroplast, and vacuole. The biomineralization of silica in SDVs is known to take place under acidic conditions which aid in the nucleation and aggregation of silica polymers (77). While a previous study has demonstrated a role for VHA in frustule development, the mechanism was not able to be identified (78). In chloroplasts, high rates of photosynthesis are supported by a CCM and it has been previously hypothesized that proton pumping within the chloroplast ER could help promote CO_2 accumulation at the pyrenoid (49). The current model for the diatom CCM includes the combined activity of carbonic anhydrase and SLC4 bicarbonate transporters. The presence of VHA to acidify the chloroplast could enhance the function of these enzymes and build a more robust CCM. Lastly, the presence of VHA diatom vacuoles could aid in shuttling a variety of nutrients and osmolytes through the tonoplast. The VHA proton pump has been identified in energizing the transport of various molecules such as nitrate and iron in the vacuoles of plants and

other single celled eukaryotes. Therefore, VHA is likely to be involved in similar functions within diatom vacuoles.

1.2 Outline of the Dissertation

At the outset of this research, the role of VHA in diatoms was limited to three studies in the pennate diatom *Phaeodactylum tricornutum*. The first study identified a role in cell wall synthesis by demonstrating reduced frustule development in cells treated with concanamycin A (78). A second study evaluated diatom genomes and identified the various subunits and isoforms of VHA, and also produced a GFP tagged VHA-c subunit localized to the endoplasmic reticulum (79). The last study measured a decrease in cellular lipid production when cells were cultured with the VHA inhibitor, bafilomycin (80). While these studies implicated VHA in several physiologies, its mechanisms and functions remained a mystery. Therefore, the goal of this dissertation is to describe how pH regulation by VHA in different subcellular locations facilitate various physiological mechanisms within diatom cells.

The characterization of VHA was carried out in the marine diatom *Thalassiosira pseudonana*, which is a model organism that carries implications for all diatoms species and therefore their influence on the ecology and biogeochemistry of earth's oceans and atmosphere. Development of a transgenic cell line of *T. pseudonana* expressing the VHA subunit B tagged with enhanced green fluorescent protein (eGFP) was pivotal for targeting VHA in multiple cell membranes and studying its functions. This dissertation can be broke down into three distinct data chapters whose objectives are as follows:

Chapter 2: Identify the role of VHA in silica biomineralization by SDV membrane localization, observe intracellular membrane dynamics of live cells, measure the effects of VHA inhibition in cell growth, activities inside the SDV, and valve morphology.

Chapter 3: Identify the role of VHA in photosynthesis by localizing VHA in the chloroplast, measure the effects of VHA inhibition on photosynthesis, and identify evolutionary linkages of a VHA mediated CCM within aquatic photosynthesis.

Chapter 4: Identify the role of VHA in vacuolar functions by localizing VHA to the tonoplast, measure the effect of VHA inhibition on vacuole acidification, and generate hypothesis for the role of proton pumping in the vacuole for nutrient storage, buoyancy, and sexual reproduction.

1.2 References

1. P. J. Keeling, Diversity and evolutionary history of plastids and their hosts. *Am. J. Bot.* **91**, 1481–1493 (2004).
2. P. J. Keeling, The endosymbiotic origin, diversification and fate of plastids. *Philos. Trans. R. Soc. B Biol. Sci.* **365**, 729–748 (2010).
3. E. Chacón-Baca, H. Beraldi-Campesi, S. R. S. Cevallos-Ferriz, A. H. Knoll, S. Golubic, 70 Ma nonmarine diatoms from northern Mexico. *Geology*. **30**, 279–281 (2002).
4. D. G. Mann, S. J. M. Droop, Biodiversity , biogeography and conservation of diatoms. *Hydrobiologia*. **336**, 19–32 (1996).
5. C. B. Field, M. J. Behrenfeld, J. T. Randerson, P. G. Falkowski, Primary production of the biosphere: Integrating terrestrial and oceanic components. *Science (80-.)*. **281**, 237–240 (1998).
6. D. M. Nelson, P. Tréguer, M. A. Brzezinski, A. Leynaert, B. Quéguiner, Production and dissolution of biogenic silica in the ocean: Revised global estimates, comparison with regional data and relationship to biogenic sedimentation. *Global Biogeochem. Cycles*. **9**, 359–372 (1995).
7. G. Sarthou, K. R. Timmermans, S. Blain, P. Tréguer, Growth physiology and fate of diatoms in the ocean: A review. *J. Sea Res.* **53**, 25–42 (2005).
8. A. Yool, T. Tyrrell, Role of diatoms in regulating the ocean’s silicon cycle. *Global Biogeochem. Cycles*. **17**, 1–21 (2003).
9. K. R. Arrigo, D. H. Robinson, D. L. Worthen, R. B. Dunbar, G. R. DiTullio, M. VanWoert, M. P. Lizotte, Phytoplankton community structure and the drawdown of nutrients and CO₂ in the Southern Ocean. *Science (80-.)*. **283**, 365–367 (1999).
10. P. Tréguer, C. Bowler, B. Moriceau, S. Dutkiewicz, M. Gehlen, O. Aumont, L. Bittner, R. Dugdale, Z. Finkel, D. Iudicone, O. Jahn, L. Guidi, M. Lasbleiz, K. Leblanc, M. Levy, P. Pondaven, Influence of diatom diversity on the ocean biological carbon pump. *Nat. Geosci.* **11** (2018), doi:10.1038/s41561-017-0028-x.
11. E. L. Cavan, A. Belcher, A. Atkinson, S. L. Hill, S. Kawaguchi, S. McCormack, B. Meyer, S. Nicol, L. Ratnarajah, K. Schmidt, D. K. Steinberg, G. A. Tarling, P. W. Boyd, The importance of Antarctic krill in biogeochemical cycles. *Nat. Commun.* **10**, 1–13 (2019).
12. P. W. Boyd, a J. Watson, C. S. Law, E. R. Abraham, T. Trull, R. Murdoch, D. C. Bakker, a R. Bowie, K. O. Buesseler, H. Chang, M. Charette, P. Croot, K. Downing, R. Frew, M. Gall, M. Hadfield, J. Hall, M. Harvey, G. Jameson, J. LaRoche, M. Liddicoat, R. Ling, M. T. Maldonado, R. M. McKay, S. Nodder, S. Pickmere, R. Pridmore, S. Rintoul, K. Safi, P. Sutton, R. Strzepak, K. Tanneberger, S. Turner, a Waite, J. Zeldis, A mesoscale phytoplankton bloom in the polar Southern Ocean stimulated by iron fertilization. *Nature*.

- 407, 695–702 (2000).
13. F. P. Dugdale, D.C., Wilkerson, Silicate regulation of new production in the equatorial Pacific upwelling. *Nature*. **391**, 270–273 (1998).
 14. R. Goericke, The structure of marine phytoplankton communities- patterns, rules and mechanisms. *CalCOFI Rep.* **52**, 182–197 (2011).
 15. L. B. Busse, E. L. Venrick, R. Antrobus, P. E. Miller, V. Vigilant, M. W. Silver, C. Mengelt, L. Mydlarz, B. B. Prezelin, Domoic acid in phytoplankton and fish in San Diego, CA, USA. *Harmful Algae*. **5**, 91–101 (2006).
 16. M. W. Silver, S. Bargu, S. L. Coale, C. R. Benitez-Nelson, A. C. Garcia, K. J. Roberts, E. Sekula-Wood, K. W. Bruland, K. H. Coale, Toxic diatoms and domoic acid in natural and iron enriched waters of the oceanic Pacific. *Proc. Natl. Acad. Sci. U. S. A.* **107**, 20762–20767 (2010).
 17. B. N. Seegers, J. M. Birch, R. Marin, C. A. Scholin, D. A. Caron, E. L. Seubert, M. D. A. Howard, G. L. Robertson, B. H. Jones, Subsurface seeding of surface harmful algal blooms observed through the integration of autonomous gliders, moored environmental sample processors, and satellite remote sensing in southern California. *Limnol. Oceanogr.* **60**, 754–764 (2015).
 18. J. K. Brunson, S. M. K. McKinnie, J. R. Chekan, J. P. McCrow, Z. D. Miles, E. M. Bertrand, V. A. Bielinski, H. Luhavaya, M. Oborník, G. J. Smith, D. A. Hutchins, A. E. Allen, B. S. Moore, Biosynthesis of the neurotoxin domoic acid in a bloom-forming diatom. *Science (80-.)*. **361**, 1356–1358 (2018).
 19. E. V. Armbrust, J. A. Berges, C. Bowler, B. R. Green, D. Martinez, N. H. Putnam, S. Zhou, A. E. Allen, K. E. Apt, M. Bechner, M. A. Brzezinski, B. K. Chaal, A. Chiovitti, A. K. Davis, M. S. Demarest, J. C. Detter, T. Glavina, D. Goodstein, M. Z. Hadi, U. Hellsten, M. Hildebrand, B. D. Jenkins, W. W. Y. Lau, T. W. Lane, F. W. Larimer, J. C. Lippmeier, S. Lucas, A. Montsant, M. Obornik, M. S. Parker, B. Palenik, G. J. Pazour, P. M. Richardson, T. A. Ryneerson, M. A. Saito, D. C. Schwartz, K. Thamtrakoln, K. Valentin, A. Vardi, F. P. Wilkerson, D. S. Rokhsar, The Genome of the Diatom. *Science (80-.)*. **306**, 79–86 (2004).
 20. C. Bowler, A. E. Allen, J. H. Badger, J. Grimwood, K. Jabbari, A. Kuo, U. Maheswari, C. Martens, F. Maumus, R. P. Otilar, E. Rayko, A. Salamov, K. Vandepoele, B. Beszteri, A. Gruber, M. Heijde, M. Katinka, T. Mock, K. Valentin, F. Verret, J. A. Berges, C. Brownlee, J. P. Cadoret, A. Chiovitti, C. J. Choi, S. Coesel, A. De Martino, J. C. Detter, C. Durkin, A. Falciatore, J. Fournet, M. Haruta, M. J. J. Huysman, B. D. Jenkins, K. Jiroutova, R. E. Jorgensen, Y. Joubert, A. Kaplan, N. Kröger, P. G. Kroth, J. La Roche, E. Lindquist, M. Lommer, V. Martin-Jézéquel, P. J. Lopez, S. Lucas, M. Mangogna, K. McGinnis, L. K. Medlin, A. Montsant, M. P. O. Le Secq, C. Napoli, M. Obornik, M. S. Parker, J. L. Petit, B. M. Porcel, N. Poulsen, M. Robison, L. Rychlewski, T. A. Ryneerson, J. Schmutz, H. Shapiro, M. Siat, M. Stanley, M. R. Sussman, A. R. Taylor, A. Vardi, P. Von Dassow, W. Vyverman, A. Willis, L. S. Wyrwicz, D. S. Rokhsar, J. Weissenbach, E. V. Armbrust, B.

- R. Green, Y. Van De Peer, I. V. Grigoriev, The *Phaeodactylum* genome reveals the evolutionary history of diatom genomes. *Nature*. **456**, 239–244 (2008).
21. A. Ogura, Y. Akizuki, H. Imoda, K. Mineta, T. Gojobori, S. Nagai, Comparative genome and transcriptome analysis of diatom, *Skeletonema costatum*, reveals evolution of genes for harmful algal bloom. *BMC Genomics*. **19** (2018), doi:10.1186/s12864-018-5144-5.
 22. T. Tanaka, Y. Maeda, A. Veluchamy, M. Tanaka, H. Abida, E. Maréchal, C. Bowler, M. Muto, Y. Sunaga, M. Tanaka, T. Yoshino, T. Taniguchi, Y. Fukuda, M. Nemoto, M. Matsumoto, P. S. Wong, S. Aburatani, W. Fujibuchi, Oil accumulation by the oleaginous diatom *Fistulifera solaris* as revealed by the genome and transcriptome. *Plant Cell*. **27**, 162–176 (2015).
 23. J. C. Traller, S. J. Cokus, D. A. Lopez, O. Gaidarenko, S. R. Smith, J. P. McCrow, S. D. Gallaher, S. Podell, M. Thompson, O. Cook, M. Morselli, A. Jaroszewicz, E. E. Allen, A. E. Allen, S. S. Merchant, M. Pellegrini, M. Hildebrand, Genome and methylome of the oleaginous diatom *Cyclotella cryptica* reveal genetic flexibility toward a high lipid phenotype. *Biotechnol. Biofuels*. **9**, 1–20 (2016).
 24. M. Lommer, M. Specht, A. S. Roy, L. Kraemer, R. Andreson, M. A. Gutowska, J. Wolf, S. V. Bergner, M. B. Schilhabel, U. C. Klostermeier, R. G. Beiko, P. Rosenstiel, M. Hippler, J. LaRoche, Genome and low-iron response of an oceanic diatom adapted to chronic iron limitation. *Genome Biol*. **13** (2012), doi:10.1186/gb-2012-13-7-r66.
 25. S. Basu, S. Patil, D. Mapleson, M. T. Russo, L. Vitale, C. Fevola, F. Maumus, R. Casotti, T. Mock, M. Caccamo, M. Montresor, R. Sanges, M. I. Ferrante, Finding a partner in the ocean: molecular and evolutionary bases of the response to sexual cues in a planktonic diatom. *New Phytol*. **215**, 140–156 (2017).
 26. T. Mock, R. P. Otilar, J. Strauss, M. McMullan, P. Paajanen, J. Schmutz, A. Salamov, R. Sanges, A. Toseland, B. J. Ward, A. E. Allen, C. L. Dupont, S. Frickenhaus, F. Maumus, A. Veluchamy, T. Wu, K. W. Barry, A. Falciatore, M. I. Ferrante, A. E. Fortunato, G. Glöckner, A. Gruber, R. Hipkin, M. G. Janech, P. G. Kroth, F. Leese, E. A. Lindquist, B. R. Lyon, J. Martin, C. Mayer, M. Parker, H. Quesneville, J. A. Raymond, C. Uhlig, R. E. Valas, K. U. Valentin, A. Z. Worden, E. V. Armbrust, M. D. Clark, C. Bowler, B. R. Green, V. Moulton, C. Van Oosterhout, I. V. Grigoriev, Evolutionary genomics of the cold-adapted diatom *Fragilariopsis cylindrus*. *Nature*. **541**, 536–540 (2017).
 27. P. Deschamps, D. Moreira, Reevaluating the green contribution to diatom genomes. *Genome Biol. Evol*. **4**, 683–688 (2012).
 28. R. Gordon, R. W. Drum, A Capillarity Mechanism for Diatom Gliding Locomotion. *Proc. Natl. Acad. Sci*. **67**, 338–344 (1970).
 29. J. D. Pickett-Heaps, A. M. M. Schmid, L. A. Edgar, *The cell biology of diatom valve formation* (Bristol. Biopress Ltd., 1990), vol. 7.
 30. M. Hildebrand, E. York, J. I. Kelz, A. K. Davis, L. G. Frigeri, D. P. Allison, M. J. Doktycz,

- Nanoscale control of silica morphology and three-dimensional structure during diatom cell wall formation. *J. Mater. Res.* **21**, 2689–2698 (2006).
31. C. E. Hamm, R. Merkel, O. Springer, P. Jurkojc, C. Maiert, K. Prechtelt, V. Smetacek, Architecture and material properties of diatom shells provide effective mechanical protection. *Nature*. **421**, 841–843 (2003).
 32. S. Yamanaka, R. Yano, H. Usami, N. Hayashida, M. Ohguchi, H. Takeda, K. Yoshino, Optical properties of diatom silica frustule with special reference to blue light. *J. Appl. Phys.* **103** (2008), doi:10.1063/1.2903342.
 33. J. Noyes, M. Sumper, P. Vukusic, Light manipulation in a marine diatom. *J. Mater. Res.* **23**, 3229–3235 (2008).
 34. K. Thamatrakoln, M. Hildebrand, Silicon Uptake in Diatoms Revisited: A Model for Saturable and Nonsaturable Uptake Kinetics and the Role of Silicon Transporters. *Plant Physiol.* **146**, 1397–1407 (2008).
 35. M. Hildebrand, K. Dahlin, B. E. Volcani, Characterization of a silicon transporter gene family in *Cylindrotheca fusiformis*: Sequences, expression analysis, and identification of homologs in other diatoms. *Mol. Gen. Genet.* **260**, 480–486 (1998).
 36. M. Hildebrand, V. B.E., W. Gassmann, J. I. Schroeder, A gene family of silicon transporters. *Nature*. **385**, 688–689 (1997).
 37. R. W. Drum, H. S. Pankratz, Post mitotic fine structure of *Gomphonema parvulum*. *J. Ultrastruct. Res.* **10**, 217–223 (1964).
 38. B. Tesson, M. Hildebrand, Extensive and intimate association of the cytoskeleton with forming silica in diatoms: Control over patterning on the meso- and micro-scale. *PLoS One*. **5** (2010), doi:10.1371/journal.pone.0014300.
 39. R. Shrestha, B. Tesson, T. Norden-Krichmar, S. Federowicz, M. Hildebrand, A. E. Allen, Whole transcriptome analysis of the silicon response of the diatom *Thalassiosira pseudonana*. *BMC Genomics*. **13**, 499 (2012).
 40. A. Scheffel, N. Poulsen, S. Shian, N. Kröger, Nanopatterned protein microrings from a diatom that direct silica morphogenesis. *Proc. Natl. Acad. Sci. U. S. A.* **108**, 3175–3180 (2011).
 41. N. Kröger, R. Deutzmann, C. Bergsdorf, M. Sumper, Species-specific polyamines from diatoms control silica morphology. *Proc. Natl. Acad. Sci.* **97**, 14133–14138 (2000).
 42. N. Poulsen, N. Kröger, Silica morphogenesis by alternative processing of silaffins in the diatom *Thalassiosira pseudonana*. *J. Biol. Chem.* **279**, 42993–42999 (2004).
 43. S. Wenzl, R. Hett, P. Riechhammer, M. Sumper, Silacidins: Highly acidic phosphopeptides from diatom shells assist in silica precipitation in vitro. *Angew. Chemie - Int. Ed.* **47**, 1729–

- 1732 (2008).
44. A. Kotsch, P. Gröger, D. Pawolski, P. H. H. Bomans, N. A. J. M. Sommerdijk, M. Schlierf, N. Kröger, Silicanin-1 is a conserved diatom membrane protein involved in silica biomineralization. *BMC Biol.* **15**, 65 (2017).
 45. B. Tesson, S. J. L. Lerch, M. Hildebrand, Characterization of a new protein family associated with the silica deposition vesicle membrane enables genetic manipulation of diatom silica. *Sci. Rep.* **7**, 1–13 (2017).
 46. D. P. Yee, M. Hildebrand, M. Tresguerres, Dynamic subcellular translocation of V-type H⁺-ATPase is essential for biomineralization of the diatom silica cell wall. *New Phytol.* **225**, 2411–2422 (2019).
 47. M. R. Badger, T. J. Andrews, S. M. Whitney, M. Ludwig, D. C. Yellowlees, W. Leggat, G. D. Price, The diversity and coevolution of Rubisco, plastids, pyrenoids, and chloroplast-based CO₂-concentrating mechanisms in algae. *Can. J. Bot.* **76**, 1052–1071 (1998).
 48. P. G. Falkowski, J. A. Raven, *Aquatic Photosynthesis* (Princeton University Press, Princeton, ed. 2nd, 2007).
 49. R. Lee Edward, P. Kugrens, Hypothesis: The ecological advantage of chloroplast ER - The ability to outcompete at low dissolved CO₂ concentrations. *Protist.* **149**, 341–345 (1998).
 50. K. Nakajima, A. Tanaka, Y. Matsuda, SLC4 family transporters in a marine diatom directly pump bicarbonate from seawater. *Proc. Natl. Acad. Sci. U. S. A.* **110**, 1767–72 (2013).
 51. M. Tachibana, A. E. Allen, S. Kikutani, Y. Endo, C. Bowler, Y. Matsuda, Localization of putative carbonic anhydrases in two marine diatoms, *Phaeodactylum tricorutum* and *Thalassiosira pseudonana*. *Photosynth. Res.* **109**, 205–221 (2011).
 52. M. Samukawa, C. Shen, B. M. Hopkinson, Y. Matsuda, Localization of putative carbonic anhydrases in the marine diatom, *Thalassiosira pseudonana*. *Photosynth. Res.* **121**, 235–249 (2014).
 53. J. R. Reinfelder, Carbon concentrating mechanisms in eukaryotic marine phytoplankton. *Ann. Rev. Mar. Sci.* **3**, 291–315 (2011).
 54. D. Ewe, M. Tachibana, S. Kikutani, A. Gruber, C. Río Bártulos, G. Konert, A. Kaplan, Y. Matsuda, P. G. Kroth, The intracellular distribution of inorganic carbon fixing enzymes does not support the presence of a C₄ pathway in the diatom *Phaeodactylum tricorutum*. *Photosynth. Res.* **137**, 263–280 (2018).
 55. R. Tanaka, S. Kikutani, A. Mahardika, Y. Matsuda, Localization of enzymes relating to C₄ organic acid metabolisms in the marine diatom, *Thalassiosira pseudonana*. *Photosynth. Res.* **121**, 251–263 (2014).
 56. T. F. Thingstad, L. Øvreås, J. K. Egge, T. Løvdaal, M. Heldal, Use of non-limiting substrates

- to increase size; a generic strategy to simultaneously optimize uptake and minimize predation in pelagic osmotrophs? *Ecol. Lett.* **8**, 675–682 (2005).
57. C. M. Boyd, D. Gradmann, Impact of osmolytes on buoyancy of marine phytoplankton. *Mar. Biol.* **141**, 605–618 (2002).
 58. M. W. Lomas, P. M. Gilbert, Comparisons of nitrate uptake, storage, and reduction in marine diatoms and flagellates. *J. Phycol.* **36**, 903–913 (2000).
 59. J. Diaz, E. Ingall, C. Benitez-nelson, D. Paterson, M. D. De Jonge, I. McNulty, J. A. Brandes, polyphosphate: A key player in geologic phosphorus sequestration. *Science (80-.)*. **13193**, 652–656 (2008).
 60. J. Nuester, S. Vogt, B. S. Twining, Localization of iron within centric diatoms of the genus *Thalassiosira*. *J. Phycol.* **48**, 626–634 (2012).
 61. A. Chiovitti, P. Molino, S. a Crawford, R. Teng, T. Spurck, R. Wetherbee, The glucans extracted with warm water from diatoms are mainly derived from intracellular chrysolaminaran and not extracellular polysaccharides. *Eur. J. Phycol.* **39**, 117–128 (2004).
 62. M. Forgac, Vacuolar ATPases: Rotary proton pumps in physiology and pathophysiology. *Nat. Rev. Mol. Cell Biol.* **8**, 917–929 (2007).
 63. S. Cidon, H. Ben-David, N. Nelson, ATP-driven proton fluxes across membranes of secretory organelles. *J. Biol. Chem.* **258**, 11684–11688 (1983).
 64. E. J. Armstrong, J. N. Roa, J. H. Stillman, M. Tresguerres, Symbiotic photosynthesis in giant clams is promoted by V-type H⁺-ATPase from host cells. *J. Exp. Biol.* **221** (2018), doi:10.1242/jeb.177220.
 65. H. Sze, J. M. Ward, S. Lai, Vacuolar H⁺-translocating ATPases from plants: Structure, function, and isoforms. *J. Bioenerg. Biomembr.* **24**, 371–381 (1992).
 66. T. Nishi, M. Forgac, The vacuolar (H⁺)-ATPases — nature’s most versatile proton pumps. *Nat. Rev. Mol. Cell Biol. Cell Biol.* **3**, 94–103 (2002).
 67. K. L. Barott, A. A. Venn, S. O. Perez, S. Tambutté, M. Tresguerres, Coral host cells acidify symbiotic algal microenvironment to promote photosynthesis. *Proc. Natl. Acad. Sci.* **112**, 607–612 (2015).
 68. Y.-T. Xiao, L.-X. Xiang, J.-Z. Shao, Vacuolar H⁺-ATPase. *Int. J. Biochem. Cell Biol.* **40**, 2002–2006 (2008).
 69. J. N. Roa, C. L. Munévar, M. Tresguerres, Feeding induces translocation of vacuolar proton ATPase and pendrin to the membrane of leopard shark (*Triakis semifasciata*) mitochondrion-rich gill cells. *Comp. Biochem. Physiol. -Part A Mol. Integr. Physiol.* **174**, 29–37 (2014).

70. S. Dröse, K. Altendorf, Bafilomycins and concanamycins as inhibitors of V-ATPases and P-ATPases. *J. Exp. Biol.* **8**, 1–8 (1997).
71. B. J. Bowman, E. J. Bowman, Mutations in subunit c of the vacuolar ATPase confer resistance to bafilomycin and identify a conserved antibiotic binding site. *J. Biol. Chem.* **277**, 3965–3972 (2002).
72. M. Huss, G. Ingenhorst, S. Ko, M. Gaßel, S. Dro, A. Zeeck, K. Altendorf, H. Wieczorek, Concanamycin A, the specific inhibitor of V-ATPases, binds to the V_o subunit c. *J. Biol. Chem.* **277**, 40544–40548 (2002).
73. K. Niikura, S. Nakajima, M. Takano, H. Yamazaki, FR177995, a novel vacuolar ATPase inhibitor, exerts not only an inhibitory effect on bone destruction but also anti-immunoinflammatory effects in adjuvant-induced arthritic rats. *Bone.* **40**, 888–894 (2007).
74. N. Kartner, Y. Yao, K. Li, G. J. Crasto, A. Datti, M. F. Manolson, Inhibition of osteoclast bone resorption by disrupting vacuolar H⁺-ATPase α 3-B2 subunit interaction. *J. Biol. Chem.* **285**, 37476–37490 (2010).
75. K. J. Parra, C. Y. Chan, J. Chen, *Saccharomyces cerevisiae* vacuolar H⁺-ATPase regulation by disassembly and reassembly: One structure and multiple signals. *Eukaryot. Cell.* **13**, 706–714 (2014).
76. T. Seidel, C. Kluge, M. Hanitzsch, J. Roß, M. Sauer, K. Dietz, D. Gollmack, Colocalization and FRET-analysis of subunits c and a of the vacuolar H⁺-ATPase in living plant cells. **112**, 165–175 (2004).
77. E. G. Vrieling, W. W. C. Gieskes, T. P. M. Beelen, Silicon deposition in diatoms: Control by the pH inside the silicon deposition vesicle. *J. Phycol.* **35**, 548–559 (1999).
78. M. Vartanian, J. Desclés, M. Quinet, S. Douady, P. J. Lopez, Plasticity and robustness of pattern formation in the model diatom *Phaeodactylum tricornutum*. *New Phytol.* **182**, 429–442 (2009).
79. A. Bussard, P. J. Lopez, Evolution of vacuolar pyrophosphatases and vacuolar H⁺-ATPases in diatoms. *J. Mar. Sci. Technol.* **22**, 50–59 (2014).
80. H. Zhang, R. Zeng, D. Chen, J. Liu, A pivotal role of vacuolar H⁺-ATPase in regulation of lipid production in *Phaeodactylum tricornutum*. *Sci. Rep.* **6**, 31319 (2016).

CHAPTER 2

Dynamic subcellular translocation of V-type H⁺-ATPase is essential for biomineralization of the diatom silica cell wall

Dynamic subcellular translocation of V-type H⁺-ATPase is essential for biomineralization of the diatom silica cell wall

Daniel P. Yee , Mark Hildebrand*[†] and Martin Tresguerres* 

Scripps Institution of Oceanography, University of California San Diego, 9500 Gilman Drive, La Jolla, CA 92093, USA

Author for correspondence:

Martin Tresguerres

Tel: +1 858 534 5895

Email: mtresguerres@ucsd.edu

Received: 11 September 2019

Accepted: 4 November 2019

New Phytologist (2019)

doi: 10.1111/nph.16329

Key words: biosilica, membrane acidification, protein trafficking, proton pump, silica biomineralization, vacuolar H⁺-ATPase.

Summary

- Diatom cell walls, called frustules, are main sources of biogenic silica in the ocean and their intricate morphology is an inspiration for nanoengineering. Here we show dynamic aspects of frustule biosynthesis involving acidification of the silica deposition vesicle (SDV) by V-type H⁺ ATPase (VHA).
- Transgenic *Thalassiosira pseudonana* expressing the VHA B subunit tagged with enhanced green fluorescent protein (VHA_B-eGFP) enabled subcellular protein localization in live cells.
- In exponentially growing cultures, VHA_B-eGFP was present in various subcellular localizations including the cytoplasm, SDVs and vacuoles. We studied the role of VHA during frustule biosynthesis in synchronized cell cultures of *T. pseudonana*. During the making of new biosilica components, VHA_B-eGFP first localized in the girdle band SDVs, and subsequently in valve SDVs. In single cell time-lapse imaging experiments, VHA_B-eGFP localization in SDVs precluded accumulation of the acidotropic silica biomineralization marker PDMPO. Furthermore, pharmacological VHA inhibition prevented PDMPO accumulation in the SDV, frustule biosynthesis and cell division, as well as insertion of the silicalemma-associated protein SAP1 into the SDVs. Finally, partial inhibition of VHA activity affected the nanoscale morphology of the valve.
- Altogether, these results indicate that VHA is essential for frustule biosynthesis by acidifying the SDVs and regulating the insertion of other structural proteins into the SDV.

Introduction

Diatoms are a diverse group of eukaryotic phytoplankton found in marine and freshwater ecosystems worldwide, and are responsible for up to 20% of the primary production on the planet (Field *et al.*, 1998). Unique for having a silica cell wall called the frustule, diatoms are the major source of biogenic silica in the ocean and play central roles in oceanic biogeochemical cycling and marine food webs (Falkowski *et al.*, 1998; Yool & Tyrrell, 2003; Falkowski *et al.*, 2004). The diatom frustule consists of an epitheca and hypotheca that assemble together, similar to a Petri dish (Fig. 1) (Pickett-Heaps *et al.*, 1990). Each half comprises a valve on top and a series of concentric ring-shaped girdle bands on the sides that enable cell elongation. Frustules are synthesized in intracellular compartments called silica deposition vesicles (SDVs), which are defined by a membrane called the silicalemma (Drum & Pankratz, 1964; Volcani & Li, 1984). After cytokinesis, a valve is synthesized in each sibling protoplast within an individual SDV close to the cleavage furrow. After valve exocytosis, each girdle band is synthesized in an individual SDV close to the

lateral sides of the cell. Silica biomineralization is aided by long-chain polyamines (Poulsen & Kröger, 2004) and proteins located inside SDVs or embedded within the silicalemma, including silicanin-1 (Sin1) (Kotzsch *et al.*, 2017) and silicalemma-associated proteins (SAPs) (Tesson *et al.*, 2017), which induce silica polymerization and guide the detailed nanoscale pattern formation of the frustule (Hildebrand *et al.*, 2018); silaffins (Kröger *et al.*, 1999) have also been shown to aid in this process but have not yet been targeted to the SDV.

The SDV is speculated to originate from the Golgi apparatus (Pickett-Heaps *et al.*, 1990) and to expand by the fusing of spherical vesicles to the silicalemma (Schmid & Schulz, 1979). A predicted acidic pH of *c.* 5 inside the SDV (Vrieling *et al.*, 1999; Herve *et al.*, 2012) is presumed to slow the polymerization of silicic acid in order to prevent uncontrolled silica deposition and allow for proper morphogenesis of the frustule (Iler, 1979). This degree of acidification suggested the involvement of the V-type H⁺-ATPase (VHA) (Gordon & Drum, 1994; Hildebrand *et al.*, 2018), an evolutionary conserved multi-subunit protein complex that uses the energy from ATP hydrolysis to transport H⁺ across biological membranes of eukaryotic cells (Nishi & Forgac, 2002; Forgac, 2007). VHA is a holoenzyme that consists of a membrane-bound V₀-domain composed of subunits a, d, e, c, c', c'', and a cytosolic V₁-domain composed of subunits A–H (Sze *et al.*,

*These authors contributed equally to this work.

[†]This article is dedicated in memory of Dr Mark Hildebrand (1958–2018), who devoted his life to advancing the biotechnological applications and elucidating the beauty and mystery of diatom cell biology.

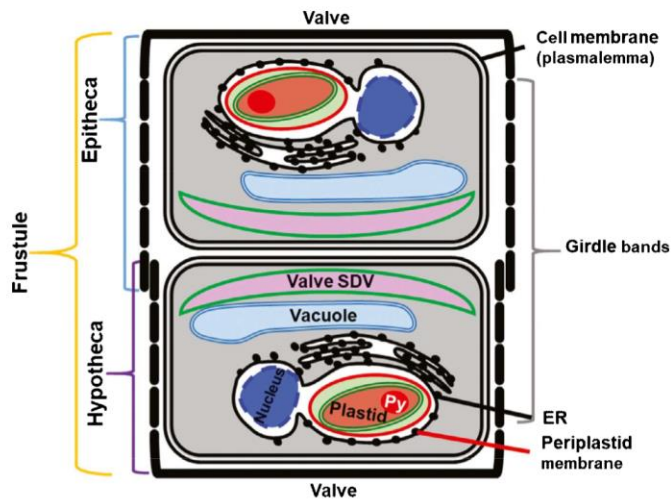


Fig. 1 Diagram of a centric diatom undergoing cell division. The frustule is composed of a hypotheca and overlapping epitheca which encapsulates the cell membrane and all other intracellular compartments. Each theca is composed of a valve and concentric rings of girdle bands. During the M phase following cytokinesis, two valves are synthesized within silica deposition vesicles (SDVs) of two daughter cells and separate the cells when exocytosed. Py, the pyrenoid; ER, endoplasmic reticulum.

1992, 2002; Kluge *et al.*, 2003; Xiao *et al.*, 2008; Bussard & Lopez, 2014; Tresguerres, 2016). The V_0 -domain forms a proteolipid ring through membranes, and the V_1 -domain hydrolyzes ATP to provide the driving force to move H^+ against its electrochemical gradient (Kawasaki-Nishi *et al.*, 2003).

V-type H^+ -ATPase was first proposed in diatom silicification in the role of acidifying clathrin-coated silica transport vesicles to prevent premature hardening of silica before delivery to SDV (Gordon & Drum, 1994). Later, a functional study using pharmacological VHA inhibitors would show reduced size and altered morphology in the frustule of the pennate diatom *Phaeodactylum tricoratum* (Vartanian *et al.*, 2009). That study suggested further investigations to confirm whether VHA directly contributed to the regulation of pH in the SDV, to study the role of VHA in vesicular trafficking and transport of material to the SDV, and to address a potential role of the vacuole in silica biomineralization. However, a subsequent investigation reported the presence of VHA subunit c in the cytoplasm and endoplasmic reticulum (Bussard & Lopez, 2014) rather than the SDV, confounding the potential role of VHA in silicification and suggesting that frustule alteration by VHA inhibitors was an indirect effect. Alternatively, VHA could be present in the silicalemma specifically during frustule formation. Indeed, a change in VHA subcellular localization is a common regulatory mechanism in other organisms; for example, acid/base stress, hormones and neurotransmitters may induce the VHA translocation from the cytoplasm to the cell plasma membrane in kidney (Pastor-Soler *et al.*, 2003), epididymis (Roy *et al.*, 2013), fish gill (Tresguerres *et al.*, 2010; Roa & Tresguerres, 2016), and insect salivary glands (Dames *et al.*, 2006).

To investigate the potential transient location of VHA in the diatom SDV and its role in biomineralization, we generated a transgenic *Thalassiosira pseudonana* cell line expressing VHA subunit B fused to enhanced green fluorescent protein (VHA_B-eGFP). We then took advantage of a synchronization method

(Hildebrand *et al.*, 2007) to determine dynamic changes in VHA subcellular location throughout the cell cycle. In the absence of silicon, *T. pseudonana* cannot make new frustules for the daughter cells and the majority of cells arrests in the Gap 1 (G1) stage of interphase. At 4 h after silicon replenishment, *c.* 50% of the cells are in the Gap 2 or mitosis (G2 + M) stages, when cells proceed to perform mitosis, build new valves, and divide (Hildebrand *et al.*, 2007). At 5–8 h after silicon replenishment, the majority of cells in the culture has divided and are in G1 of the next cell division cycle. Frustule biosynthesis was visualized by staining with 2-(4-pyridyl)-5-((4-(2-dimethylaminoethylaminocarbonyl) methoxy)phenyl)oxazole (PDMPO), an acidotropic dye that selectively incorporates into newly biomineralized silica (Shimizu *et al.*, 2001). VHA activity was downregulated by incubating cell cultures with the highly specific pharmacological inhibitor, concanamycin A (Dröse & Altendorf, 1997; Huss *et al.*, 2002). Higher temporal resolution of VHA_B-eGFP translocation to SDVs was visualized by time-lapse super-resolution confocal microscopy. Additionally, we used *T. pseudonana* expressing SAPI-eGFP fusion proteins to interrogate a putative role of VHA activity on the delivery of silicon-polymerizing proteins to the SDV. Lastly, wild-type *T. pseudonana* cultures were incubated with partial-inhibiting concentrations of concanamycin A and their frustules were imaged using scanning electron microscopy (SEM) to observe effects of VHA activity downregulation on silica biomineralization.

Materials and Methods

Culture conditions

Thalassiosira pseudonana (CCMP1335) cultures were grown axenically in artificial seawater (ASW) medium (Darley &

Volcani, 1969) supplemented with 1 mM Na_2SiO_3 . Wild-type and VHA_B-eGFP expressing cultures were grown on an orbital shaker under continuous illumination by cool-white fluorescent lamps at 70 $\mu\text{mol photons m}^{-2} \text{s}^{-1}$ at 18°C. Cell lines expressing SAP1-eGFP were grown under 16 h : 8 h, light : dark conditions to overcome a negative growth phenotype resulting from light-induced overexpression of the SAP1 under control of the *fcg*-promoter.

Transgenic diatoms expressing fluorescently labeled VHA_B and SAP1

Proteins labeled with eGFP were expressed under the control of the native or *fcg* promoters. For native expression of Thaps3_40522 (VHA_B), DNA fragments including the full-length coding sequence of the gene, 500 bp upstream of the first methionine, and 500 bp downstream of the stop codon were amplified from *T. pseudonana* genomic DNA, and cloned into the Gateway destination vector pMHL_71 with eGFP at the end of the coding sequence. For *fcg* expression of Thaps3_40522 (VHA_B) and Thaps3_25736 (SAP1), the full-length coding sequence of the gene was amplified from *T. pseudonana* genomic DNA, and cloned into Gateway destination vector pMHL_79 with eGFP at the end of the coding sequence. All transformation vectors were cotransformed with a pMHL_09 expressing the *nat1* gene which confers nourseothricin resistance by biolistic gene gun method (Poulsen *et al.*, 2006). Liquid cultures grown in ASW media containing 100 $\mu\text{g ml}^{-1}$ nourseothricin were enriched for cells expressing eGFP using several rounds of fluorescence-activated cell sorting on a BD Influx Cell Sorter (BD Biosciences, San Jose, CA, USA), from which single colonies expressing eGFP were selected for on ASW agar plates containing nourseothricin.

Similar localizations were observed in *T. pseudonana* expressing VHA_B-eGFP under control of the native (Supporting Information Fig. S1) and *fcg* promoters (Fig. 2), indicating that choice of promoter did not influence localization of the fusion protein. However, cells expressing *fcg*-VHA_B-eGFP were able to be imaged longer by fluorescence microscopy and were used for all experiments involving the VHA_B-eGFP fusion protein.

Synchronized cell cycle localization of VHA_B-eGFP and PDMPO

For synchronization of the cell cycle, starter cultures of *T. pseudonana* expressing *fcg*-VHA_B-eGFP grown to 2×10^6 cells ml^{-1} were centrifuged at 4000 *g* for 10 min and washed twice with silicon-free (Si-) ASW before being resuspended at 1.0×10^6 cells ml^{-1} in 500 ml of Si- ASW. Following 24 h of silicon starvation, sodium silicate was added at 200 μM final concentration to initiate cell-cycle progression, and PDMPO; LysoSensor YellowBlue DND-160 (Life Technologies, Carlsbad, CA, USA), an acidotropic silica biomineralization marker, was added at 0.125 μM final concentration to visualize low-pH compartments and newly synthesized biosilica. VHA_B-eGFP and PDMPO localization were tracked in cells sampled

from $t=0$ to $t=8$ h at the start of each hour by fluorescence microscopy on a Zeiss Axio Observer.Z1 inverted microscope. Visual analysis and calculations of VHA and PDMPO localization were carried out by recording cells with eGFP signal and/or PDMPO signal in the valve SDV out of the total cell population using the CELL COUNTS plugin in Fiji (Schindelin *et al.*, 2019). In parallel experiments, 2.5 μl of a 1 mM concanamycin A (AdipoGen BVT-0237; $\geq 98\%$ purity) stock solution prepared in dimethyl sulfoxide (DMSO) was added at 5 nM to 500 ml cell cultures to inhibit VHA activity (Dröse & Altendorf, 1997; Bowman & Bowman, 2002; Huss *et al.*, 2002); equal volumes of DMSO were added in control experiments to account for potential side-effects of DMSO on diatom cells. The filter sets used for GFP was Zeiss #38HE (Ex 470/40 nm, FT 495 nm, Em 525/50 nm), for PDMPO was Zeiss #21HE (Ex 387/15 nm, FT 409 nm, Em 510/90 nm), and for Chl autofluorescence was Zeiss #05 (Ex 395-440 nm, FT 460 nm, Em 470 nm).

Super-resolution confocal microscopy

For single-cell time-lapse imaging, 2 ml of exponentially growing *T. pseudonana* cell culture expressing VHA_B-eGFP was transferred to a 35 mm poly-d-lysine-coated glass-bottom Petri dish. Cells were allowed to adhere to the Petri dish bottom for 15 min followed by the addition of 2 ml of ASW medium and PDMPO was added for a final concentration of 0.125 μM . Dishes were mounted on a Warner Instruments (Camden, CT, USA) QE-1HC Quick Exchange Heated/Cooled stage chamber controlled by CL-200 Dual Channel Temperature Controller maintained at 18°C. Cells were imaged with a Zeiss LSM800 inverted confocal microscope equipped with a Zeiss Plan-Apochromat $\times 63$ (1.4) Oil DIC M27 objective, and Zeiss Airyscan super-resolution detector. Two channels were acquired to monitor eGFP (Ex 488 nm with 0.5% laser power, Em 509 nm, detection 490–535 nm) and PDMPO (Ex 335 nm at 0.6% laser power, Em 530 nm, detection 490–575 nm) fluorescence. Images were collected at 3 min intervals for 4 h with Zeiss Definite Focus stabilization enabled.

VHA_B mRNA expression

Thaps3_40522 (VHA_B) mRNA expression level fragments per kilobase per million reads mapped (FPKM) was acquired from transcriptomics analysis of RNAseq data collected from time-course experiments following silicon replenishment from biological duplicates of synchronized *T. pseudonana* cultures (Abbriano Burke, 2017). Raw reads from individual samples were demultiplexed based on a perfect barcode match, and TOPHAT (v.2.0.6) running BOWTIE 2 (v.2.0.2) was used for strand-specific mapping of RNAseq reads to the *T. pseudonana* reference genome assembly (Thaps3) obtained from the Joint Genome Institute (JGI): (<http://genome.jgi.doe.gov/Thaps3/Thaps3.download.ftp.html>). CUFFLINKS (v.2.2.1) was used to assemble transcripts, and the assembly was used for AUGUSTUS gene model prediction. Raw counts to AUGUSTUS-generated gene models were generated using HTSEQ-COUNT (HTSEQ 0.6.1p1). Normalized counted and

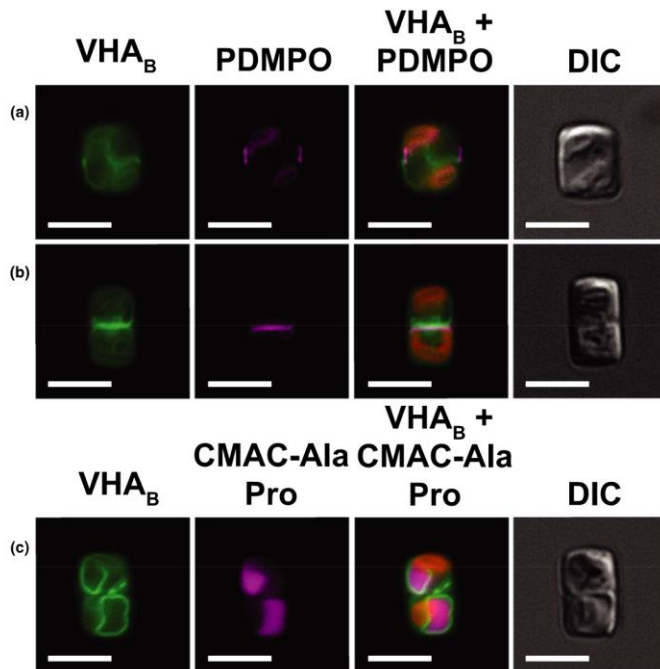


Fig. 2 V-type H^+ -ATPase (VHA) localization in multiple subcellular compartments. Representative images of exponentially growing *Thalassiosira pseudonana* expressing fcp-VHA B subunit tagged with enhanced green fluorescent protein (fcp-VHA_B-eGFP) in: (a) a girdle band silica deposition vesicle (SDV); (b) valve SDVs; and (c) vacuole tonoplast. Green, VHA_B-eGFP; red, Chl; magenta, 2-(4-pyridyl)-5-((4-(2-dimethylaminoethyl)-aminocarbonyl)methoxy)phenyl)oxazole (PDMPPO) (a, b), CMAC-Ala-Pro (c); white, colocalization of VHA_B-eGFP and PDMPPO (a, b). Bars, 5 µm.

differential expression analysis was done using the DESeq2_1.6.3 package.

VHA_B protein abundance

Subsamples of synchronized wild-type *T. pseudonana* expressing VHA_B-eGFP were harvested at $t = 0$ before silicon replenishment, and every hour thereafter ($t = 1-8$ h), by centrifugation at maximum speed at 4°C for 5 min followed by freezing of the pellet on dry ice. Protein was extracted in a 2× Extraction Buffer (125 mM Tris, pH 6.8, and 138 mM sodium dodecyl sulfate) by boiling at 95°C for 5 min, pelleting at maximum speed, and recovering the supernatant for Western blot analysis. Protein concentration was determined with the Bio-Rad D/C Protein Assay Kit and BSA protein standard. Western blots were performed by separating 23 µg of total protein in a 10% polyacrylamide mini gel (60 V, 20 min; 120 V, 90 min) and transferring to a polyvinylidene difluoride (PVDF) membrane. Equivalent protein loading was confirmed by Ponceau staining of total protein on the PVDF membranes (Romero-Calvo *et al.*, 2010). Membranes were blocked in 3% milk-blocking buffer and incubated with custom monoclonal VHA_B primary antibody (1 : 100) at 4°C overnight. Membranes were washed three times with Tris-buffered saline + 0.1% TWEEN 20 (T-BST) and incubated with goat-anti-mouse horseradish peroxidase antibody (1 : 10 000) at room temperature

for 1 h. Membranes were developed with Bio-Rad Western Clarity ECL and analyzed in a Bio-Rad Universal III Hood using IMAGEQUANT software (Bio-Rad, Hercules, CA, USA).

SEM imaging of frustules

Wild-type *T. pseudonana* synchronized by silicon starvation was incubated with 200 µM Na₂SiO₃ for 2 h, then exposed to 0 (control), 0.4, 1.0, and 2.0 nM concanamycin A for 22 h. At $t = 24$ h, 20 ml of each cell culture was pelleted and frozen on dry ice. Frustules were acid-washed by resuspending pellets in 50 µl of milli-Q H₂O (resistivity of 18.2 MΩ cm at 25°C) and vortexing with 200 µl 100% H₂SO₄. Samples were then boiled for 10 min, cooled on ice before adding a small amount of KNO₃, and boiled again for 10 min. Next, 800 µl of H₂O was added to samples before centrifuging at 1500 g for 10 min; the supernatant was discarded. These steps were repeated, without vortexing, to remove all intracellular contents. After washing with H₂O three times, frustules were resuspended in 200 ml of 100% ethanol for storage and air-dried onto stubs at ambient conditions for SEM imaging. Acid-cleaned frustules were imaged on Zeiss Sigma 500 SEM at the California Institute for Telecommunications and Information Technology Nano3 facility at UCSD. Quantification of normal and altered valves was completed using the CELL COUNTS plugin in Fiji (Schindelin *et al.*, 2019).

Results

Subcellular localization of VHA_B-eGFP in *T. pseudonana*

Diatoms expressing VHA_B-eGFP under control of the *fcy* promoter from exponentially growing (i.e. not synchronized) cultures displayed heterogeneous VHA_B-eGFP subcellular localization. VHA_B-eGFP was generally found faintly throughout the cytoplasm in all cells. In addition, more concentrated VHA_B-eGFP signal was present in the silicalemma of girdle band SDVs (Fig. 2a) and valve SDVs of dividing cells (based on colocalization with PDMPO; Fig. 2b) or in vacuole tonoplasts (based on colocalization with the vacuolar marker CMAC Ala-Pro; Fig. 2c).

VHA_B mRNA and protein expression in synchronized cell cultures

Next, we quantified VHA_B mRNA and protein abundance along the cell cycle of *T. pseudonana* cultures synchronized by silicon starvation and replenishment (Fig. 3). Expression of mRNA was measured using an Illumina (La Jolla, CA, USA) HiSeq 2000 sequencer. VHA_B mRNA had a peak at $t = 4$ h that was *c.* 3.2-fold higher compared with $t = 0$ h (4501 vs 1391 FPKMs). VHA_B mRNA abundance then decreased to basal values (*c.* 1116 FPKMs) by $t = 8$ h. Expression of VHA_B protein was quantified by Western blotting and revealed two bands, one at *c.* 55 kDa (corresponding to native VHA_B) and another at *c.* 88 kDa (corresponding to transgenic VHA_B plus the 33 kDa eGFP tag) (Fig. S2). Native VHA_B protein abundance had a *c.* 3.2-fold peak between $t = 3$ h and $t = 5$ h (Fig. 3). The Western blots also showed that the level of VHA_B-eGFP protein overexpression over native VHA_B was moderate, with a maximum of *c.* 2.4-fold at $t = 1$ h and nearly equal levels from $t = 4$ h and onwards.

These mRNA and protein abundance peaks occurred between $t = 4$ h and $t = 5$ h, which coincided with initiation of valve formation and maximum cell length during the G2 + M phase of the cell cycle observed in previous synchrony experiments conducted with *T. pseudonana* (Hildebrand *et al.*, 2007). While this pattern of VHA_B expression is consistent with synthesis of new

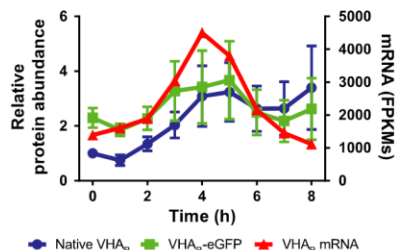


Fig. 3 Relative VHA B subunit (VHA_B) protein abundance ($n = 5$, error bars = \pm SE) and mRNA expression (FPKM) from synchronized *Thalassiosira pseudonana* cultures following silicon replenishment. FPKM, fragments per kilobase per million reads mapped.

© 2019 The Authors
New Phytologist © 2019 New Phytologist Trust

VHA_B protein for valve SDVs, the presence of VHA_B in multiple subcellular localization shown in Fig. 2 prevents assessment of its significance to cell physiology.

VHA_B-eGFP and PDMPO localization in SDVs of synchronized cells

To investigate the physiological role of VHA throughout the cell cycle of *T. pseudonana*, VHA_B-eGFP subcellular localization was tracked alongside frustule morphogenesis using the acidotropic silica biomineralization marker PDMPO using fluorescence microscopy. In synchronized cultures, analysis of PDMPO accumulation in the valve SDV in control and concanamycin A-treated cells (Fig. 4a) revealed a strong relationship between VHA_B-eGFP translocation to the valve SDV, valve formation, and progression of the cell cycle. In the period $t = 0$ –3 h after silicon replenishment, VHA_B-eGFP and PDMPO signals in the valve SDV were minimal, with both occurring in *c.* 5% of the population. The observed peak of roughly one-third of the cell population exhibiting both VHA_B-eGFP and PDMPO in the valve SDV at $t = 4$ h matches previous reports that the majority of synchronized *T. pseudonana* begin synthesizing the valves at 3.5 h after silicon replenishment (Hildebrand *et al.*, 2007). At $t = 5$ h, PDMPO signal in newly synthesized valves increased to *c.* 67% and reached a maximum of *c.* 88% after $t = 7$ h. However, VHA_B-eGFP signal in the valve SDV decreased to *c.* 14% of the cells at $t = 5$ h, and then to a minimum of *c.* 2% by $t = 8$ h. This is consistent with VHA leaving the silicalemma after the completion of valve synthesis.

Dynamics of VHA_B-eGFP localization and silica biomineralization in SDVs of synchronized cells

Fig. 4(b) shows representative VHA_B-eGFP expressing cells corresponding to the hours following silicon replenishment and phases of the cell cycle. In the G1 phase ($t = 0$ –2 h) following silicon replenishment, VHA_B-eGFP was present throughout the cytoplasm and more prominently in vacuole tonoplasts (Fig. 4bi). Further along in the G1 phase, VHA_B-eGFP was present in a single girdle band SDV which colocalized with PDMPO, marking newly synthesized girdle bands (Fig. 4bii). At the beginning of the G2 + M phase ($t = 3$ –6 h), VHA_B-eGFP accumulated along with a diffuse signal from PDMPO in the middle of the cell where valve synthesis occurs (Fig. 4biii). Further into the G2 + M phase, VHA_B-eGFP was present in the valve SDVs while PDMPO signal became concentrated and bound within the newly synthesized valves (Fig. 4biv). VHA_B-eGFP was maintained in valve SDVs as valve synthesis neared completion (Fig. 4bv). By the end of the G2 + M phase, the new PDMPO-labeled valves were exocytosed and the two cells divided. As the daughter cells transitioned to the next G1 phase ($t = 6$ –8 h), VHA_B-eGFP was again present in girdle band SDVs while a majority of VHA_B-eGFP was present in tonoplasts, presumably to serve in physiological functions carried out by vacuoles (Fig. 4bvi).

Having established a clear relationship between VHA and SDVs, the functional effect of abolishing VHA activity using the

New Phytologist (2019)
www.newphytologist.com

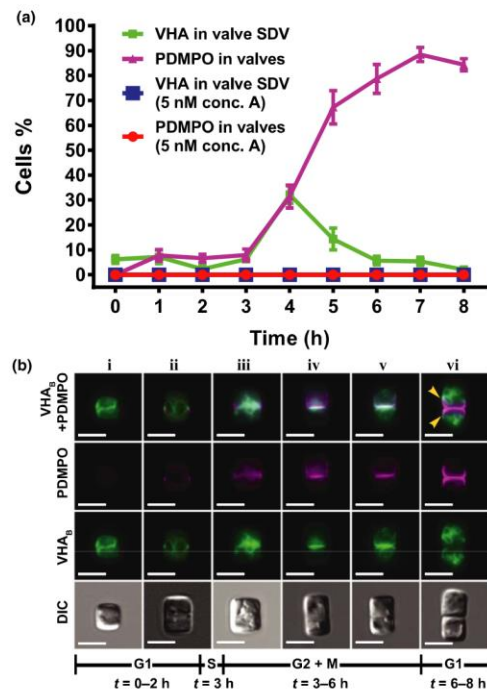


Fig. 4 (a) V-type H⁺-ATPase (VHA) dynamics in the valve-specific silica deposition vesicles (SDVs) throughout the cell cycle. Percentage of cells with VHA B subunit tagged with enhanced green fluorescent protein (VHA_B-eGFP) in the valve-specific SDVs, and 2-(4-pyridyl)-5-((4-(2-dimethylaminoethyl-aminocarbonyl) methoxy)phenyl)oxazole (PDMPO) signal in valves in control and concanamycin A (conc. A)-treated cultures. VHA and PDMPO localization were analyzed using the CELL_COUNTER tool in IMAGEJ on c. 280 cells per time point (c. 2500 cells total; n = 3; error bars are ± SE). (b) Representative cell images of VHA_B subcellular localization throughout the cell cycle in *Thalassiosira pseudonana* expressing fcp-VHA_B-eGFP: (i) cytoplasmic and tonoplast localization during G1 phase; (ii) tonoplast and girdle band SDV localization during G1 phase; (iii) accumulation at the site of valve biosynthesis; (iv, v) initial (iv) and later stage (v) concentration in the valve SDVs during the G2 + M phase; (vi) cytoplasmic, girdle band SDV, and tonoplast localization in the G1 phase of two daughter cells. Green, VHA_B-eGFP; magenta, PDMPO; white, colocalization of VHA_B-eGFP and PDMPO; red, Chl; DIC, differential interference contrast. Yellow arrows in (vi) indicate girdle bands. Bars, 5 μm.

highly specific inhibitor concanamycin A (5 nM) was investigated. Cell cultures treated with concanamycin A displayed no VHA_B-eGFP signal in SDVs throughout the synchronized time-course (Fig. 4a). Concanamycin A also prevented the accumulation of PDMPO in valves throughout the time-course (Fig. 4a), which indicated that frustule biosynthesis was inhibited and was consistent with the lack of cell division even after 24 h of exposure to the drug. Cells exposed to concanamycin A showed VHA_B-eGFP distributed as a diffuse signal throughout the

cytoplasm with a slightly denser signal in the middle of the cell, but lacking the concentrated signal typical of intracellular membrane labeling (Fig. 5a–c). Additional images of concanamycin A-treated cells are shown in Fig. S3.

Live cell time-lapse imaging of VHA_B-eGFP dynamics

The dynamics of VHA_B-eGFP translocation in SDVs was investigated using time-lapse super-resolution confocal fluorescence microscopy analysis of single *T. pseudonana* cells expressing fcp-VHA_B-eGFP incubated with PDMPO during the G2 + M phase (corresponding to $t = 4$ h of the synchrony, and defined here as $t = 0$ min) (Fig. 6). At $t = 0$ min, VHA_B-eGFP was predominantly in the tonoplasts of two adjacent vacuoles. At $t = 6$ min, a distinct VHA_B-eGFP signal began to accumulate at the center of the cell marking the membranes of two adjacent valve SDVs. Three minutes later, at $t = 9$ min, PDMPO began to mark new valves and VHA_B-eGFP signal expanded further along the middle region of the cell. By $t = 27$ min, VHA_B-eGFP had made its way across the entire middle plane and a strong colocalization with PDMPO became visible. By $t = 66$ min the VHA signal in the SDVs began to decrease while PDMPO remained trapped within mature valve biosilica. At $t = 93$ min, VHA_B-eGFP signal in the SDV was nearly absent, and by $t = 111$ min, VHA_B-eGFP was only faintly visible in the plasma membrane of each daughter cell. VHA_B-eGFP signal was always present in vacuole tonoplasts which appeared to be associated with the valve SDVs up until $t = 93$ min. A movie of this time-lapse can be found in Video S1.

The VHA_B-eGFP dynamics in girdle band SDVs was captured in two attached daughter cells in the G1 phase (Fig. 7). This approach was adopted to consistently identify cells in the G1 phase following valve biosynthesis in the G2 + M phase for high-magnification focusing for super-resolution imaging. At $t = 0$ min, each cell already had newly synthesized girdle bands which extend from the valves and are labeled with PDMPO. In the top cell, VHA_B-eGFP was concentrated in the vacuole tonoplasts which could be seen in close association with a new girdle band SDV (similar to the association with the valve SDVs shown in Fig. 6). In the period $t = 24$ –57 min, VHA_B-eGFP colocalized with PDMPO in girdle band SDVs. By $t = 60$ min, VHA_B-eGFP had left the girdle band SDV while PDMPO remained in the newly synthesized girdle band. Similar observations were made in the lower cell, but it was delayed by c. 10 min relative to the top cell. A movie of this time-lapse showing the completion of both upper and lower girdle bands can be found in Video S2.

Effects of VHA inhibition on SAP1 incorporation into the SDV

Next, we examined whether VHA activity is required for the incorporation of the structural protein SAP1 into SDVs in cultures of *T. pseudonana* expressing fcp-SAP1-eGFP. First, we confirmed the previously described localization of SAP1 (Tesson *et al.*, 2017) in the silicemmas of SDVs of both girdle bands (Fig. 8a) and valves (Fig. 8b). In dividing cells, SAP1 appeared to be trafficked through the cytoplasm in a single

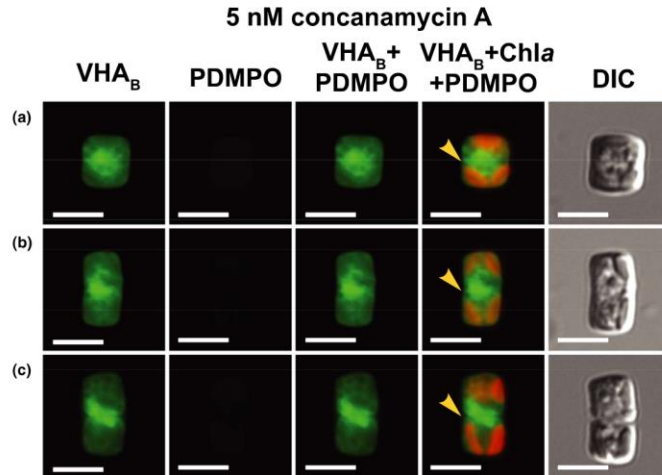


Fig. 5 Inhibition of V-type H⁺-ATPase (VHA) activity prevents frustule biosynthesis. (a–c) Representative images of synchronized *Thalassiosira pseudonana* expressing fcp-VHA B subunit tagged with enhanced green fluorescent protein (fcp-VHA_B-eGFP) treated with 5 nM concanamycin A. Green, VHA_B-eGFP; magenta, 2-(4-pyridyl)-5-((4-(2-dimethylaminoethyl-aminocarbonyl) methoxy)phenyl)oxazole (PDMPO); white, colocalization of VHA_B-eGFP and PDMPO; red, Chl; DIC, differential interference contrast. Yellow arrowheads highlight VHA accumulation near the location where the valve biosynthesis normally occurs. Bars, 5 μm.

vesicle that attached to valve SDVs and fused into the silicella (Fig. S4a–f). Following cytokinesis, SAP1 was again found within a single vesicle adjacent to newly formed valves in each daughter cell (Fig. 8c). However, in cells exposed to 5 nM concanamycin A, SAP1 accumulated in the middle of the cell, in multiple vesicles that varied in size (Figs 8d–f, S4g–i). Similar to the VHA inhibition experiments captured in Figs 4(a) and 5, 5 nM concanamycin A prevented PDMPO accumulation in SDVs, indicating inhibition of frustule biosynthesis. However, intense PDMPO signal was observed in a few SAP1-containing vesicles (Fig. 8f), suggesting they were acidic and that silica may have biomineralized in those compartments despite VHA inhibition. We tentatively suggest this is related to SAP1 overexpression.

Effects of VHA inhibition on valve nanostructure

Finally, we exposed *T. pseudonana* cultures to submaximal concanamycin A concentrations (0–2 nM) to examine the effects of reduced VHA activity on growth and valve ultrastructure. A dose–response growth curve revealed that cultures exposed to 0.4 nM concanamycin A resulted in a c. 25% decrease in growth rate and c. 36% decrease in final cell density compared with the control treatment (Fig. 9a). About one-quarter of the valves from diatoms exposed to 0.4 nM concanamycin displayed altered morphology, while the remaining valves were probably synthesized before exposure to concanamycin A and therefore looked normal. Compared with valves from control diatoms (Fig. 9b), altered valves exhibited decreased deposition of silica, and lacked features

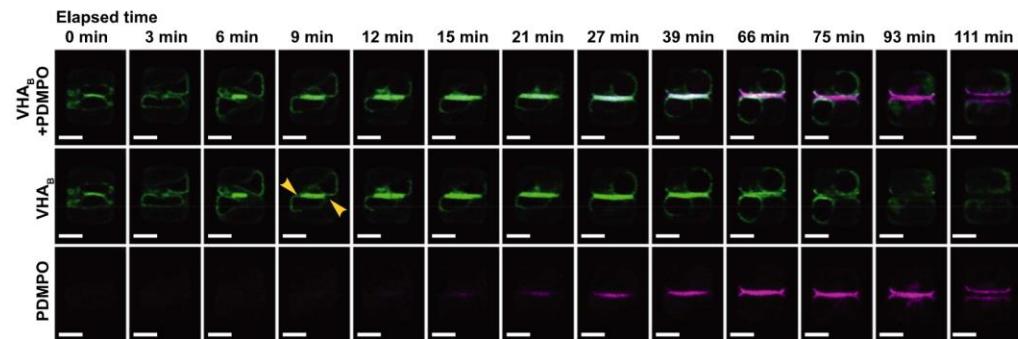


Fig. 6 Time-lapse during valve biosynthesis. Selected images from time-lapse super-resolution confocal fluorescence microscopy of *Thalassiosira pseudonana* expressing fcp-VHA B subunit tagged with enhanced green fluorescent protein (fcp-VHA_B-eGFP) incubated with 2-(4-pyridyl)-5-((4-(2-dimethylaminoethyl-aminocarbonyl) methoxy)phenyl)oxazole (PDMPO) are shown during valve biosynthesis (Supporting Information Video S1). Green, VHA_B-eGFP; magenta, PDMPO; white, colocalization of VHA_B-eGFP and PDMPO. Yellow arrowheads highlight association of vacuoles with silica deposition vesicles (SDVs). Bars, 2.5 μm.

characteristic of the distal surface of valves (Fig. 9c–e). While ribs were present in the altered valves, they lacked defined ridges and were composed of more granular silica nanoparticles. As a result of reduced silica deposition, some of the valves were bent at the edges making them less round (Fig. 9c), suggesting a decrease in rigidity. The portula was also deformed and the fuloportulae were mislocated away from the outer edges, and found closer to the center of the valve (Fig. 9c). Suboptimal VHA activity additionally affected the nanopore-containing space in between ribs (Fig. 9c): in some frustules it was only partially filled, and in the most extreme cases it was entirely absent. Additional images of altered valves are shown in Fig. S5.

Discussion

Our results demonstrate that VHA is responsible for the acidification of *T. pseudonana* SDVs which is essential for silica biomineralization *in vivo*, and identify the dynamic translocation of VHA to SDVs as a novel mechanism for frustule biosynthesis. Combining transgenic diatoms expressing VHA_B-eGFP and synchronization of the cell cycle by silicon depletion and replenishment allowed us to study the order of events that led to SDV acidification, silicon biomineralization and cell division. Under our experimental conditions, the average duration of the cell cycle is *c.* 8 h. During G1 (*t* = 0–2 h after silicon replenishment), VHA_B-eGFP is found in the cytoplasm and concentrated in vacuole tonoplasts and then to girdle band SDVs for the synthesis of girdle bands which expand the cell. At the onset of G2 and during mitosis (*t* = 3–6 h), VHA_B-eGFP translocates from vacuoles to valve SDVs of each daughter cell to produce the two new

valves required for the cells to separate. Time-lapse imaging using super-resolution confocal microscopy showed that VHA_B-eGFP presence in the SDV precedes accumulation of the acidotrophic dye PDMPO, which in turn is completely abolished by the highly specific VHA inhibitor concanamycin A. Altogether, this indicates that VHA acidifies the SDV and that this acidification is essential for frustule biosynthesis. After the new valves are exocytosed (*t* = 6–8 h), cells enter G1 of the next cell cycle and VHA_B-eGFP is turned over by translocating to the plasma membrane, leaving behind PDMPO-labeled frustules and confirming the dynamic nature of VHA. These results support the previous suggestion that the SDV integrate with the plasma membrane after frustule exocytosis (Kotzsch *et al.*, 2017).

The essential role of VHA activity on diatom frustule formation is a result of at least two potential processes. First, VHA probably provides the acidic pH that has long been predicted inside the SDV which may aide in shaping and arranging silica nanospheres, and enabling the proper function of silica-forming proteins (Iler, 1979; Kröger *et al.*, 1999, 2000, 2002; Sumper & Kröger, 2004; Kotzsch *et al.*, 2017). Although P-type H⁺-ATPases have been identified in diatoms (Bussard & Lopez, 2014), they are not inhibited at the nanomolar concentrations of concanamycin A used in our study (Dröse & Altendorf, 1997). Given the specificity of concanamycin A for VHA, and its suppressive effect on frustule synthesis as well as cell division in cultures, our results suggest that VHA is the only proton pump involved in SDV acidification. Second, VHA inhibition blocked the delivery of SAP1-containing vesicles to SDVs, pointing out a potential role of VHA in regulating vesicle fusion to the silicella. This function may depend on SDV acidification itself

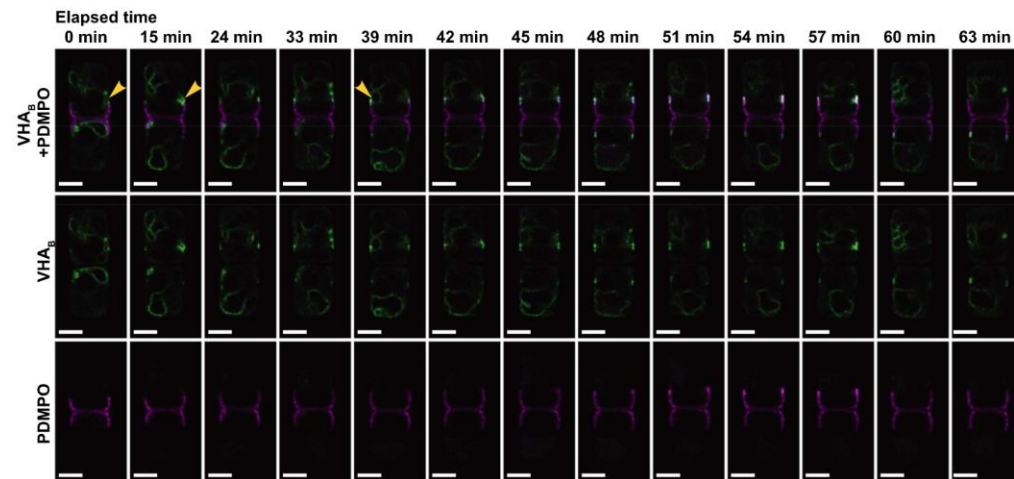


Fig. 7 Time-lapse during girdle band biosynthesis. Selected images from time-lapse super-resolution confocal fluorescence microscopy of two attached *Thalassiosira pseudonana* cells expressing fcp-VHA B subunit tagged with enhanced green fluorescent protein (fcp-VHA_B-eGFP) incubated with 2-(4-pyridyl)-5-((4-(2-dimethylaminoethyl-aminocarbonyl) methoxy)phenyl)oxazole (PDMPO) are shown during girdle band biosynthesis (Supporting information Video S2). Green, VHA_B-eGFP; magenta, PDMPO; white, colocalization of VHA_B-eGFP and PDMPO. Yellow arrowheads highlight association of vacuoles with SDVs. Bars, 2.5 μ m.

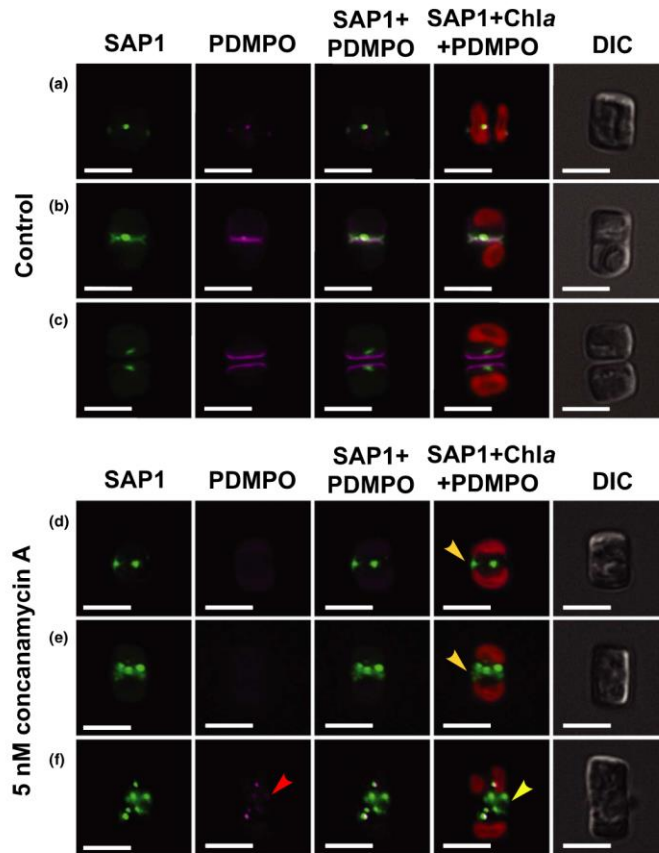


Fig. 8 Inhibition of V-type H^+ -ATPase (VHA) activity prevents insertion of SAP1 into the silica deposition vesicle (SDV). Representative images of cell cycle-synchronized *Thalassiosira pseudonana* expressing fcp-SAP1-eGFP. (a–c) Control cells; (d–f) cells incubated with 5 nM concanamycin A. Green, SAP1-eGFP; magenta, 2-(4-pyridyl)-5-((4-(2-dimethylaminoethyl-aminocarbonyl) methoxy)phenyl)oxazole (PDMPO); white, colocalization of SAP1-eGFP and PDMPO; red, Chl; DIC, differential interference contrast. Yellow arrowheads highlight SAP1 near the location where the valve biosynthesis normally occurs; the red arrow highlights the concentration of PDMPO in SAP1 vesicles. Bars, 5 μ m.

or on the recruitment of the vesicle fusion machinery by VHA as reported in other cells (Maxson & Grinstein, 2014). If this is true, another outstanding question is whether VHA activity is required for the fusion of vesicles trafficking other components to the SDV of newly forming frustules, including other structural proteins found in SDV membranes and substrates of the insoluble organic matrices known to comprise frustules (Tesson & Hildebrand, 2013; Kotzsch *et al.*, 2016). Alternatively, inhibition of VHA by concanamycin A may prevent SDV formation, leaving SDV-associated proteins without a final location to target to.

In addition to the SDV, we found that VHA_B -eGFP is present in the vacuole tonoplast in cells in various cell stages (Figs 2c, 4b, 6, 7), which opens new questions about the regulatory mechanisms behind differential VHA subcellular localization and coordination of vacuolar function and cell division. Interestingly, the tonoplast appeared to maintain an association with the SDV, and may act as a reservoir for newly synthesized VHA. The proximity of vacuoles near locations of valve and girdle band synthesis

suggests the transfer of VHA-containing tonoplast to the silicella during valve biogenesis, providing insights into the potential origin of SDV membrane material such as lipids and other proteins. In cultures treated with a fully inhibiting dose of concanamycin A, cells that were in the process of dividing had increased VHA_B -eGFP in the site where the new valves would form; however, they lacked a defined SDV (Figs 5a–c, S3). In these cells, we hypothesize that VHA_B -eGFP was localized in a nonrigid SDV membrane representative of an early stage in valve formation, which is consistent with previous observations of very early stages of valve formation with deformed but recognizable silica structure (Hildebrand, 2010) and a folded appearance similar to a 'taco' shell (Hildebrand *et al.*, 2007). An interesting concept to consider is whether the normal SDV shape directly depends on VHA activity. To prevent aberrant valve structure, the SDV must become fully expanded before or at least concurrent with completion of the base layer. Thus, SDV expansion would be a property of the organic material comprising the SDV,

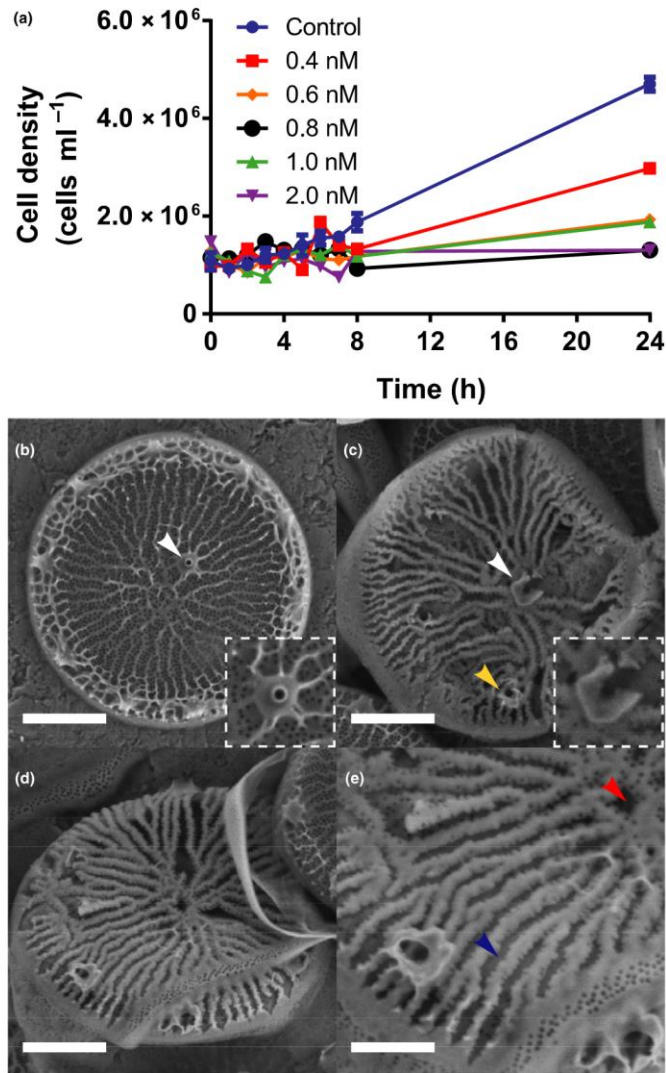


Fig. 9 Suboptimal V-type H⁺-ATPase (VHA) activity results in abnormal valve nanostructure. (a) Growth curves of *Thalassiosira pseudonana* cultures under various concanamycin A concentrations ($n = 2$; error bars are \pm SE). Valve nanostructure was examined by scanning electron microscopy after 22 h growth in control (b) or 0.4 nM concanamycin A (c–e) conditions. (b, c) Insets shows central portula at $\times 2$ magnification; white arrowheads, central portula; (c) yellow arrowhead, displaced fuloportula; (e) blue arrowhead, ribs lacking ridges; red arrowhead, unfilled nanopore base layer. Bars: 1 μ m (b–d); 0.5 μ m (e).

and not the silica itself. In addition, several *T. pseudonana* silicification proteins exhibit reversible aggregation as pH is decreased (Kotzsch *et al.*, 2016, 2017), suggesting that VHA-dependent acidification induces protein aggregation and organization inside the SDV, resulting in a subsequent change in SDV topology and expansion.

The halting of cell division by a high concanamycin A dose together with the presence of VHA_B-eGFP in multiple subcellular compartments unfortunately prevented the generation of

VHA gene knockouts as a result of lack of growth and potential unspecific effects on other physiological processes, respectively. As an alternative, we examined the effect of VHA pharmacological knockdown on valve morphology by growing synchronized *T. pseudonana* cultures in a partially inhibiting concanamycin A dose. These cells divided at *c.* 75% of the normal rate which yielded a mix of normal valves that were generated before the addition of concanamycin A, and newly formed valves with an abnormal morphology. While the ribs in the silica base layer had

relatively minor malformations, the nanopore network in the areas between the ribs was partially or entirely missing, and the portula and fuloportulae were deformed and occasionally displaced from their normal locations. These results suggest that a fully acidified SDV is more essential for maturation of the distal surface ridges above the ribs of the valves and porous base layer of nanopores. Interestingly, a SAP1 knockdown (Tesson *et al.*, 2017) and Sin1 knockout (Görllich *et al.*, 2019) also resulted in aberrant patterning deposition of the silica network in the distal valve surface, further supporting the link between VHA function and recruitment of SAP1-containing vesicles to the SDV.

Conclusion

This study confirms the decades-long hypotheses (Gordon & Drum, 1994) that VHA is the enzyme directly responsible for SDV acidification *in vivo*. It also identified that VHA activity regulates the trafficking and fusion of vesicles containing the structural protein SAP1 into the SDV, and revealed that frustule formation is a highly dynamic process that includes intimate interactions between SDVs and vacuoles. In addition to revealing those novel basic mechanistic aspects of diatom frustule biosynthesis, this study has identified interesting areas for future research. Is VHA activity important for the trafficking of other proteins to the SDV or biogenesis of the SDV? What is the function of VHA in the vacuole? What are the regulatory mechanisms behind differential VHA subcellular localization throughout the cell cycle? Can we take advantage of this information to manipulate VHA activity and nanoengineer frustules with specific porosity, silica nanosphere size and ornamentation?

The dominance of diatoms over other phytoplankton groups is presumed to be due, in part, to their ability to use silica as a substrate for growth. Compared with carbon, making cell walls out of silica provides energy savings (Raven, 1983), and silica cell walls have been proposed to act as a pH buffer to provide more CO₂ and promote photosynthesis (Milligan & Morel, 2002). Thus, understanding the mechanisms responsible for diatom silicification carries broader implications for understanding the role of diatoms in the global carbon cycle and primary production in the oceans.

Acknowledgements



The project described was supported by awards from the National Institute of Health Training Grant in Marine Biotechnology (T32GM067550) and the Edna Bailey Sussman Foundation to DPY, and the UCSD Frontiers of Innovation Scholars Program to MT. We would like to thank Dr Roshan Shrestha for providing plasmids and assisting with diatom cloning and transformations, Dr Raffaella Abbriano Burke for analysis of RNAseq data, and Dr Amro Hamdoun for providing advice on live cell imaging.

Author contributions

DPY, MH and MT designed research; DPY performed the research; DPY, MH and MT analyzed data and interpreted the

results; and DPY, MH and MT wrote the manuscript. MH and MT contributed equally to this work.

ORCID

Martin Tresguerres  <https://orcid.org/0000-0002-7090-9266>
Daniel P. Yee  <https://orcid.org/0000-0002-2085-5538>

References

- Abbriano BR. 2017. *Insights into the molecular regulation of growth and carbon flux in marine diatoms*, PhD thesis. San Diego, La Jolla, CA, USA: University of California.
- Bowman BJ, Bowman EJ. 2002. Mutations in subunit c of the vacuolar ATPase confer resistance to bafilomycin and identify a conserved antibiotic binding site. *Journal of Biological Chemistry* 277: 3965–3972.
- Bussard A, Lopez PJ. 2014. Evolution of vacuolar pyrophosphatases and vacuolar H⁺-ATPases in diatoms. *Journal of Marine Science and Technology* 22: 50–59.
- Dames P, Zimmermann B, Schmidt R, Rein J, Voss M, Schewe B, Walz B, Baumann O. 2006. cAMP regulates plasma membrane vacuolar-type H⁺-ATPase assembly and activity in blowfly salivary glands. *Proceedings of the National Academy of Sciences, USA* 103: 3926–3931.
- Darley WM, Volcani BE. 1969. Role of silicon in diatom metabolism: a silicon requirement for deoxyribonucleic acid synthesis in the diatom *Cylindrotheca fusiformis* Reimann and Lewin. *Experimental Cell and Research* 58: 334–342.
- Drose S, Altendorf K. 1997. Bafilomycins and concanamycins as inhibitors of V-ATPases and P-ATPases. *Journal of Experimental Biology* 8: 1–8.
- Drum RW, Pankratz HS. 1964. Post mitotic fine structure of *Gamphonema parvulum*. *Journal of Ultrastructure Research* 10: 217–223.
- Falkowski PG, Barber RT, Smetacek V. 1998. Biogeochemical controls and feedbacks on ocean primary production. *Science* 281: 200–207.
- Falkowski PG, Grzebyk D, Katz ME, Knoll AH, Quigg A, Raven JA, Schofield O, Taylor FJR. 2004. The evolution of modern eukaryotic phytoplankton. *Science* 305: 354–360.
- Field CB, Behrenfeld MJ, Randerson JT, Falkowski PG. 1998. Primary production of the biosphere: Integrating terrestrial and oceanic components. *Science* 281: 237–240.
- Forgac M. 2007. Vacuolar ATPases: rotary proton pumps in physiology and pathophysiology. *Nature Reviews Molecular Cell Biology* 8: 917–929.
- Gordon R, Drum RW. 1994. The chemical basis of diatom morphogenesis. *International Review of Cytology* 150: 243–372.
- Görllich S, Pawolski D, Zlotnikov I, Kröger N. 2019. Control of biosilica morphology and mechanical performance by the conserved diatom gene *Silicanin-1*. *Communications Biology* 2: 1–8.
- Herve V, Derr J, Quinet M, Moisan L, Lopez PJ. 2012. Multiparametric analyses reveal the pH-dependence of silicon biomineralization in diatoms. *PLoS ONE* 7: e46722.
- Hildebrand M. 2010. 3D imaging of diatoms with ion-abrasion electron microscopy. *Journal of Structural Biology* 166: 316–328.
- Hildebrand M, Frigeri LG, Davis AK. 2007. Synchronized growth of *Thalassiosira pseudonana* (Bacillariophyceae) provides novel insights into cell-wall synthesis processes in relation to the cell cycle. *Journal of Phycology* 740: 730–740.
- Hildebrand M, Lerch SJL, Shrestha RP. 2018. Understanding diatom cell wall silicification—moving forward. *Frontiers in Marine Science* 5: 1–19.
- Huss M, Ingenhorst G, Ko S, Gafel M, Dro S, Zeeck A, Altendorf K, Wiczorek H. 2002. Concanamycin A, the specific inhibitor of V-ATPases, binds to the V_o subunit c. *Journal of Biological Chemistry* 277: 40544–40548.
- Iler RK. 1979. *The chemistry of silica: solubility, polymerization, colloid and surface properties, and biochemistry*. New York, USA: Wiley-Interscience.
- Kawasaki-Nishi S, Nishi T, Forgac M. 2003. Proton translocation driven by ATP hydrolysis in V-ATPases. *FEBS Letters* 545: 76–85.
- Kluge C, Lahr J, Hanitzsch M, Bolte S, Gollmack D, Dietz K. 2003. New insight into the structure and regulation of the plant vacuolar H⁺-ATPase. *Journal of Bioenergetics and Biomembranes* 35: 377–388.

- Kotzsch A, Gröger P, Pawolowski D, Bomans PHH, Sommerdijk NAJM, Schlierf M, Kröger N. 2017. Silicanin-1 is a conserved diatom membrane protein involved in silica biomineralization. *BMC Biology* 15: 65.
- Kotzsch A, Pawolowski D, Milentyev A, Shevchenko A, Scheffel A, Poulsen N, Shevchenko A, Kröger N. 2016. Biochemical composition and assembly of biosilica-associated insoluble organic matrices from the diatom *Thalassiosira pseudonana*. *Journal of Biological Chemistry* 291: 4982–4997.
- Kröger N, Deutzmann R, Bergsdorf C, Sumper M. 2000. Species-specific polyamines from diatoms control silica morphology. *Proceedings of the National Academy of Sciences, USA* 97: 14133–14138.
- Kröger N, Deutzmann R, Sumper M. 1999. Polycationic peptides from diatom biosilica that direct silica nanosphere formation. *Science* 286: 1129–1132.
- Kröger N, Lorenz S, Brunner E, Sumper M. 2002. Self-assembly of highly phosphorylated silaffins and their function in biosilica morphogenesis. *Science* 298: 584–586.
- Maxson ME, Grinstein S. 2014. The vacuolar-type H⁺-ATPase at a glance – more than a proton pump. *Journal of Cell Science* 127: 4987–4993.
- Milligan AJ, Morel FMM. 2002. A proton buffering role for silica in diatoms. *Science* 297: 1848–1850.
- Nishi T, Forgac M. 2002. The vacuolar (H⁺)-ATPases — nature's most versatile proton pumps. *Nature Reviews Molecular Cell Biology* 3: 94–103.
- Pastor-Soler N, Beaulieu V, Litvin TN, Da Silva N, Chen Y, Brown D, Buck J, Levin LR, Breton S. 2003. Bicarbonate-regulated adenylyl cyclase (sAC) is a sensor that regulates pH-dependent V-ATPase recycling. *Journal of Biological Chemistry* 278: 49523–49529.
- Pickett-Heaps JD, Schmid AMM, Edgar LA. 1990. The cell biology of diatom valve formation. In: Round FE, Chapman DJ, eds. *Progress in phycological research*. Bristol, UK: Biopress Ltd, 1–168.
- Poulsen N, Chesley PM, Kröger N. 2006. Molecular genetic manipulation of the diatom *Thalassiosira pseudonana* (Bacillariophyceae). *Journal of Phycology* 42: 1059–1065.
- Poulsen N, Kröger N. 2004. Silica morphogenesis by alternative processing of silaffins in the diatom *Thalassiosira pseudonana*. *Journal of Biological Chemistry* 279: 42993–42999.
- Raven JA. 1983. The transport and function of silicon in plants. *Biological Reviews* 58: 179–207.
- Roa JN, Tresguerres M. 2016. Soluble adenylyl cyclase is an acid-base sensor in epithelial base-secreting cells. *American Journal of Physiology – Cell Physiology* 311: C340–C349.
- Romero-Calvo I, Ocón B, Martínez-Moya P, Suárez MD, Zarzuelo A, Martínez-Augustín O, de Medina FS. 2010. Reversible Ponceau staining as a loading control alternative to actin in Western blots. *Analytical Biochemistry* 401: 318–320.
- Roy JW, Hill E, Ruan YC, Vedovelli L, Paunescu TG, Brown D, Breton S. 2013. Circulating aldosterone induces the apical accumulation of the proton pumping V-ATPase and increases proton secretion in clear cells in the caput epididymis. *American Journal of Physiology – Cell Physiology* 305: CA36–CA46.
- Schindelin J, Arganda-carreras I, Frise E, Kaynig V, Longair M, Pietzsch T, Preibisch S, Rueden C, Saalfeld S, Schmid B et al. 2019. Fiji: an open-source platform for biological-image analysis. *Nature Methods* 9: 676–682.
- Schmid AMM, Schulz D. 1979. Wall morphogenesis in diatoms: Deposition of silica by cytoplasmic vesicles. *Protoplasma* 100: 267–288.
- Shimizu K, Del Amo Y, Brzezinski MA, Stucky GD, Morse DE. 2001. A novel fluorescent silica tracer for biological silicification studies. *Chemistry and Biology* 8: 1051–1060.
- Sumper M, Kröger N. 2004. Silica formation in diatoms: the function of long-chain polyamines and silaffins. *Journal of Materials Chemistry* 14: 2059–2065.
- Sze H, Schumacher K, Müller ML, Padmanaban S, Taiz L. 2002. A simple nomenclature for a complex proton pump: VHA genes encode the vacuolar H⁺-ATPase. *Trends in Plant Science* 7: 157–161.
- Sze H, Ward JM, Lai S. 1992. Vacuolar H⁺-translocating ATPases from plants: Structure, function, and isoforms. *Journal of Bioenergetics and Biomembranes* 24: 371–381.
- Tesson B, Hildebrand M. 2013. Characterization and localization of insoluble organic matrices associated with diatom cell walls: Insight into their roles during cell wall formation. *PLoS ONE* 8: e61675.
- Tesson B, Lerch SJL, Hildebrand M. 2017. Characterization of a new protein family associated with the silica deposition vesicle membrane enables genetic manipulation of diatom silica. *Scientific Reports* 7: 1–13.
- Tresguerres M. 2016. Novel and potential physiological roles of vacuolar-type H⁺-ATPase in marine organisms. *Journal of Experimental Biology* 219: 2088–2097.
- Tresguerres M, Parks SK, Salazar E, Levin LR, Goss GG, Buck J. 2010. Bicarbonate-sensing soluble adenylyl cyclase is an essential sensor for acid/base homeostasis. *Proceedings of the National Academy of Sciences, USA* 107: 442–447.
- Vartanian M, Desclés J, Quinet M, Douady S, Lopez PJ. 2009. Plasticity and robustness of pattern formation in the model diatom *Phaeodactylum tricorutum*. *New Phytologist* 182: 429–442.
- Volcani BE, Li CW. 1984. Aspects of silicification in wall morphogenesis of diatoms. *Philosophical Transactions of the Royal Society B: Biological Sciences* 304: 519–528.
- Vrieling EG, Gieskes WWC, Beelen TPM. 1999. Silicon deposition in diatoms: Control by the pH inside the silica deposition vesicle. *Journal of Phycology* 35: 548–559.
- Xiao Y-T, Xiang L-X, Shao J-Z. 2008. Vacuolar H⁺-ATPase. *International Journal of Biochemistry and Cell Biology* 40: 2002–2006.
- Yool A, Tyrrell T. 2003. Role of diatoms in regulating the ocean's silicon cycle. *Global Biogeochemical Cycles* 17: 1–21.

Supporting Information

Additional Supporting Information may be found online in the Supporting Information section at the end of the article.

Fig. S1 Representative images of exponentially growing *T. pseudonana* natively expressing VHA_B-eGFP.

Fig. S2 Western blots of VHA_B protein abundance in *T. pseudonana* cultures throughout the cell cycle along with corresponding Ponceau-stained blots.

Fig. S3 Representative images of cell cycle-synchronized *T. pseudonana* expressing fcp-VHA_B-eGFP incubated with 5 nM concanamycin A.

Fig. S4 Representative images of cell cycle-synchronized *T. pseudonana* expressing fcp-SAP1-eGFP $-/+$ 5 nM concanamycin A.

Fig. S5 Suboptimal VHA activity results in altered valve nanostructure, examined by SEM after 22 h growth in 0.4 nM concanamycin A conditions.

Video S1 Time-lapse imaging video of *T. pseudonana* expressing fcp-VHA_B-eGFP during valve biosynthesis (MP4 803 kb).

Video S2 Time-lapse imaging video of *T. pseudonana* expressing fcp-VHA_B-eGFP during girdle band biosynthesis (MP4 888 kb).

Please note: Wiley Blackwell are not responsible for the content or functionality of any Supporting Information supplied by the authors. Any queries (other than missing material) should be directed to the *New Phytologist* Central Office.

Article title: Dynamic subcellular translocation of V-type H⁺-ATPase is essential for biomineralization of the diatom silica cell wall

Authors: Daniel P. Yee, Mark Hildebrand, Martin Tresguerres

Article acceptance date: 4 November 2019

The following supporting information is available for this article:

Fig. S1 VHA localization in multiple subcellular compartments. Representative images of exponentially growing *T. pseudonana* natively expressing VHA_B-eGFP in **(a)** vacuole tonoplast and cytosol, **(b)** valve SDV and vacuole tonoplast, and **(c)** vacuole tonoplast and cytosol post cell division. Green: VHA_B-eGFP; red: chlorophyll; differential interference contrast. Scale bar: 5 μm.

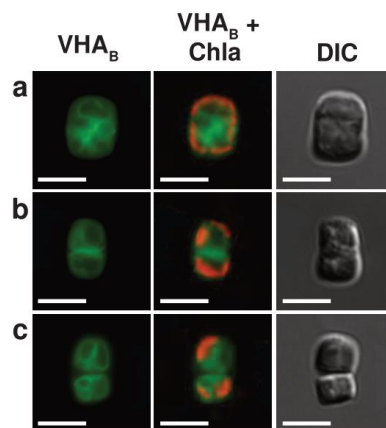


Fig. S2 VHA_B protein abundance in *T. pseudonana* cultures throughout the cell cycle. VHA_B protein abundance was quantified by Western blotting using a monoclonal VHA_B antibody in *T. pseudonana* cultures expressing fcp-VHA_B-eGFP at the indicated times following silicon re-addition. **(a-e)** Western blots of replicate cultures. The ~56 KDa band corresponds to native VHA_B; the ~89 KDa band corresponds to VHA_B-eGFP. **(f-j)** Ponceau stained blots confirmed equivalent total protein loaded per lane for each corresponding blot.

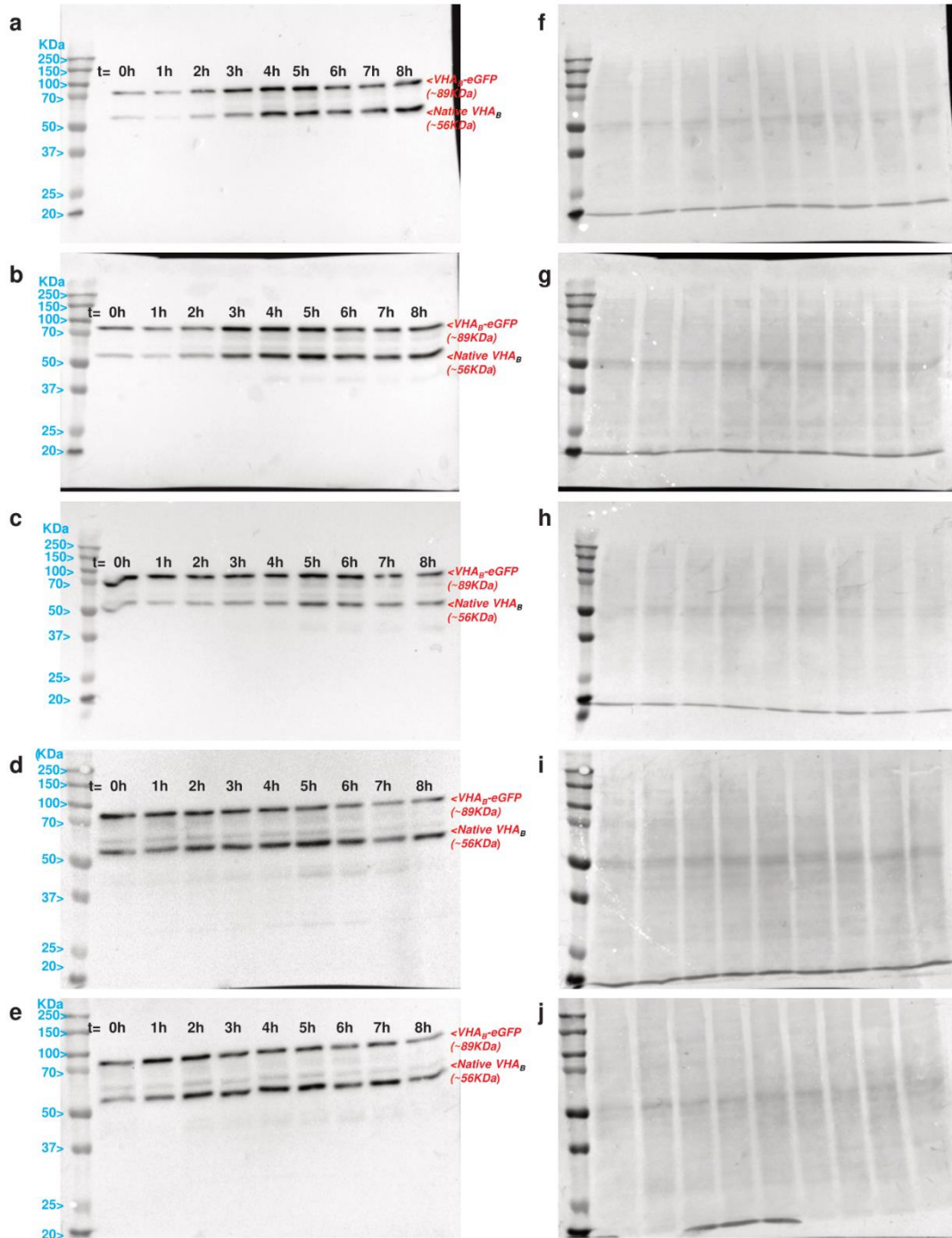
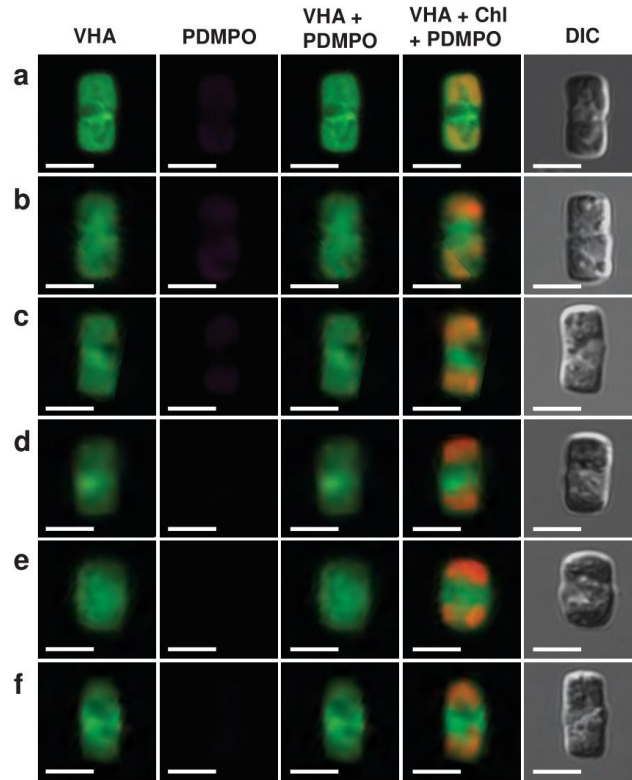


Fig. S3 Inhibition of VHA activity prevents SDV acidification and frustule formation (this figure expands on **Fig. 5**). **(a-f)** Representative images of cell cycle synchronized *T. pseudonana* expressing fcp-VHA_B-eGFP incubated with 5 nM concanamycin A. Green: VHA_B-eGFP; magenta: PDMPO; white: colocalization of VHA_B-eGFP and PDMPO; red: chlorophyll; differential interference contrast. Scale bar: 5 μm.



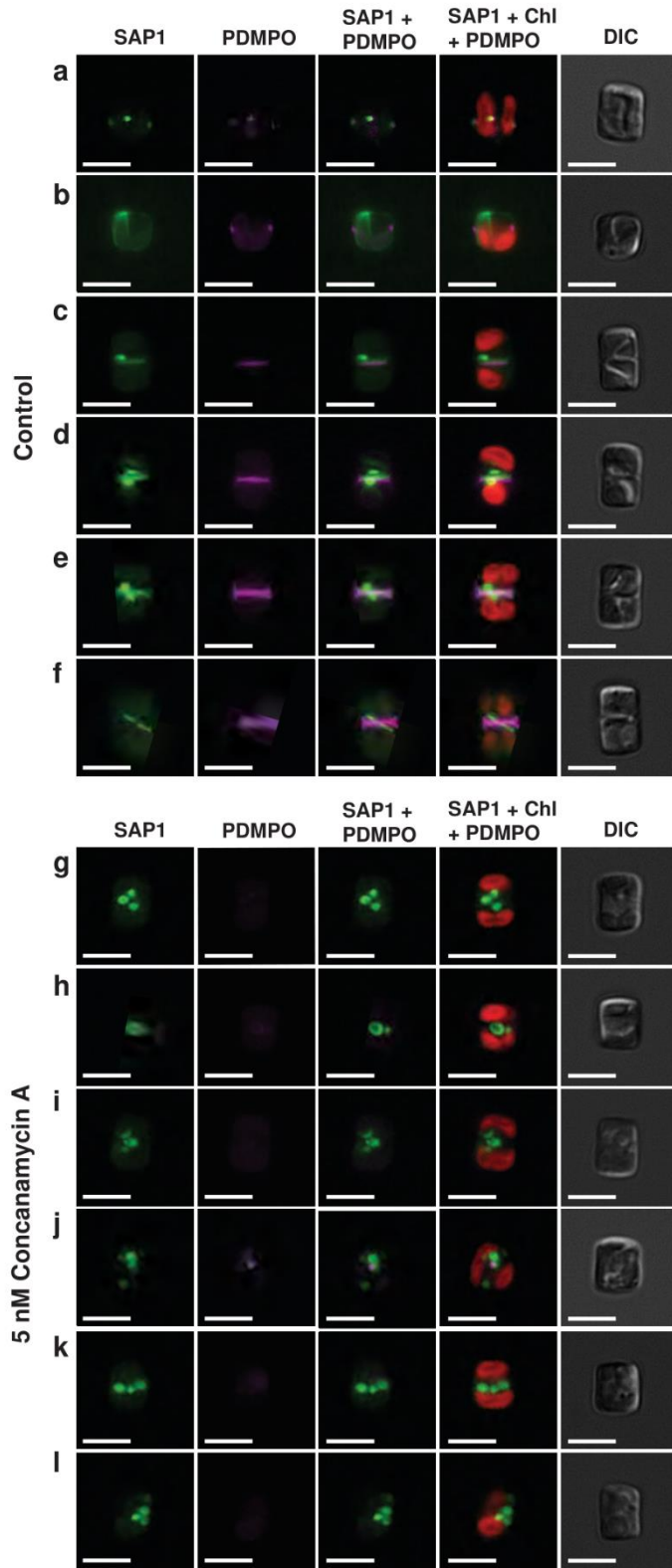
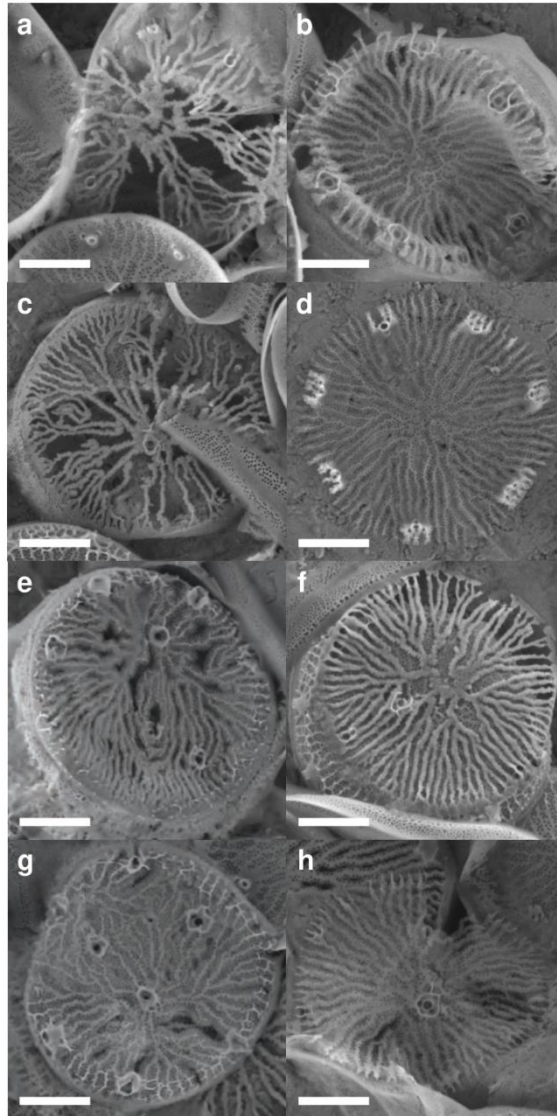


Fig. S4 Inhibition of VHA activity prevents insertion of SAP1 into the SDV (this figure expands on **Fig. 8**). Representative images of cell cycle synchronized *T. pseudonana* expressing fcp-SAP1-eGFP. **(a-f)** Control cells. **(g-l)** Cells incubated with 5 nM concanamycin A. Green: SAP1-eGFP; magenta: PDMPO; white: colocalization of SAP1-eGFP and PDMPO; red: chlorophyll; differential interference contrast. Scale bar: 5 μ m.

Fig. S5 (a-h) Suboptimal VHA activity results in a range of altered valve nanostructure, examined by SEM after 22h incubation with 0.4 nM concanamycin A conditions (this figure expands on **Fig. 9**). Scale bars: 1 μ m.



Video S1 Time-lapse imaging video of *T. pseudonana* expressing fcp-VHA_B-eGFP during valve biosynthesis [MP4 803 kb] (see separate file)

Video S2 Time-lapse imaging video of *T. pseudonana* expressing fcp-VHA_B-eGFP during girdle band biosynthesis [MP4 888 kb](see separate file)

Chapter 2, in full, is a reprint of the material as it appears in **Yee, D. P.**, Hildebrand, H., & Tresguerres, M. (2019). Dynamic subcellular translocation of V-type H⁺-ATPase is essential for diatom silica cell wall biomineralization. *New Phytologist*, 225.6, 2411-2422. The dissertation author was the primary investigator and author of this paper.

CHAPTER 3

Evolution of a V-type H⁺-ATPase-mediated carbon concentrating mechanism in secondary endosymbiotic phytoplankton

3.1 Abstract

The vast majority of contemporary marine eukaryotic phytoplankton species originated from a secondary endosymbiosis event with red algae, and as a result, their photosynthesizing plastids are surrounded by additional membranes derived from the ancestral phagocytic event. However, the physiological role and ecological advantage of these membranes remains largely unknown. Using fluorescent tagging and super-resolution confocal microscopy, we identified the conserved proton pumping enzyme V-type H⁺-ATPase (VHA) in the membranes surrounding the plastid of the marine diatom, *Thalassiosira pseudonana*. Analyses of O₂-production and ¹⁴C-fixation revealed that VHA activity was responsible for at least ~18% (and as much as 50%) of photosynthetic activity under the entire range of ecologically-relevant light intensities. Equivalent results in the diatom *Phaeodactylum tricornutum* and the coccolithophore *Emiliania huxleyi*, but not the green alga *Chlorella sp.* suggested VHA is part of a carbon concentrating mechanism (CCM) around plastids acquired by secondary endosymbiosis. Based on the estimated contribution of eukaryotic phytoplankton, this VHA-powered CCM is responsible for at least 10% of annual primary production on earth.

3.2 Introduction

Diatoms are some of the most efficient photosynthesizers on the planet and account for ~20% of earth's annual primary production (1, 2). Well known for their ornate silica shells, diatoms can form dense blooms in nutrient-rich upwelling regions of the ocean (3, 4) and outcompete other phytoplankton by readily adjusting to a wide range of environmental conditions, which allow them to achieve fast and stable growth rates (5, 6). Like many other phytoplankton, diatoms operate a robust carbon concentrating mechanism (CCM) to saturate ribulose-1,5-bisphosphate carboxylase/oxygenase (RuBisCO) with CO₂ and maintain high photosynthetic rates.

The diatom CCM consists of carbonic anhydrases (CAs) distributed to the plasmalemma, cytosol, mitochondria, and chloroplast (7–9), and solute carrier 4 (SLC4) HCO_3^- transporters in the plasmalemma (10). In conjunction, these proteins move dissolved inorganic carbon (DIC) from the surrounding water to the site of carbon fixation. However, the driving forces for this transport and the mechanisms that influence internal pH -which has a key effect on carbonate chemistry and therefore on the efficiency of a CCM, remain unknown (11).

Diatoms arose ~275 million years ago during an unprecedented CO_2 minimum in earth's atmosphere (12). The secondary endosymbiosis of a red alga by a eukaryotic host resulted in two additional membranes surrounding the original cyanobacterial ancestor: the periplastid membrane derived from the plasmalemma of the red algal symbiont, and the plastid endoplasmic reticulum (ER) derived from the phagosomal membrane of the heterotrophic host (13). More than two decades ago, it was hypothesized that these additional membranes and ensuing compartments would enable a proton pump to maintain an acidic environment around the plastid to concentrate CO_2 , thereby providing a selective advantage for success in a low CO_2 atmosphere (14). More recently, an equivalent CCM has been identified in contemporary photosymbiotic corals and giant clams, in which symbiotic algae are kept within a compartment acidified by the proton pump V-type H^+ -ATPase (VHA) (15, 16). Indeed, compartmentalization is a common strategy of symbioses that allows a host to control and mediate chemical exchange with the symbiont (17). Although plastids are fully integrated organelles of diatom cells, the physiological adaptations that persist to this day may help identify convergent strategies of evolution in aquatic photosymbioses. In this chapter, we investigate the role of pH regulation of the chloroplast by VHA and elucidate the evolution of photosynthesis in aquatic environments.

3.3 Results & Discussion

The VHA proton pump is a conserved protein complex that hydrolyzes ATP to transport H^+ ions across biological membranes against its electrochemical gradient. Consisting of a V_0 membrane domain and a V_1 cytosolic domain, the activity of VHA can be regulated through maintenance as a reversibly assembled holoenzyme, localization in different cellular membranes, and supply of ATP (18, 19). In the marine centric diatom *Thalassiosira pseudonana*, mRNA expression of various VHA subunits ranged from 150 to over 10,000 FPKMs in actively growing and stationary cells, showing VHA is constitutively expressed (Fig. S3.1). Using transgenic *T. pseudonana* expressing VHA subunit B tagged with enhanced green fluorescence protein, we recently showed that VHA dynamically translocates between the cytoplasm, vacuoles, and the silica deposition vesicle (SDV) where it lowers pH and promotes silica biomineralization (20). Here, we report that VHA is also localized in the membranes surrounding the chloroplast of *T. pseudonana* (Fig. 3.1). Co-localization of VHA around the chloroplast marked with the acidotropic fluorescent dye PDMPO (21) suggests an acidification of the plastid microenvironment to \leq pH 5.5. At this pH, the majority of dissolved inorganic carbon (DIC) exists as CO_2 which would help satisfy a CCM for photosynthesis.

Similar to corals (15) and giant clams (16), pharmacological inhibition of VHA activity resulted in a significant decrease in photosynthetic O_2 production in *T. pseudonana* (Fig. 3.2). To determine if this mechanism is conserved in other phytoplankton we also tested VHA inhibition on photosynthetic O_2 production in the pennate diatom *Phaeodactylum tricornutum*, coccolithophore *Emiliana huxleyi*, and green alga *Chlorella sp.* Three-day averages of gross oxygen production rates under control and concanamycin A treatments were calculated for each organism (Fig. 3.2A). We found that VHA enhanced oxygen production by an average of ~20, 16,

and 39% in *T. pseudonana*, *P. tricornutum*, and *E. huxleyi*, respectively, but had no effect in *Chlorella* (Fig. 3.2B). The latter species did not undergo a secondary endosymbiotic event, and therefore its plastids are not surrounded by additional phagocytic membranes present in diatoms and coccolithophores. Statistical significance of results were analyzed (Table S3.1), while culture conditions from this experiment are described in Fig. S3.2 captions.

Overall, this result indicates VHA plays a conserved role in the CCM of a broad range of taxa. Because *Chlorella* was unaffected by VHA inhibition, we postulate that the presence of the third and fourth plastid membranes are required for this mechanism to take place. In addition to creating a compartment to trap acid and CO₂, the phagosomal origins of these membranes establish an evolutionary blueprint for possessing VHA (14). This is further supported by VHA playing a role in the CCM of photosymbiotic algae in corals and giant clams (15, 16). In these contemporary tertiary endosymbioses, the host derived symbiosome membrane is synonymous to the phagosomal membranes of the ancestral hosts of secondary endosymbionts and provides evidence for a convergent evolutionary strategy in aquatic photosynthesis.

To confirm the role of VHA in promoting carbon fixation and not just O₂ production, we generated photosynthesis versus irradiance (P-E) curves *via* incubations of *T. pseudonana* with ¹⁴C-Na₂CO₃ in the presence or absence of VHA inhibitor. To mimic the range of environmental conditions found in nature, we tested irradiances ranging from 0 to ~1800 μmols photons m⁻² sec⁻¹, used culture media with different DIC and micronutrient conditions, and introduced DIC shifts away from ambient culture conditions to measure the response of VHA activity. In order to capture the various cell cycle stages and associated physiological statuses that occur during pre-blooming, blooming, and post-blooming periods, these incubations were performed over three consecutive days of culturing (Fig. S3.3-4). Curve fitting parameters were analyzed for statistical significance

difference between control and concanamycin A treatments (Table S3.2), while culture conditions for this experiment are described in Fig. S3.5 captions.

A reduction in photosynthetic carbon fixation was measured in all conditions treated with concanamycin A, accounting on average for 23% of the total rate. Maximal photosynthetic rates varied over the three days of sampling reflecting changes in metabolic activity and DIC content of the media. Overall, P-E curves indicate *T. pseudonana* experiences little to no photoinhibition at high light, likely due to a robust xanthophyll cycle (22). Reductions in photosynthetic rate by VHA inhibition appeared to change in response to irradiance, suggesting VHA activity is sensitive to photosynthetic output. Analysis of P-E curves from FSW control treatments under ambient DIC showed an increase in cellular photosynthetic rates from day 1 to 2, and smaller increases at sub-saturating irradiance levels between days 2 to 3 (Fig. S3.6A). In ASW medium, overall rates decreased over the three days correlating with decreasing DIC levels in the media (Fig. S3.6B). Despite the limitation of DIC in ASW, growth was similar between media (Fig. S3.5). To better reflect the contribution of the CCM to photosynthesis, we recalculated these rates as a ratio to the DIC in the media and see that photosynthesis performed more efficiently under the most limiting DIC concentrations on day 3 compared to days 1-2 (Fig S3.6C-D), indicating a highly active CCM.

For cells in FSW under ambient DIC, VHA contributed between ~14-20%, 14-21%, and 32-38% of photosynthesis across the range of irradiances on days 1-3, respectively (Fig. 3.3A-C). When the same cells were exposed to lower DIC, there was an increase in VHA contribution to photosynthesis at sub-saturating irradiances up to 35%, 38%, and 52% on days 1-3, respectively. However, VHA contribution to photosynthesis decreased at higher irradiances, beginning at ~550 $\mu\text{mol photons m}^{-2} \text{ sec}^{-1}$ on days 1-2, and ~300 $\mu\text{mol photons m}^{-2} \text{ sec}^{-1}$ on day 3 compared to FSW with ambient DIC. This reduction in VHA contribution at higher irradiance may reflect a

point at which the energetic cost of VHA become detrimental. In ASW where DIC is naturally low, VHA contribution ranged from ~6-15% at sub-saturating irradiances and averaged ~10% at saturating irradiances across all days (Fig. 3.3D-F). When additional DIC was supplemented, VHA contribution to photosynthesis also increased to ~33-40% over the three days at sub-saturating irradiances, indicating an upregulation of the VHA activity for the CCM.

For measurements in ASW and FSW under ambient DIC levels, there is less variability in VHA contribution to photosynthesis in response to irradiance (Fig. 3.3, black curves). However, modifying DIC resulted in dynamic shifts in VHA activity between low and high irradiances (Fig. 3.3, red curves). Interestingly, there were large increases in VHA activity at sub-saturating irradiances ($<500 \mu\text{mol photons m}^{-2} \text{sec}^{-1}$) which better represents the light environment diatoms experience during blooms (23). Phytoplankton experience fluctuations in light as they migrate throughout the water column and it appears diatoms can modulate VHA activity to optimize photosynthesis in a dynamic light environment. Overall, these results not only confirm that VHA enhances photosynthesis by contributing to the CCM of *T. pseudonana*, but also demonstrate how diatoms modulate photosynthetic efficiency relative to energetic demand, irradiance, and DIC in the environment.

3.4 Conclusion

In addition to a silica shell and an active xanthophyll cycle for dealing with light stress (24), the operation of a steady and efficient CCM contributes to the competitive success of diatoms. The abiotic conditions that diatoms experience in nature are in constant flux, with light and DIC being the substrates most important to photosynthesis. For phytoplankton living in a low CO_2 atmosphere such as today, a more compartmentalized chloroplast enables cells to better optimize the conditions for photosynthesis irrespective of extracellular conditions. Given that VHA is

constitutively expressed throughout the cell cycle and is able to dynamically translocate in diatom cells (20), makes it well-suited to responding rapidly to environmental fluctuations and efficiently maintain high photosynthetic rates.

Previous research has led to the development of model involving carbonic anhydrase and SLC4 bicarbonate transporters for the diatom CCM. In *T. pseudonana* carbonic anhydrases have been localized to the surface of the plasmalemma, cytosol, mitochondria, and chloroplast (7). Meanwhile in *P. tricornutum*, SLC4 bicarbonate transporters have been targeted to the plasmalemma (10), as well as chloroplast membranes (unpublished data referenced in (25)). Our results support the inclusion of VHA in this model which would further enhance the efficiency of the CCM. In the case for diatoms and coccolithophores, acidification of the lumen of the chloroplast ER and periplastid membranes would shift the equilibrium of imported HCO_3^- towards CO_2 and facilitate diffusion in towards the RuBisCO rich pyrenoid (Fig. 3.4). Additionally, VHA may also serve a dual role in providing the proton motive force to energize SLC4 transporters which are sodium dependent (11). Our results from identifying VHA in the role of the CCM also corroborates evidence showing VHA inhibition led to reduction in lipid accumulation in *P. tricornutum* which may have resulted from reduced photosynthetic production (26).

Our study provides conclusive evidence that VHA participates in the CCM of diatoms and can enhance photosynthesis between ~18-50%. Given that diatoms account for a fifth of the earth's primary production, we estimate that VHA activity is responsible for up to 10% of global photosynthesis. We also show that VHA enhances photosynthesis in coccolithophores, but not chlorophytes. Along with similar studies in photosymbioses of dinoflagellates with cnidarians and mollusks (15, 16), these results suggest an evolutionarily conserved VHA-dependent mechanism to enhance photosynthetic rate in photosymbiotic associations with phytoplankton from red algal

origins. Further experiments should continue to assess this mechanism in other aquatic photoautotrophs to elucidate the evolutionary underpinnings and assess the full contributions of VHA to global primary production.

3.5 Methods

Culturing and Growth Conditions

Cultures of *T. pseudonana* (CCMP1335) expressing VHA_B-eGFP were grown axenically in ASW medium (27) supplemented with 1 mM Na₂SiO₃ or with filtered seawater (FSW) from the Scripps Pier supplemented with F/2 nutrients (28), while cultures of *P. tricornutum*, *E. huxleyi*, and *Chlorella* were maintained in FSW only. Inoculum cultures were maintained in 50 ml volumes in 125 mL Erlenmeyer flasks on an orbital shaker under continuous illumination by cool-white fluorescent lamps at 70 $\mu\text{mol photons m}^{-2} \text{ s}^{-1}$ at 18°C. Inoculum grown to $\sim 2 \times 10^6$ cells ml⁻¹ were used to inoculate 1 liter bioreactor tubes bubbled with air and under continuous illumination by cool-white fluorescent lamps at ~ 100 $\mu\text{mol photons m}^{-2} \text{ s}^{-1}$ at 18°C at 1×10^5 cells ml⁻¹.

Daily measurements including cell counts, chlorophyll content, pH, and total CO₂ (TCO₂) were collected over the duration of all culturing experiments, and were used to calculate cellular chlorophyll content, specific growth rates, and carbonate chemistry. Cell counts were obtained on a Neubauer hemacytometer chamber in combination with a Zeiss light microscope. Chlorophyll was measured on a Turner fluorometer following overnight extraction in 100% methanol at -20°C. Relative fluorescence units was recorded before and after the addition of two drops 0.1 N HCl. and total chlorophyll was calculated by the method described in Holm-Hansen *et al.* (29).

Culture pH was measured using an UltraBASIC pH meter (Denver Instruments) equipped with an Orion glass pH electrode (ThermoFisher Scientific) calibrated with NBS standard buffer.

Total CO₂ was measured using a Corning 965 Carbon Dioxide Analyzer with technical duplicates taken in between measurements of 10 mM Na₂CO₃ standards. Dissolved inorganic carbon (DIC) species in the cultures was calculated using CO2Sys_v2.1 (30) after inputting salinity, temperature, pH and TCO₂ values.

Transgenic diatoms expressing fluorescently labeled VHA_B

VHA subunit B labelled with eGFP was expressed under the control of the *fcp* promoter. For Thaps3_40522 (VHA_B) the full-length coding sequence of the gene was amplified from *T. pseudonana* genomic DNA, and cloned into Gateway destination vector pMHL_79 with eGFP at the end of the coding sequence. The final vector was co-transformed with a pMHL_09 expressing the *nat1* gene which confers nourseothricin resistance by biolistic gene gun method (31). Liquid cultures grown in ASW medium containing 100 µg/ml nourseothricin were enriched for cells expressing eGFP using several rounds of fluorescence-activated cell sorting on a BD Influx Cell Sorter (BD Biosciences), from which single colonies expressing eGFP were selected for on ASW agar plates containing nourseothricin.

Transcriptomics

The VHA mRNA expression levels Fragments Per Kilobase Million (FPKM) was acquired from transcriptomics analysis of RNAseq data collected from time-course experiments through silicon starvation and following silicon replenishment from biological duplicates of synchronized *T. pseudonana* cultures (32). Raw reads from individual samples were demultiplexed based on a perfect barcode match, and TopHat (v2.0.6) running Bowtie 2 (version 2.0.2) was used for strand-specific mapping of RNAseq reads to the *T. pseudonana* reference genome assembly (Thaps3) obtained from the Joint Genome Institute (JGI):

(<http://genome.jgi.doe.gov/Thaps3/Thaps3.download.ftp.html>). Cufflinks (v.2.2.1) was used to assemble transcripts, and the assembly was used for AUGUSTUS gene model prediction. Raw counts to AUGUSTUS generated gene models were generated using htseq-count (HTSeq 0.6.1p1). Normalized counted and differential expression analysis was done using the DESeq2_1.6.3 package.

Fluorescence microscopy

Super-resolution confocal microscopy was used for *T. pseudonana* expressing VHA_B-eGFP were stained with the acidotropic pH stain 2-(4-pyridyl)-5-((4-(2-dimethylaminoethylaminocarbonyl)methoxy)phenyl)oxazole (PDMPO); LysoSensor YellowBlue DND-160 (Life Technologies) at a final concentration of 0.125 μ M. Cells were then transferred to a 35 mm poly-d-lysine coated glass bottom petri dish and mounted on a Warner Instruments QE-1HC Quick Exchange Heated/Cooled stage chamber controlled by CL-200 Dual Channel Temperature Controller maintained at 18 °C. Cells were imaged with a Zeiss LSM800 inverted confocal microscope equipped with a Zeiss Plan-Apochromat 63 \times (1.4) Oil DIC M27 objective, and Zeiss Airyscan super-resolution detector. Z-stacks of three channels were acquired to monitor eGFP (Ex 488 nm with 0.3% laser power, Em 509 nm, and detection 490-535 nm), PDMPO (Ex 335 nm at 0.5% laser power, Em 530 nm, detection 550-650 nm), and chlorophyll (Ex 488 nm with 0.2% laser power, Em 667 nm, detection 450-700 nm) fluorescence.

¹⁴C photosynthesis versus irradiance (P-E) curves

Photosynthesis-irradiance (P-E) curves were generated by incubating cells in a modified ¹⁴C bicarbonate incorporation technique by Lewis & Smith (1983). For FSW, lower DIC concentrations were reached by adding HCl and bubbling off CO₂ with air, while for ASW, higher levels of DIC was reached by supplemental Na₂CO₃ addition. P-E incubations were carried out at

18°C and at 18 irradiances ranging from 0 to 1804 $\mu\text{mol photons m}^{-2} \text{sec}^{-1}$ illuminated by a 150W tungsten-halogen lamp. Total photosynthetically available radiation (PAR, 400-700 nm) was measured in each chamber with a Spherical Micro Quantum Sensor US-SQS (Heinz Walz, GmbH). For each P-E curve, 100 μl of a 1 mCi $^{14}\text{C Na}_2\text{CO}_3$ (Perkin-Elmer) solution was added to 25 mL of diatom culture at a final concentration of 4 $\mu\text{Ci ml}^{-1}$. Spiked culture was aliquoted in 1 ml volumes into 21 pre-chilled 7 ml borosilicate glass scintillation vials. Eighteen of these vials were illuminated for 1 hour in the P-E incubator while three remaining vials were immediately acidified with 150 μl of 12N HCl to drive off inorganic carbon and determine background activity for time-zero (T0) samples. Three total radioactivity (TA) samples were generated by combining 50 μL of spiked culture with 200 μL of phenylethylamine (source) topped off with 5 mL of Ecolite(+) scintillation cocktail (MP Biomedicals) and capped immediately. Incubations were terminated after 1 hour by switching off the lamps and adding 150 μl of 12N HCl to each vial. All acidified samples were allowed to drive off inorganic carbon overnight in a fume hood and topped off with 5 mL of Ecolite(+) and capped the next day for counting radioactivity on a Beckman Coulter LS6500 liquid scintillation counter.

Carbon productivity rates were calculated from disintegrations per minute (DPM) by the equation:

$$\text{Production (mg C l}^{-1} \text{ hr}^{-1}) = (\text{DPM}_{\text{sample}} / \text{Vol}_{\text{sample}}) * (\text{W} * \text{Vol}_{\text{TA}} / \text{DPM}_{\text{TA}}) * (1.05 / \text{T}),$$

where $\text{DPM}_{\text{sample}}$ is the T0 corrected activity per sample, $\text{Vol}_{\text{sample}}$ is volume of culture per sample, W is the DIC concentration of the culture, Vol_{TA} is volume of culture in TA samples, DPM_{TA} is the activity per TA sample, 1.05 is the discrimination factor for lower uptake of ^{14}C compared to ^{12}C , and T is the time duration of the incubations. The resulting P-E curves were parameterized and fit with the equations by Platt et al. (1980) using the Phytotools R-package.

Photosynthetic oxygen measurements

Oxygen production was measured on a Hansatech Oxy-lab Clark-type oxygen electrode operated with O2view software (Hansatech Instruments) to control illumination with a red LED and stirring within the water-jacketed chamber maintained at 18°C. Net oxygen production was measured by calculating the slope of oxygen concentration over 10 minutes of illumination with 1000 $\mu\text{mol photons m}^{-2} \text{sec}^{-1}$, and respiration was measured for over 1 minute post-illumination. Gross oxygen production rate was calculated by the equation:

$$\text{O}_{2\text{gross}} = \text{O}_{2\text{net}} - \text{respiration}$$

Statistics

For oxygen measurements, paired t-test were carried out between control and concanamycin A treatments for each species (Fig. 2A), and one sample t-tests were carried out for % contribution of VHA for each species (Fig. 2B). P-values showing statistical differences are summarized in Table 3.1.

For P-E curves, paired t-test were carried out on parameterized values of P_{max} (photosynthesis maximum), α (initial slope), and E_k (saturation irradiance) between control and concanamycin A treatments for all media and DIC conditions. P-values showing statistical differences are summarized in Table 3.2.

3.6 References

1. C. B. Field, M. J. Behrenfeld, J. T. Randerson, P. G. Falkowski, Primary production of the biosphere: Integrating terrestrial and oceanic components. *Science* (80-.). **281**, 237–240 (1998).
2. D. M. Nelson, P. Tréguer, M. A. Brzezinski, A. Leynaert, B. Quéguiner, Production and dissolution of biogenic silica in the ocean: Revised global estimates, comparison with regional data and relationship to biogenic sedimentation. *Global Biogeochem. Cycles*. **9**, 359–372 (1995).
3. K. R. Arrigo, D. K. Perovich, R. S. Pickart, Z. W. Brown, G. L. Van Dijken, K. E. Lowry,

- M. M. Mills, M. A. Palmer, W. M. Balch, F. Bahr, N. R. Bates, C. Benitez-Nelson, B. Bowler, E. Brownlee, J. K. Ehn, K. E. Frey, R. Garley, S. R. Laney, L. Lubelczyk, J. Mathis, A. Matsuoka, B. G. Mitchell, G. W. K. Moore, E. Ortega-Retuerta, S. Pal, C. M. Polashenski, R. A. Reynolds, B. Schieber, H. M. Sosik, M. Stephens, J. H. Swift, Massive phytoplankton blooms under arctic sea ice. *Science* (80-.). **336**, 1408 (2012).
4. C. Lancelot, E. Hannon, S. Becquevort, C. Veth, H. J. W. De Baar, Modeling phytoplankton blooms and carbon export production in the Southern Ocean: Dominant controls by light and iron in the Atlantic sector in Austral spring 1992. *Deep. Res. Part I Oceanogr. Res. Pap.* **47**, 1621–1662 (2000).
 5. P. Boelen, W. H. van de Poll, H. J. van der Strate, I. A. Neven, J. Beardall, A. G. J. Buma, Neither elevated nor reduced CO₂ affects the photophysiological performance of the marine Antarctic diatom *Chaetoceros brevis*. *J. Exp. Mar. Bio. Ecol.* **406**, 38–45 (2011).
 6. J. N. Young, S. A. Kranz, J. A. L. Goldman, P. D. Tortell, F. M. M. Morel, Antarctic phytoplankton down-regulate their carbon-concentrating mechanisms under high CO₂ with no change in growth rates. *Mar. Ecol. Prog. Ser.* **532**, 13–28 (2015).
 7. M. Samukawa, C. Shen, B. M. Hopkinson, Y. Matsuda, Localization of putative carbonic anhydrases in the marine diatom, *Thalassiosira pseudonana*. *Photosynth. Res.* **121**, 235–249 (2014).
 8. S. Kikutani, K. Nakajima, C. Nagasato, Y. Tsuji, A. Miyatake, Y. Matsuda, Thylakoid luminal θ -carbonic anhydrase critical for growth and photosynthesis in the marine diatom *Phaeodactylum tricorutum*. *Proc. Natl. Acad. Sci.* **113**, 9828–9833 (2016).
 9. M. Tachibana, A. E. Allen, S. Kikutani, Y. Endo, C. Bowler, Y. Matsuda, Localization of putative carbonic anhydrases in two marine diatoms, *Phaeodactylum tricorutum* and *Thalassiosira pseudonana*. *Photosynth. Res.* **109**, 205–221 (2011).
 10. K. Nakajima, A. Tanaka, Y. Matsuda, SLC4 family transporters in a marine diatom directly pump bicarbonate from seawater. *Proc. Natl. Acad. Sci. U. S. A.* **110**, 1767–72 (2013).
 11. Y. Matsuda, B. M. Hopkinson, K. Nakajima, C. L. Dupont, Y. Tsuji, Mechanisms of carbon dioxide acquisition and CO₂ sensing in marine diatoms: A gateway to carbon metabolism. *Philos. Trans. R. Soc. B Biol. Sci.* **372** (2017), doi:10.1098/rstb.2016.0403.
 12. R. A. Berner, Z. Kothavala, Geocarb III: A revised model of atmospheric CO₂ over phanerozoic time. *Am. J. Sci.* **301**, 182–204 (2001).
 13. P. J. Keeling, Diversity and evolutionary history of plastids and their hosts. *Am. J. Bot.* **91**, 1481–1493 (2004).
 14. R. Lee Edward, P. Kugrens, Hypothesis: The ecological advantage of chloroplast ER - The ability to outcompete at low dissolved CO₂ concentrations. *Protist.* **149**, 341–345 (1998).
 15. K. L. Barott, A. A. Venn, S. O. Perez, S. Tambutté, M. Tresguerres, Coral host cells acidify

- symbiotic algal microenvironment to promote photosynthesis. *Proc. Natl. Acad. Sci.* **112**, 607–612 (2015).
16. E. J. Armstrong, J. N. Roa, J. H. Stillman, M. Tresguerres, Symbiont photosynthesis in giant clams is promoted by V-type H⁺ -ATPase from host cells. *J. Exp. Biol.* **221** (2018), doi:10.1242/jeb.177220.
 17. G. Chomicki, G. D. A. Werner, S. A. West, E. T. Kiers, Compartmentalization drives the evolution of symbiotic cooperation. *Philos. Trans. R. Soc. B Biol. Sci.* **375** (2020), doi:10.1098/rstb.2019.0602rstb20190602.
 18. M. Forgac, Vacuolar ATPases: Rotary proton pumps in physiology and pathophysiology. *Nat. Rev. Mol. Cell Biol.* **8**, 917–929 (2007).
 19. M. Tresguerres, Novel and potential physiological roles of vacuolar-type H⁺ -ATPase in marine organisms. *J. Exp. Biol.* **219**, 2088–2097 (2016).
 20. D. P. Yee, M. Hildebrand, M. Tresguerres, Dynamic subcellular translocation of V-type H⁺ -ATPase is essential for biomineralization of the diatom silica cell wall. *New Phytol.* **225**, 2411–2422 (2019).
 21. Z. Diwu, C. S. Chen, C. Zhang, D. H. Klaubert, R. P. Haugland, A novel acidotropic pH indicator and its potential application in labeling acidic organelles of live cells. *Chem. Biol.* **6**, 411–418 (1999).
 22. H. P. Dong, Y. L. Dong, L. Cui, S. Balamurugan, J. Gao, S. H. Lu, T. Jiang, High light stress triggers distinct proteomic responses in the marine diatom *Thalassiosira pseudonana*. *BMC Genomics.* **17**, 1–14 (2016).
 23. L. J. Hoffman, I. Peeken, K. Lochte, Iron, silicate, and light co-limitation of three Southern Ocean diatom species. *Polar Biol.* **31**, 1067–1080 (2008).
 24. C. Dimier, F. Corato, F. Tramontano, C. Brunet, Photoprotection and xanthophyll-cycle activity in three marine diatoms. *J. Phycol.* **43**, 937–947 (2007).
 25. B. M. Hopkinson, C. L. Dupont, Y. Matsuda, The physiology and genetics of CO₂ concentrating mechanisms in model diatoms. *Curr. Opin. Plant Biol.* **31**, 51–57 (2016).
 26. H. Zhang, R. Zeng, D. Chen, J. Liu, A pivotal role of vacuolar H⁺-ATPase in regulation of lipid production in *Phaeodactylum tricornutum*. *Sci. Rep.* **6**, 31319 (2016).
 27. W. M. Darley, B. E. Volcani, Role of silicon in diatom metabolism: a silicon requirement for deoxyribonucleic acid synthesis in the diatom *Cylindrotheca fusiformis* Reimann and Lewin. *Exp. Cell Res.* **58**, 334–342 (1969).
 28. R. R. L. Guillard, in *Culture of Marine Invertebrate Animals*, W. L. Smith, M. H. Chanley, Eds. (Springer, Boston, 1975; https://doi.org/10.1007/978-1-4615-8714-9_3), pp. 29–60.

29. O. Holm-Hansen, C. J. Lorenzen, R. W. Holmes, J. D. H. Strickland, Fluorometric determination of chlorophyll. *ICES J. Mar. Sci.* **30**, 3–15 (1965).
30. E. Lewis, D. Wallace, Program Developed for CO₂ System Calculations ORNL/CDIAC-105, Carbon Dioxide Information Analysis Centre, (1998), pp. 1–29.
31. N. Poulsen, P. M. Chesley, N. Kröger, Molecular genetic manipulation of the diatom *Thalassiosira pseudonana* (Bacillariophyceae). *J. Phycol.* **42**, 1059–1065 (2006).
32. R. Abbriano Burke, Insights into the molecular regulation of growth and carbon flux in marine diatoms. *thesis, Univ. California, San Diego* (2017) (available at <https://escholarship.org/uc/item/5c152112>).
33. M. Lewis, J. Smith, A small volume, short-incubation-time method for measurement of photosynthesis as a function of incident irradiance. *Mar. Ecol. Prog. Ser.* **13**, 99–102 (1983).
34. T. Platt, C. L. Gallegos, W. G. Harrison, Photoinhibition of Photosynthesis in Natural Assemblages of Marine Phytoplankton. *J. Mar. Res.* **38** (1980), pp. 687–701.

Chapter 3 Figures

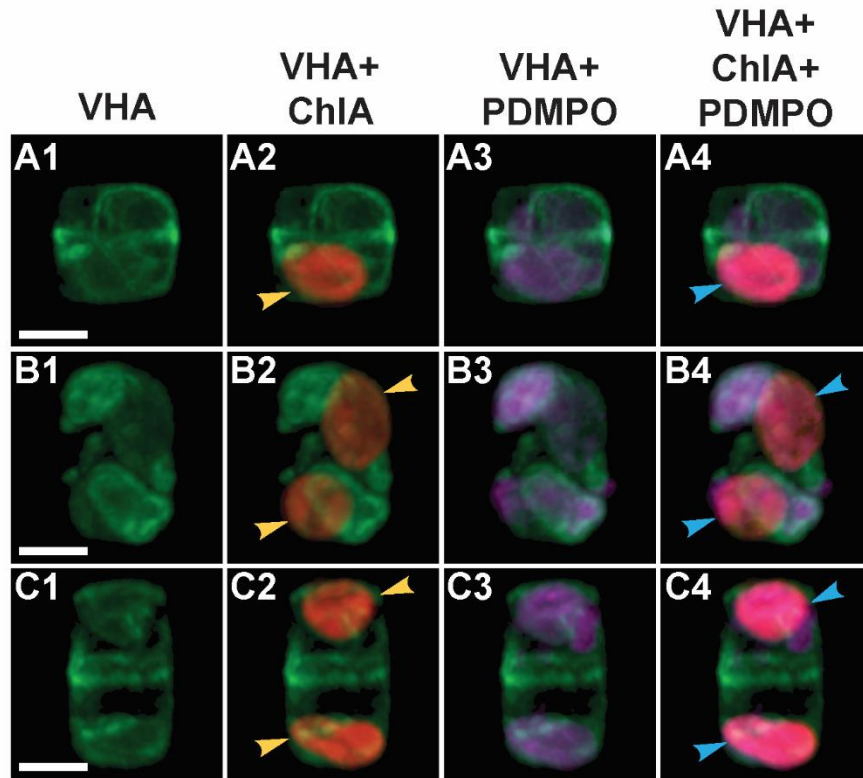


Fig. 3.1 Super-resolution confocal 3-D projections of *T. pseudonana* expressing VHA_B tagged with eGFP. The presence of VHA is detected in the membranes surrounding the chloroplasts (yellow arrow), accumulation of PDMPO within the chloroplasts suggest an acidification of $\text{pH} \leq 5.5$ (blue arrows) at several cell stages (A-C). Green: VHA_B-eGFP; red: chlorophyll; magenta: PDMPO; pink: co-localization of chlorophyll and PDMPO. Scale bar: 5 μm .

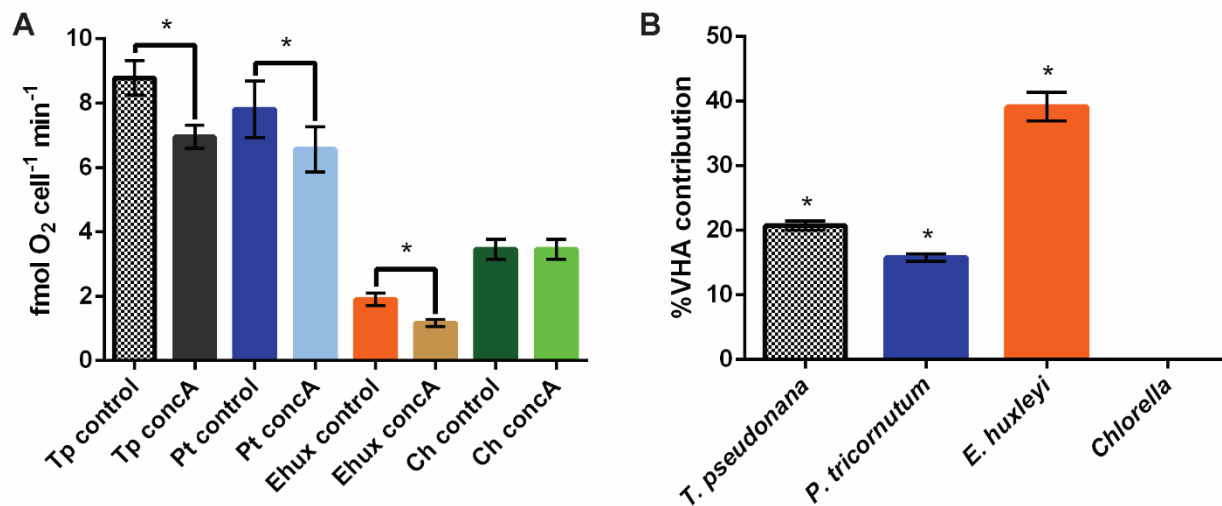


Fig. 3.2 (A) Three averages of cellular oxygen evolution rates in *T. pseudonana*, *P. tricornutum*, *Chlorella* sp., and *E. huxleyi*. Inhibition of VHA was carried out by addition of 10 nM concanamycin A, control treatments contained equivalent amounts of DMSO (1 μ L/mL). (B) Average calculated contribution of VHA to photosynthesis in for each species. (Error bars = SEM; n = 3; asterisk denotes statistical significance).

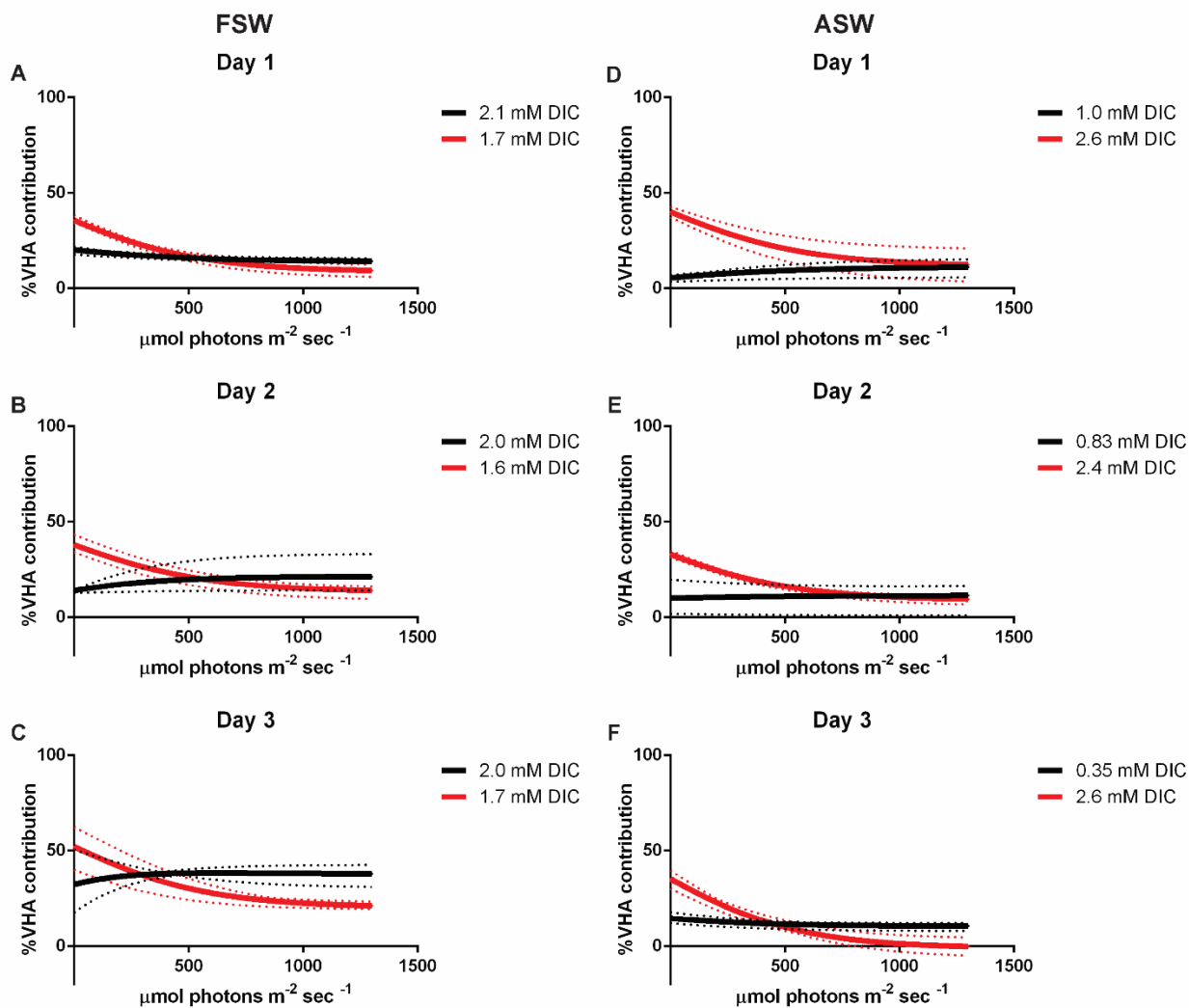


Fig. 3.3 Average calculated contributions of VHA to cellular carbon fixation rates in *T. pseudonana* up to 1300 $\mu\text{mol photons m}^{-2} \text{sec}^{-1}$. Black lines represent measurements carried out under ambient DIC, and red lines represent measurements carried out under modified DIC in FSW or ASW media (n=3, except for ASW Day 1- 2.6 mM DIC where n=2; dotted lines= range).

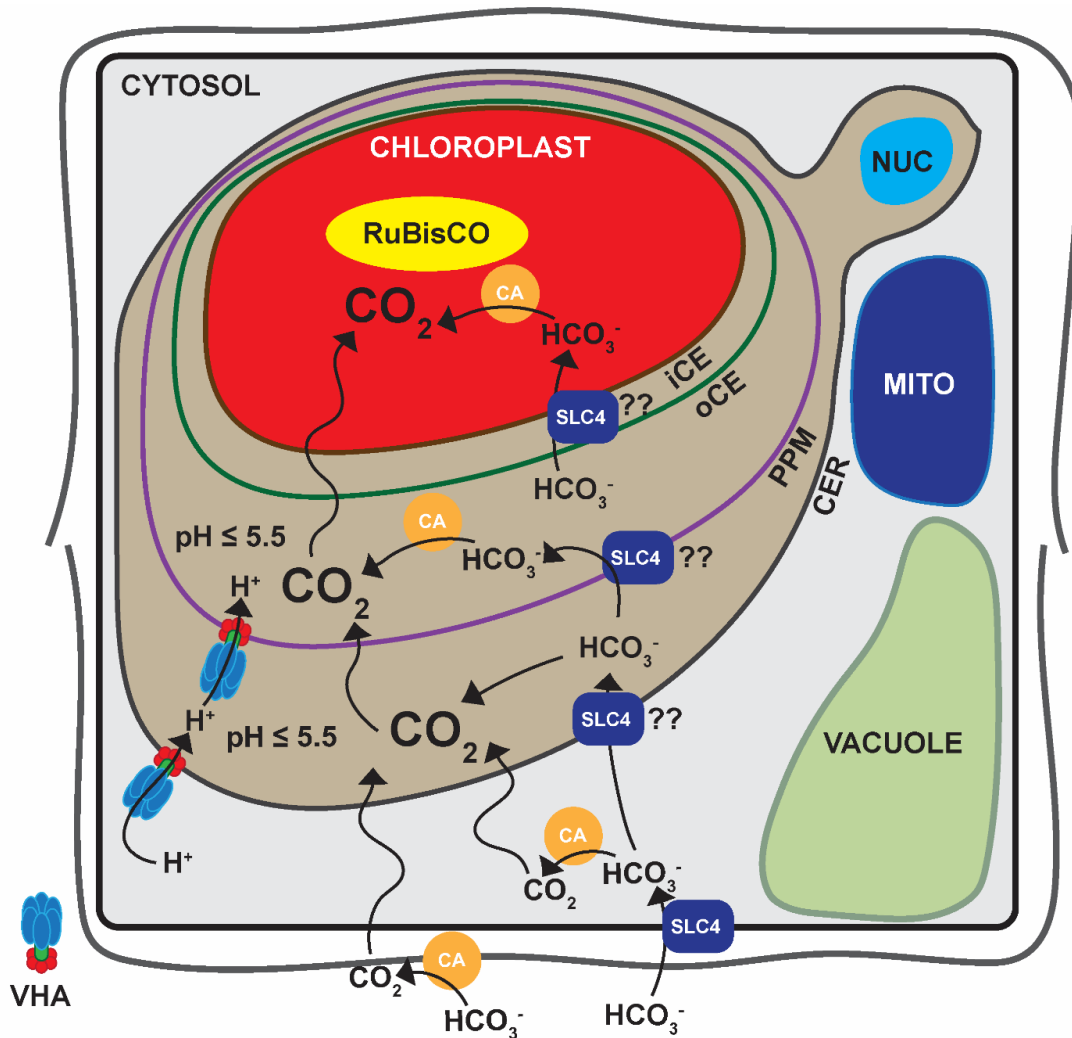


Fig. 3.4 Diagram of a hypothetical model for a VHA mediated CCM in diatoms. Orange circles represent different isoforms of CAs which have been localized but whose activity has not yet been confirmed in *T. pseudonana* (7). Blue rectangles are for SLC4 isoforms which have been localized in the plasmalemma (10) but also suspected in the chloroplast membranes (unpublished data referenced in (25)) of *P. tricornutum*. Bicarbonate is brought into the cell by active transport through SLC4 in the plasmalemma, at pH 7.2-7.5 in the cytosol most of HCO_3^- gets shuttle through SLC4 in the CER. Within the CER and PPM, $\text{pH} \leq 5.5$ is achieved via proton pumping by VHA and much of the HCO_3^- equilibrates towards CO_2 which can diffuse inward to the pyrenoid and gets carboxylated by RuBisCO. Unequilibrated HCO_3^- can continue to be shuttled to the pyrenoid by SLC4 which is potentially located within the chloroplast. The presence of CAs can generate CO_2 at all times to maintain diffusion gradients in towards the pyrenoid. The compartmental abbreviations are: V-type H^+ -ATPase (VHA), carbonic anhydrase (CA), solute carrier 4 HCO_3^- transporters (SLC4), chloroplast endoplasmic reticulum (CER), periplastid membrane (PPM), outer-chloroplast envelope (oCE), inner-chloroplast envelope (iCE), mitochondria (MITO), and nucleus (NUC).

Chapter 3 Supplemental Figures

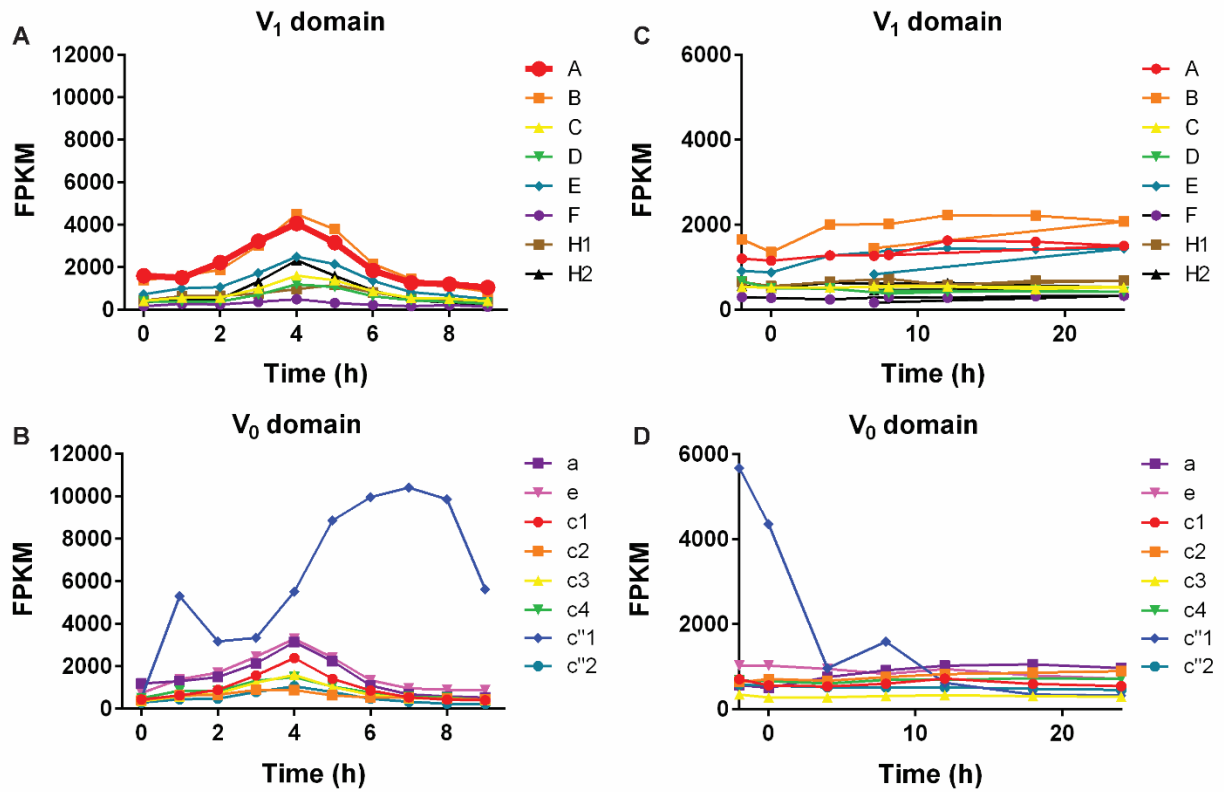


Fig. S3.1 Time-course of transcriptomic profiles of VHA mRNA abundances in *T. pseudonana* during synchronized growth following silicon starvation (A-B), and during halted growth during silicon starvation (C-D).

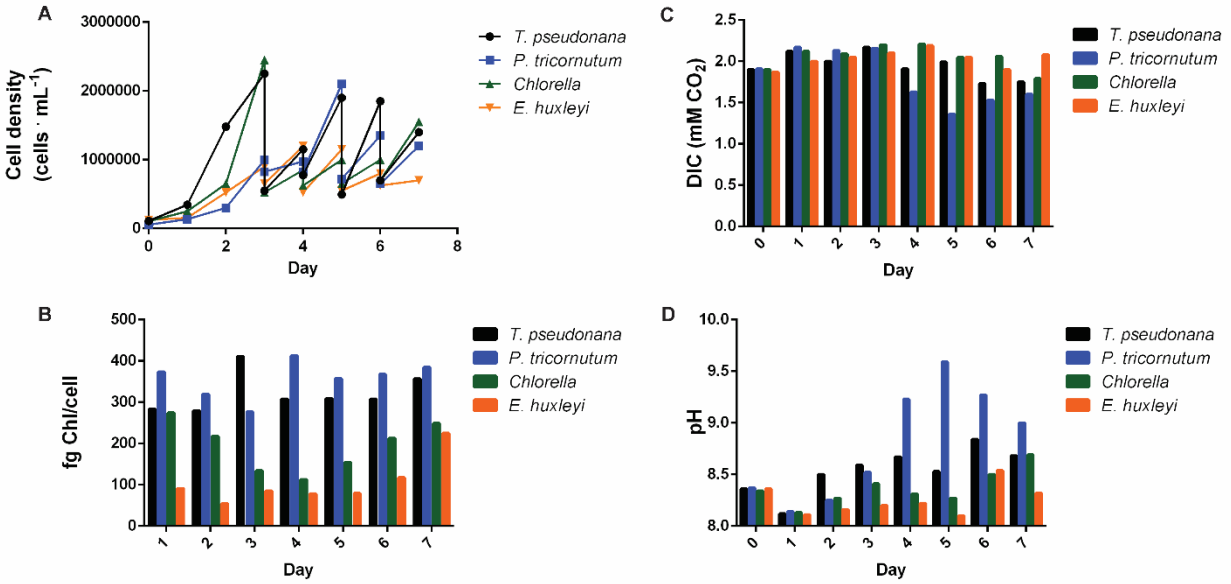


Fig. S3.2 Culture conditions for *T. pseudonana*, *P. tricornutum*, *Chlorella* sp., and *E. huxleyi* cultured on F/2 supplemented natural seawater medium.

Cultures of *P. tricornutum*, *E. huxleyi*, and *Chlorella* were grown alongside *T. pseudonana* for 3 days, after which they were diluted daily over four days to maintain cells in exponential growth for replicate measurements of oxygen production. In the first three days, growth was greatest in *T. pseudonana*, followed by *Chlorella*, *E. huxleyi*, and *P. tricornutum*. However, once dilutions began, both diatoms generally performed better than *Chlorella*, while *E. huxleyi* performed the worst with growth slowing after each dilution (Fig. S3.2A). Cellular chlorophyll content in the both diatoms remained relatively stable compared to *Chlorella* and *E. huxleyi* which began to accumulate chlorophyll during dilutions, likely due to light stress (Fig. S3.2B). DIC levels remained relatively stable across all days of culturing except in *P. tricornutum* which experienced a significant decrease to <1.5 mM CO₂ during dilutions (Fig. S3.2C). As expected, there was an inverse relationship between pH and DIC, with a large increase in culture pH for *P. tricornutum* during dilutions, however, this did not appear to negatively affect cell growth (Fig. S3.2D).

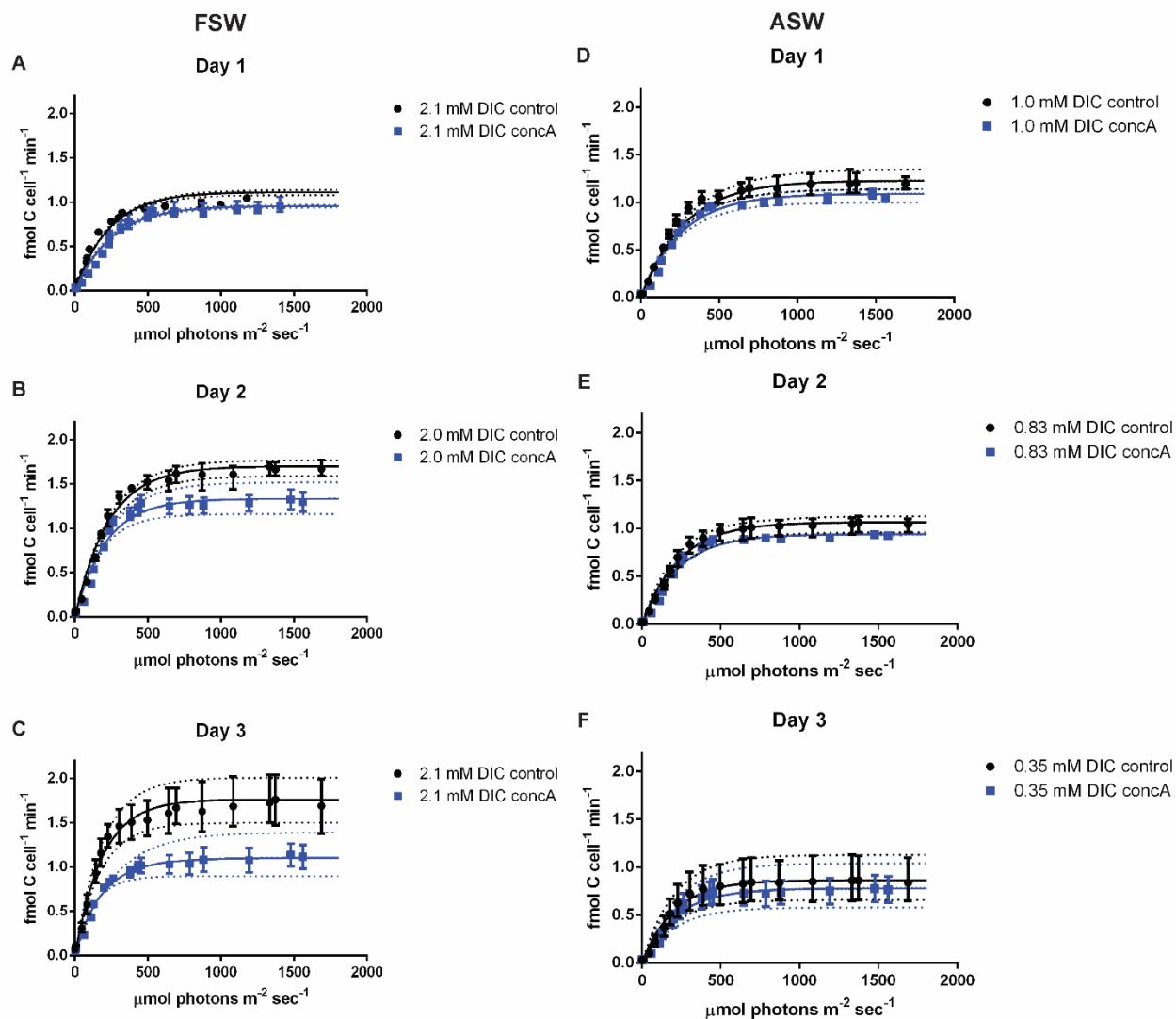


Fig. S3.3 Average cell normalized ¹⁴C PvE curves for *T. pseudonana* +/- 10 nM concanamycin A sampled over 3 days of culturing in FSW (A-C) and ASW medium with ambient DIC (D-F) (n=3 except for ASW Day 1 control where n=2, error bars= SEM, dotted lines= range).

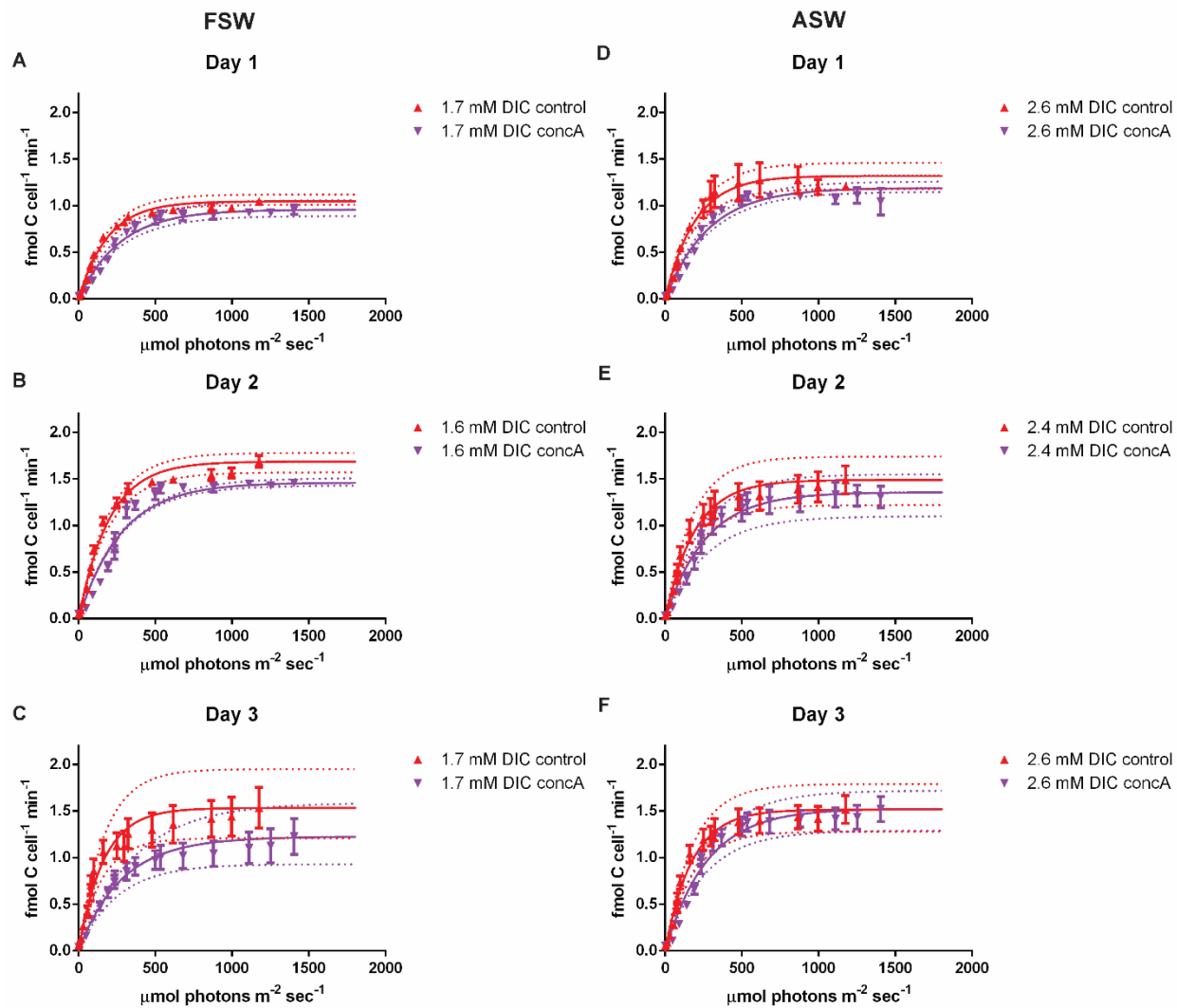


Fig. S3.4 Average cell normalized ¹⁴C PvE curves for *T. pseudonana* +/- 10 nM concanamycin A sampled over 3 days of culturing in FSW (A-C) and ASW medium with modified DIC (D-F) (n=3, error bars= SEM, dotted lines= range).

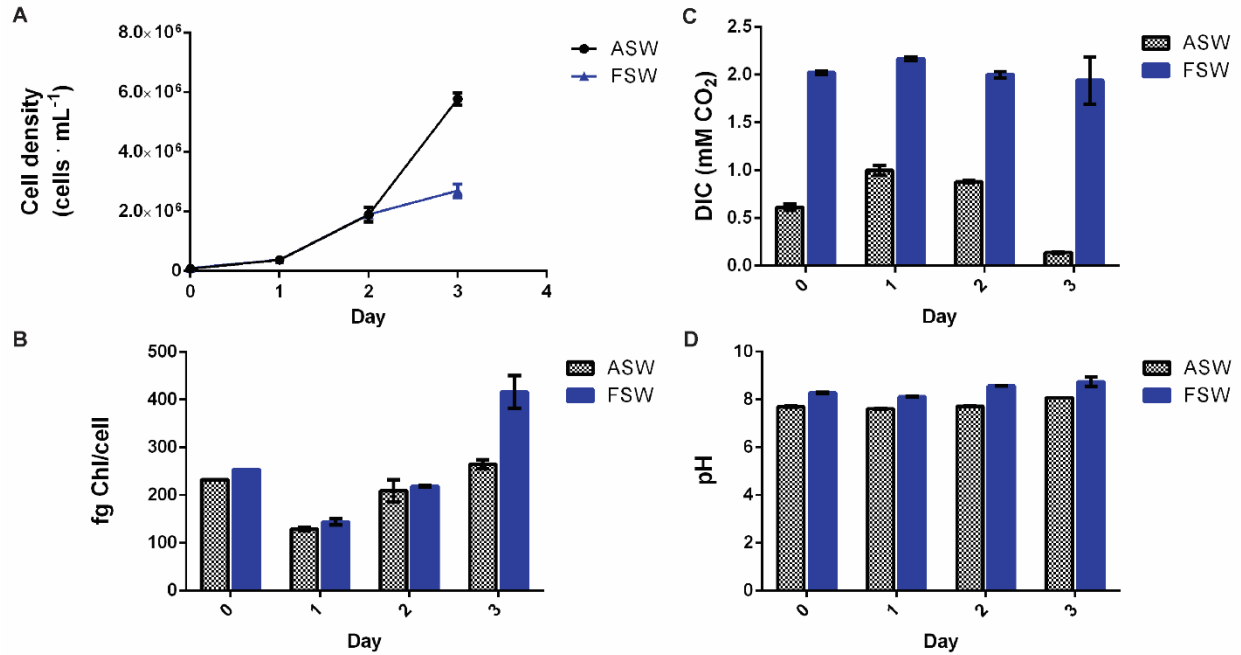


Fig. S3.5 Culture conditions for *T. pseudonana* cultured on ASW and FSW medium (n=3, error bars= SEM).

Cell counts and cellular chlorophyll content (indicating the photo-acclimation state of the cells) were similar between the two culture media in days 0-2 (Fig. S3.5A-B). This was despite measurements of water chemistry in the two culture media showing DIC concentrations in ASW were less than half that present FSW, and slightly more acidic across the four days measured (Fig. S3.5C-D). This observation suggests that *T. pseudonana* can adapt to wide range of DIC concentrations in order to satisfy the photosynthetic demands of the cell. Growth began to slow in FSW compared to ASW on day 3, likely due to lower nitrogen content in F/2 nutrient recipe.

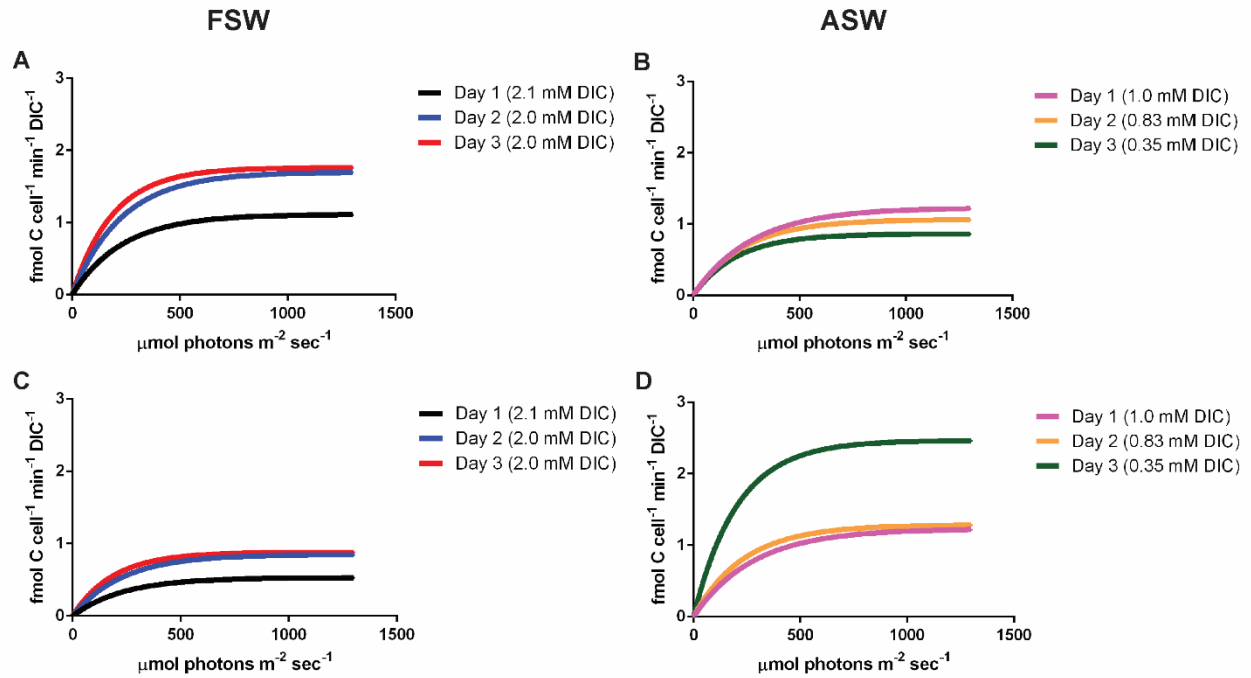


Fig. S3.6 Curve fitting of average cell normalized ^{14}C PvE rates for for *T. pseudonana* controls sampled over 3 days of culture in FSW and ASW medium (A-B), and recalculated curve fittings presented as a ratio to DIC in the media (C-D).

Chapter 3 Tables

Table 3.1 P-values for significant difference in gross O₂ production between control and concanamycin A treatments (left), and % VHA contribution (right) (nd= no difference measured; n= 3).

	Paired t-test		% VHA contribution
	P-value	P-value summary	P-value
<i>T. pseudonana</i>	0.009	**	0.0013
<i>P. tricornutum</i>	0.0203	*	0.0015
<i>E. huxleyi</i>	0.0125	*	0.0031
<i>Chlorella sp.</i>	nd	nd	nd

Table 3.2 P-values for significant difference in cellular carbon fixation rates between control and concanamycin A treatments of various P-E curve fitting parameters (n= 3 were p-values are present; ns= not significant; n/a= low n prevented statistical analysis).

	P-value											
	F/2 ambient DIC			F/2 reduced DIC			ASW ambient DIC			ASW reduced DIC		
	Day 1	Day 2	Day 3	Day 1	Day 2	Day 3	Day 1	Day 2	Day 3	Day 1	Day 2	Day 3
P _{max}	0.0058	0.0754	0.0056	0.0351	0.0347	0.0075	0.0742	0.1624	0.0015	n/a	0.046	0.8487
alpha	0.0023	0.0009	0.1138	0.005	0.0122	0.0499	0.0369	0.227	0.0155	n/a	0.0275	0.0203
E _k	0.0467	0.3246	0.9224	0.0039	0.0133	0.098	0.1253	0.7167	0.1077	n/a	0.0024	0.0214
P-value summary												
	F/2 ambient DIC			F/2 reduced DIC			ASW ambient DIC			ASW reduced DIC		
	Day 1	Day 2	Day 3	Day 1	Day 2	Day 3	Day 1	Day 2	Day 3	Day 1	Day 2	Day 3
P _{max}	**	ns	**	*	*	**	ns	ns	**	n/a	*	ns
alpha	**	***	ns	**	*	*	*	ns	*	n/a	*	*
E _k	*	ns	ns	**	*	ns	ns	ns	ns	n/a	**	*

Chapter 3, in full, is in preparation for submission as Yee, D.P., Shimasaki, B.L., & Tresguerres, M. Evolution of a V-type H⁺-ATPase-mediated carbon concentrating mechanism in secondary endosymbiotic phytoplankton. The dissertation author was the primary investigator and author of this paper.

CHAPTER 4

The potential roles of V-type H⁺-ATPase in the function diatom vacuoles

4.1 Abstract

Vacuoles make up a significant portion of the cell volume and have long been purported as the site of nutrient accumulation in diatoms. In addition to providing a reservoir for storage, diatom vacuoles are used to provide buoyancy to offset the weight of their silica shells and enable vertical migration in the water column. Despite the many functions of the vacuole, little is known about the mechanisms that facilitate these roles. Fluorescent tagging of V-type H⁺-ATPase (VHA) in *Thalassiosira pseudonana* revealed a strong presence in vacuole tonoplasts at various cell stages. Pharmacological inhibition of VHA reduced pH in the vacuole, indicating a role for acidification in the function of the vacuole. Therefore, mechanisms of VHA mediated transport nitrogen, carbon, iron, and phosphorous through the vacuole are proposed with implications for buoyancy, nutrient metabolism, and sexual reproduction in diatoms.

4.2 Introduction

By their simplest definition, vacuoles are ubiquitous organelles in eukaryotic cells that provide a chemical environment separated from the cytoplasm. However, the specific physiological function of vacuoles varies depending on the cell type, organism, and environment they inhabit. The evolution of vacuolar functions is likely driven by conditions limiting cellular metabolism such as the availability of vital nutrients and the turnover of toxic compounds (1). Vacuoles also serve to increase cell size and the intracellular surface area to volume ratio, thereby enabling a higher capacity for unique biochemical reactions and cellular adaptations to occur. Because synthesizing vacuoles is energetically costly, the amount of vacuolization can vary across organisms. In plants, maintaining large vacuoles is advantageous for storing and concentrating nutrients that may otherwise be limiting in the environment.

This paradigm holds true for large vacuoles in diatoms, whose planktonic lifestyles depend heavily on the seasonal and physical ocean processes to obtain nutrients for growth. Nevertheless, diatoms have overcome these challenges and become some of the most successful primary producers on the planet (2, 3). Some of the strategies of diatoms include the use of silica, an abundant yet underutilized mineral, as a substrate for building their protective cell walls called frustules, and the operation of a robust carbon concentrating mechanism (CCM); these features were presented in Chapters 2 and 3 respectively. Additionally, diatoms are able to adjust their metabolism for storing nutrients during and after blooms, and can also transition to a vegetative state in response to prolonged nutrient stress by forming resting spores that reproduce sexually (4). Diatoms possess large vacuoles which can make up to 90% of the cells' total volume (5). In addition to storing nutrients, diatom vacuoles are also important for maintaining buoyancy within the water column. Indeed, the large diatom vacuoles can be filled up with “light” ions such as Na^+ , NH_4^+ , and H^+ that offset their heavy silicified frustules (1). It has been proposed that having large vacuoles in combination with a silica frustule enables a “large yet small” strategy whereby diatoms can remain physically large to avoid grazing predation while maintaining a reduced cytoplasm and an associated “small” metabolism (6). Although the diatom vacuole is known to be acidic (7), the molecular mechanisms that mediate the transport of molecules across the vacuolar membrane (known as the tonoplast) remain poorly understood. While several eukaryotic transporters may energize molecular activities in the vacuole, a leading candidate is the V-type H^+ -ATPase (VHA) which is an evolutionarily conserved multi-subunit proton pump that regulates the pH of various intracellular compartments in eukaryotic cells (8), and which I identified as essential for diatom frustule formation and CCM in Chapters 2 and 3, respectively. In this chapter, I have reviewed the

literature about putative vacuolar biomechanisms in diatoms and provide results supporting a role of VHA in these processes.

VHA localization and function in diatom vacuoles

In plant vacuoles, VHA can serve in secondary active transport of molecules to facilitate nutrient storage (9) and osmolyte transport for generating turgor pressure for cell expansion (10, 11). While it has been suggested that VHA functions in diatom vacuoles for nitrogen uptake (12), past studies tagging the c-subunit with enhanced green fluorescent protein (eGFP) did not detect the enzyme in the tonoplast of the marine diatom *Phaeodactylum tricornutum* (13).

As described in Chapter 2, transgenic *Thalassiosira pseudonana* expressing VHA subunit B with eGFP (VHA_B-eGFP) allowed me to visualize the presence of VHA in multiple subcellular compartments including the tonoplast of vacuoles, which were identified by staining with the vacuolar marker CMAC-Ala-Pro (Fig. 4.1). Based on the accumulation and fluorescence of the acidotropic pH stain PDMPO, the intra-vacuolar pH was ≤ 5.5 (Fig. 4.2A-B). Furthermore, application of the specific VHA inhibitor concanamycin A completely abolished the PDMPO signal in the vacuole (Fig. 4.2C-D). The presence of VHA in the tonoplast together with the observed concanamycin-dependent vacuolar PDMPO accumulation indicates that VHA plays an important role in vacuolar acidification, and provides the foundation for predicting potential roles in various vacuolar functions.

Nitrogen metabolism and nitrate storage

Nitrogen is known to limit phytoplankton productivity in the oceans, therefore, it is crucial that diatoms have a way to sequester nitrogen when it becomes available. While there is an energetic preference for NH_4^+ , NO_3^- is the more abundant in seawater. Nitrate uptake and assimilation is directly connected to photosynthetically driven carbon metabolism and the

synthesis of amino acids. However, in experiments with diatoms grown on diel cycles, diatoms have been shown to uptake NO_3^- even in the dark (14). Additionally, it has been shown that several diatom species increase NO_3^- uptake rates when extracellular concentrations are above $60 \mu\text{mol N L}^{-1}$, and likely partition NO_3^- into vacuoles (15). Nitrate has been reported to make up ~84% of inorganic nitrogen pools (15), and as high as 99% in *T. pseudonana* grown exponentially (16). The uptake of NO_3^- into the cytoplasm is known to occur by diffusion and carrier mediated transport. In the diatom *Cylindrotheca fusiformis* three NO_3^- transporters (NRT1/2/3) have been characterized (17) and are also found in the genome of *T. pseudonana*. However, most studies of nitrogen metabolism in diatoms involve nitrogen reductases, such as nitrate reductase, which has been localized to the plasmamembrane and cytoplasm of diatoms to reduce NO_3^- to NO_2^- (18, 19). Meanwhile, mechanisms of storing NO_3^- in diatom vacuoles remain unknown.

Intriguingly, VHA mediated NO_3^- storage has been demonstrated in plants where mutants for in VHA subunits targeting the vacuole led to reduced vacuolar NO_3^- content (9). This activity was later linked to a voltage-gated chloride channel (CLC) that behaves as a NO_3^-/H^+ exchanger in which proton pumping into the vacuole drives the exchange of NO_3^- into the vacuole (20). In the pennate diatom *P. tricornutum*, nitrate reductase mutants upregulated transcripts of putative CLC- NO_3^- transporters along with several VHA subunits (12). Furthermore, mutants had swollen vacuoles, which was attributed to an inability to reduce NO_3^- to NO_2^- for metabolism, resulting in vacuolar accumulation of NO_3^- . The authors proposed that NO_3^- transport into the vacuoles is mediated by CLC- NO_3^- transporters coupled to VHA, and that NO_3^- accumulation is partly responsible for swelling of the vacuoles. Based on this combined evidence, the diagram in Fig. 4.3A shows a model for the secondary active transport of NO_3^- into the diatom vacuole. In this

model, NRT imports NO_3^- into the cytosol which is shuttled into the vacuole by VHA mediated secondary active transport through CLC NO_3^-/H^+ exchangers.

Ammonium storage

While vacuolar NO_3^- accumulation in diatoms be essential for survival, it is an unlikely strategy for actively growing cells. Due to its mass, a large concentration of NO_3^- in the vacuole would offset buoyancy, causing cells to sink out of the photic zone. Alternatively, the accumulation of $\text{NH}_3/\text{NH}_4^+$ in vacuoles would be a “lighter” way to store nitrogen in the cell. Despite NH_4^+ concentrations being much lower than NO_3^- in seawater, diatoms can preferentially uptake NH_4^+ (21). Therefore, a mechanism for accumulating $\text{NH}_3/\text{NH}_4^+$ in diatom vacuoles may also exist.

In eukaryotes, NH_4^+ is shuttled through ammonium transporters (AMT) and have been characterized in the marine diatom *Cylindrotheca fusiformis* (22). Expression of AMT mRNA has been shown to be constitutive under various nitrogen conditions but particularly upregulated in response to N-limitation in several diatom species (23). In plants, the mechanism of AMT1 was shown to function as a NH_4^+ uniporter or NH_3/H^+ cotransporter and was in the plasma membrane of root cells (24). Meanwhile, diatoms also possess aquaporin (AQP) channels which can transport CO_2/NH_3 by diffusion gradients. In *T. pseudonana*, AQP1 has been localized to the tonoplast while AQP2 was present in both the tonoplast and chloroplast ER (25).

Alkylamine tracer studies have shown that diatoms can accumulate NH_4^+ at high concentrations within the cell, and speculated that the acidic environment of vacuoles generated by proton pumps is an ideal storage location for NH_4^+ and other weak bases (7). Given that strong preference for NH_4^+ utilization of many diatoms, and the presence of AQPs in the tonoplast, I propose VHA promotes NH_4^+ storage in diatom vacuoles. For actively growing cells were NH_4^+ is preferentially used, NH_4^+ is imported through plasma membrane AMT1 transporters. In order

to prevent NH_4^+ from equilibrating towards NH_3 it must be shuttled into an acidic compartment such as vacuoles and chloroplasts. From the cytosol, $\text{NH}_3/\text{NH}_4^+$ diffuses through tonoplast AQP channels via electrochemical gradients where the acidic environment of the vacuole converts all NH_3 to NH_4^+ for storage (Fig. 4.3B). Simultaneously, $\text{NH}_3/\text{NH}_4^+$ also diffuses through AQP in the ER membrane where it can be used for amino acid synthesis in chloroplasts. The ability to sequester NH_4^+ in the vacuole can further help diatoms outcompete other phytoplankton in nature.

Chrysolaminarin storage

During silicon or nitrogen starvation diatoms halt their growth and redirect their carbon metabolism towards the production of storage molecules such as lipids and carbohydrates (26, 27). The major storage carbohydrate found in diatoms is a water soluble β -1,3-glucan called chrysolaminarin. Chrysolaminarin is synthesized from uridine diphosphate (UDP)-glucose by the UDP-glucose pyrophosphorylase (UGP) and chrysolaminarin synthase (CS) enzymes (28, 29). Following synthesis, chrysolaminarin molecules are linked and assembled by 1,6- β -transglycosylases (TGS) found in the tonoplast (30) and stored in vacuoles (31).

While accumulation of chrysolaminarin occurs in the vacuole, it is unknown whether synthesis takes place in the chloroplast, cytosol, or vacuole. In all scenarios, glucose or β -1,3-glucan would need to be transported through the tonoplast. While the presence of ABC glucan transporters (32, 33) are unknown, the glucose transporters (GLUT) are have been identified in diatom genomes (Thaps3_3268472; Thaps3_269158) (34). Based on this information, I propose that glucose derived from photosynthesis diffuses from chloroplasts to vacuoles through GLUT3 transporters. In the vacuole, glucose is synthesized into chrysolaminarin in a cascading pathway involving UGP, CS, and TGS (Fig. 4.3C). Although glucose is transported via facilitated diffusion through GLUT, the viscosity of β -glucans is known to increase under acidic pH(35). The enhanced stability of

chrysolaminarin under acidic pH may increase the rate of chrysolaminarin synthesis and promote diffusion of glucose through GLUT3, making the vacuole's acidic environment ideal for storing chrysolaminarin.

Iron storage

Iron is recognized as a major limiting nutrient to diatom productivity in the oceans. In high-nutrient low-chlorophyll (HNLC) waters, iron fertilization has been found to stimulate diatom blooms (36–38). Therefore, diatoms must have evolved robust uptake and storage mechanisms to compete for iron once it becomes available (39). While iron storage is carried out by ferritin in the pennate diatom *P. tricornutum*, it appears to be absent in *T. pseudonana* and other centric diatoms (40). A putative natural resistance-associated macrophage protein (NRAMP) gene identified in *T. pseudonana* but not *P. tricornutum*, was significantly upregulated in response to increased iron availability (41). NRAMPs are proton-coupled metal-ion transporters which shuttle Fe(II) and other divalent metals (42). In *Arabidopsis* seedlings, NRAMPs function in releasing iron stores from vacuoles (43). Given that iron stores have been identified in the vacuoles of two centric diatoms *T. pseudonana* and *Thalassiosira weissflogii* (44), I propose that following iron sequestration, VHA provides the proton motive forces for H⁺ coupled iron transport out of vacuoles through NRAMPs found in tonoplast of centric diatoms (Fig. 4.3D).

Phosphate storage

Although phosphorous is not as limiting as nitrogen and iron for phytoplankton growth in the environment, it is still an important nutrient that is vital to many cellular processes including the synthesis of proteins, nucleic acids, and phospholipids. While diatoms have evolved to sequester various nutrients away from competitors, some evidence suggests they are less efficient at storing phosphate (45). However, experiments investigating the responses of diatoms to P-

limitation reveal strong shifts in phosphorous metabolism (46, 47). From these studies vacuolar transporter chaperone (VTC) and vacuolar phosphate transporter (VPT) 1 have been found to be transcriptionally upregulated under P-limitation, and VPT1 and VTC2 were recently localized in the tonoplast of *P. tricornutum* (48). The study also identified two H⁺/P co-transporters (*PtHP1/2*) in which *PtHP2* was targeted to the plasma membrane while *PtHP1* localization remains unconfirmed.

In yeast, VTCs are present in the vacuolar membrane to produce the storage compound polyphosphate (49). Meanwhile in plants, VPT1 was found to mediate phosphate transport into vacuoles (50), while orthologs of *PtHP* facilitating proton coupled efflux of phosphate out of the vacuole (51). Polyphosphate has been demonstrated to accumulate as a storage molecule in diatoms (52) and is likely stored in the vacuole. Therefore, I propose a mechanism similar to plants where phosphate entering the vacuole through VPT1 provides the substrate for VTC to produce polyphosphate, afterwards phosphate is distributed from the vacuole by proton coupled efflux through H⁺/P cotransporters driven by secondary active transport of protons by VHA (Fig. 4.3E).

Buoyancy & Auxosporulation

Diatoms play a significant role in carbon and nutrient export from surface waters and biogeochemical cycles in the ocean (37, 53, 54). The sinking of diatom biomass after massive blooms is due to their large size and weight of silica frustules. However, in actively growing cells, diatoms may exhibit vertical migratory behaviors based on the distribution of nutrients and light in the water column by modulation their buoyancy (55). One way diatoms can regulate their buoyancy is by the storing lighter or heavier ions in their large vacuoles (1). A study of osmolyte composition from different phytoplankton found that positively buoyant phytoplankton tended to contain ammonium versus negatively buoyant phytoplankton which contained more carbohydrates

(56). This observation is consistent with the physiology of nitrogen metabolism in diatoms where actively growing cells switch from ammonium utilization to nitrate accumulation in vacuoles to induce sinking following N-limitation. Furthermore, N-limitation also results in a shift in carbon metabolism to accumulation chrysolaminarin in vacuoles which would also reduce buoyancy in the cell.

Indeed, the end of a phytoplankton bloom is usually marked by the exhaustion of nutrients and a shift in metabolism resulting in the loss of buoyancy and sinking of diatom cells. Another occurrence is the transformation of diatoms from a state of vegetative asexual cell division to resting auxospores which reproduce sexually. Auxosporulation has been observed in both centric and pennate diatom species (4, 57–59) which occurs after the fertilization of a large oocyte by a small flagellated spermatocyte, and is important for restoring cell size after generational shrinking after repeated cell divisions and mating of genetic traits (60, 61). Auxospores are characterized by a large vacuoles which restrict other organelles to a thin peripheral band of cytoplasm adjacent to the plasma membrane (62). As the early spore enlarges, it breaks out of the parent frustule and balloons to a spherical shape lacking a cell wall, but eventually synthesizes siliceous scales as it matures. In cultures of *T. pseudonana* expressing VHA_B-eGFP, cells undergoing auxosporulation have been observed with VHA in the tonoplast of the large vacuoles along with SDV membranes synthesizing siliceous scales (Fig. 4.4). Based on similar mechanisms in vegetative diatom cells proposed in this chapter, I propose that VHA drives the import of osmolytes through various transporters to aide in buoyancy, nutrient accumulation, and expansion of vacuoles.

In natural diatom assemblages following nitrogen limitation, vegetative cells were observed to sink as they transitioned to sexual reproduction but would rise back to the photic zone after auxosporulation (63). While phosphorous appears to remain constant, there are minor

increases in nitrogen and large increases in silicic acid quotas in auxospores following N- and P-limitation (4). While increase in silicic acid is likely due to production of siliceous scales, the increase in nitrogen may be due to changes in nitrogen metabolism and buoyancy. Since ammonium compounds have been suggested to provide buoyancy in diatom cells (55, 56), I propose that the $\text{NH}_3/\text{NH}_4^+$ transport mechanism presented in Fig. 4.3B also serves to regulate buoyancy in auxospores.

4.3 Conclusion

Mechanistic understanding of vacuolar function in diatoms is limited, and in this chapter, I present multiple functions of vacuoles in diatom biology. Localization of VHA to the tonoplast in *T. pseudonana* suggests acidification plays an important role in the physiological functions of the vacuole. In plants and other unicellular eukaryotes with large vacuoles, VHA has been shown to play a crucial role in the transport of different solutes through tonoplasts. A combination of literature reviews and my localization data showing VHA acidifies diatom vacuoles enabled me to generate multiple hypothesis for VHA mediated nitrogen, carbon, iron, and phosphate transport through the vacuole. I also show that VHA is present in diatom auxospores and is active in acidifying vacuoles where it may function in generating buoyancy by facilitating vacuolar expansion and storage of osmolytes such as NH_4^+ . While it is hard to imagine the vacuole being so multifunctional, linking all of these functions to VHA opens the possibility of these mechanisms taking place simultaneously over a range of cell physiologies. There is also evidence that diatoms possess different types of vacuoles which further broadens the range of possibilities (31). Overall, these preliminary results and observations highlights the importance of pH regulating mechanisms in the cell. Future work to characterize the role of VHA in these roles should measure the effects

of blocking VHA on nutrient accumulation and buoyancy. In doing so we may begin to better understand the dynamic and multifunctional role vacuoles serve in diatom cells.

4.4 Methods and Materials

Culture conditions

Cultures of *T. pseudonana* (CCMP1335) expressing VHA_B-eGFP were grown axenically in ASW medium supplemented with 1 mM Na₂SiO₃ or F/2 medium prepared with natural seawater filtered from the Scripps Pier. Cultures were maintained in 50 ml volumes in 125 mL Erlenmeyer flasks on an orbital shaker under continuous illumination by cool-white fluorescent lamps at 70 $\mu\text{mol photons m}^{-2} \text{ s}^{-1}$ at 18°C.

Transgenic diatoms expressing fluorescently labeled VHA_B

VHA subunit B labelled with eGFP was expressed under the control of the *fcp* promoter. For Thaps3_40522 (VHA_B) the full-length coding sequence of the gene was amplified from *T. pseudonana* genomic DNA, and cloned into Gateway destination vector pMHL_79 with eGFP at the end of the coding sequence. The final vector was co-transformed with a pMHL_09 expressing the *nat1* gene which confers nourseothriscin resistance by biolistic gene gun method (64). Liquid cultures grown in ASW medium containing 100 $\mu\text{g/ml}$ nourseothriscin were enriched for cells expressing eGFP using several rounds of fluorescence-activated cell sorting on a BD Influx Cell Sorter (BD Biosciences), from which single colonies expressing eGFP were selected for on ASW agar plates containing nourseothriscin.

Fluorescence microscopy

Epifluorescence microscopy was used for *T. pseudonana* expressing VHA_B-eGFP were stained with vacuolar stain (7-amino-4-chloromethylcoumarin, L-alanyl-L-proline amide (CMAC-Ala-Pro) (ThermoFisher Scientific) for a final concentration of 0.1 μM . The images were

collected with an Zeiss Axio Observer.Z1 inverted microscope, and filter sets used for GFP was Zeiss #38HE (Ex 470/40 nm, FT 495 nm, Em 525/ 50 nm), for CMAC-Ala-Pro was Zeiss #21HE (Ex 387/15 nm, FT 409 nm, Em 510/90 nm), and for Chl autofluorescence was Zeiss #05 (Ex 395-440 nm, FT 460 nm, Em 470 nm).

Super-resolution confocal microscopy was used for *T. pseudonana* expressing VHA_B-eGFP stained with the acidotropic pH stain 2-(4-pyridyl)-5-((4-(2-dimethylaminoethylaminocarbamoyl)methoxy)phenyl)oxazole (PDMPO); LysoSensor YellowBlue DND-160 (Life Technologies) at a final concentration of 0.125 μ M. Concanamycin A (Adipogen Life Sciences) was added at a final concentration of 10 nM in VHA inhibited cells. Cells were then transferred to a 35 mm poly-d-lysine coated glass bottom petri dish and mounted on a Warner Instruments QE-1HC Quick Exchange Heated/Cooled stage chamber controlled by CL-200 Dual Channel Temperature Controller maintained at 18 °C. Cells were imaged with a Zeiss LSM800 inverted confocal microscope equipped with a Zeiss Plan-Apochromat 63 \times (1.4) Oil DIC M27 objective, and Zeiss Airyscan super-resolution detector. Z-stacks of three channels were acquired to monitor eGFP (Ex 488 nm with 0.3% laser power, Em 509 nm, detection 490-535 nm), PDMPO (Ex 335 nm at 0.5% laser power, Em 530 nm, detection 550-650 nm), and chlorophyll (Ex 488 nm with 0.2% laser power, Em 667 nm, detection 450-700 nm) fluorescence.

4.5 References

1. J. A. Raven, The Vacuole : a Cost-Benefit Analysis. *Adv. Bot. Res.* **25**, 59–86 (1997).
2. C. B. Field, M. J. Behrenfeld, J. T. Randerson, P. G. Falkowski, Primary production of the biosphere: Integrating terrestrial and oceanic components. *Science (80-.)*. **281**, 237–240 (1998).
3. D. M. Nelson, P. Tréguer, M. A. Brzezinski, A. Leynaert, B. Quéguiner, Production and dissolution of biogenic silica in the ocean: Revised global estimates, comparison with regional data and relationship to biogenic sedimentation. *Global Biogeochem. Cycles.* **9**, 359–372 (1995).
4. O. Oku, A. Kamatani, Resting spore formation and phosphorus composition of the marine diatom *Chaetoceros pseudocurvisefus* under various nutrient conditions. *Mar. Biol.* **123**, 393–399 (1995).
5. T. J. Smayda, The suspension and sinking of phytoplankton in the sea. *Mar. Geol.* **8**, 353–414 (1970).
6. T. F. Thingstad, L. Øvreås, J. K. Egge, T. Løvdal, M. Haldal, Use of non-limiting substrates to increase size; a generic strategy to simultaneously optimize uptake and minimize predation in pelagic osmotrophs? *Ecol. Lett.* **8**, 675–682 (2005).
7. P. A. Wheeler, J. A. Hellebust, Uptake and Concentration of Alkylamines by a Marine Diatom. *Plant Physiol.* **67**, 367–372 (1981).
8. M. Forgac, Vacuolar ATPases: Rotary proton pumps in physiology and pathophysiology. *Nat. Rev. Mol. Cell Biol.* **8**, 917–929 (2007).
9. M. Krebs, D. Beyhl, E. Görlich, K. A. S. Al-rasheid, I. Marten, Y. Stierhof, Arabidopsis V-ATPase activity at the tonoplast is required for efficient nutrient storage but not for sodium accumulation. **107**, 3251–3256 (2010).
10. K. Schumacher, D. Vafeados, M. McCarthy, H. Sze, T. Wilkins, J. Chory, The *Arabidopsis* det3 mutant reveals a central role for the vacuolar H⁺ -ATPase in plant growth and development. *Genes Dev.* **13**, 3259–3270 (1999).
11. S. Padmanaban, X. Lin, I. Perera, Y. Kawamura, H. Sze, Differential Expression of Vacuolar H⁺ -ATPase Subunit c Genes in Tissues Active in Membrane Trafficking and Their Roles in Plant Growth as Revealed by RNAi. *Plant Physiol.* **134**, 1514–1526 (2004).
12. J. K. McCarthy, S. R. Smith, J. P. McCrow, M. Tan, H. Zheng, K. Beerli, R. Roth, C. Lichtle, U. Goodenough, C. P. Bowler, C. L. Dupont, A. E. Allen, Nitrate Reductase Knockout Uncouples Nitrate Transport from Nitrate Assimilation and Drives Repartitioning of Carbon Flux in a Model Pennate Diatom. *Plant Cell.* **29**, 2047–2070 (2017).
13. A. Bussard, P. J. Lopez, Evolution of vacuolar pyrophosphatases and vacuolar H⁺-ATPases

- in diatoms. *J. Mar. Sci. Technol.* **22**, 50–59 (2014).
14. R. W. Eppley, J. L. Coatsworth, Uptake of Nitrate and Nitrite By *Ditylum Brightwellii*-Kinetics and Mechanisms. *J. Phycol.* **4**, 151–156 (1968).
 15. M. W. Lomas, P. M. Gilbert, Comparisons of nitrate uptake, storage, and reduction in marine diatoms and flagellates. *J. Phycol.* **36**, 903–913 (2000).
 16. S. J. Bender, C. A. Durkin, C. T. Berthiaume, R. L. Morales, E. V. Armbrust, Transcriptional responses of three model diatoms to nitrate limitation of growth. *Front. Mar. Sci.* **1**, 1–15 (2014).
 17. M. Hildebrand, K. Dahlin, Nitrate transporter genes from the diatom *Cylindrotheca fusiformis* (Bacillariophyceae): mRNA levels controlled by nitrogen source and by the cell cycle. *J. Phycol.* **36**, 702–713 (2000).
 18. N. K. Amy, R. H. Garrett, Purification and Characterization of the Nitrate Reductase from the Diatom *Thalassiosira pseudonana*. *Plant Physiol.* **54**, 629–637 (1974).
 19. G. J. Jones, F. M. M. Morel, Plasmalemma Redox Activity in the Diatom *Thalassiosira*. *Plant Physiol.* **87**, 143–147 (1988).
 20. A. De Angeli, D. Monachello, G. Ephritikhine, J. M. Frachisse, S. Thomine, F. Gambale, H. Barbier-Brygoo, The nitrate/proton antiporter AtCLCa mediates nitrate accumulation in plant vacuoles. *Nature.* **442**, 939–942 (2006).
 21. Q. Dortch, P. A. Thompson, P. J. Harrison, Short-term interaction between nitrate and ammonium uptake in *Thalassiosira pseudonana*: Effect of preconditioning nitrogen source and growth rate. *Mar. Biol.* **110**, 183–193 (1991).
 22. M. Hildebrand, Cloning and functional characterization of ammonium transporters from the marine diatom *Cylindrotheca fusiformis* (Bacillariophyceae). *J. Phycol.* **41**, 105–113 (2005).
 23. A. Rogato, A. Amato, D. Iudicone, M. Chiurazzi, M. I. Ferrante, M. R. d’Alcalà, The diatom molecular toolkit to handle nitrogen uptake. *Mar. Genomics.* **24**, 95–108 (2015).
 24. L. Yuan, D. Loqué, S. Kojima, S. Rauch, K. Ishiyama, E. Inoue, H. Takahashi, N. Von Wiréna, The organization of high-affinity ammonium uptake in *Arabidopsis* roots depends on the spatial arrangement and biochemical properties of AMT1-type transporters. *Plant Cell.* **19**, 2636–2652 (2007).
 25. H. Matsui, B. M. Hopkinson, K. Nakajima, Y. Matsuda, Plasma Membrane-Type Aquaporins from Marine Diatoms Function as CO₂/ NH₃ Channels and Provide Photoprotection. *Plant Physiol.* **178**, 345–357 (2018).
 26. P. G. Roessler, Effects of Silicon Deficiency on Lipid Composition and Metabolism in the Diatom *Cyclotella Cryptica*. *J. Phycol.* **24**, 394–400 (1988).

27. E. Granum, S. Kirkvold, S. M. Myklestad, Cellular and extracellular production of carbohydrates and amino acids by the marine diatom *Skeletonema costatum* : diel variations and effects of N depletion. **242**, 83–94 (2002).
28. P. C. Roessler, UDPglucose pyrophosphorylase activity in the diatom *Cyclotella cryptica*. Pathway of chrysolaminarin biosynthesis. *J. Phycol.* **498**, 494–498 (1987).
29. M. Hildebrand, K. Manandhar-shrestha, R. Abbriano, Effects of chrysolaminarin synthase knockdown in the diatom *Thalassiosira pseudonana*: Implications of reduced carbohydrate storage relative to green algae. *Algal Res.* **23**, 66–77 (2017).
30. W. Huang, C. Río Bártulos, P. G. Kroth, Diatom Vacuolar 1,6- β -Transglycosylases can Functionally Complement the Respective Yeast Mutants. *J. Eukaryot. Microbiol.* **63**, 536–546 (2016).
31. A. Chiovitti, P. Molino, S. a Crawford, R. Teng, T. Spurck, R. Wetherbee, The glucans extracted with warm water from diatoms are mainly derived from intracellular chrysolaminaran and not extracellular polysaccharides. *Eur. J. Phycol.* **39**, 117–128 (2004).
32. G. A. Cangelosi, G. Martinetti, J. A. Leigh, C. H. I. C. Lee, C. Theines, E. W. Nester, Role of *Agrobacterium tumefaciens* ChvA Protein in Export of B-1,2-Glucan. *J. Bacteriol.* **171**, 1609–1615 (1989).
33. S. W. Stanfield, L. Ielpi, D. O. B. D. R. Helinski, G. S. Ditta, The ndvA Gene Product of *Rhizobium meliloti* Is Required for 1- (1--2) Glucan Production and Has Homology to the ATP-Binding Export Protein HlyB. **170**, 3523–3530 (1988).
34. Y. Zheng, A. H. Quinn, G. Sriram, Experimental evidence and isotopomer analysis of mixotrophic glucose metabolism in the marine diatom *Phaeodactylum tricornutum*. *Microb. Cell Fact.* **12** (2013).
35. M. Salmenkallio-Marttila, T. Suortti, K. Autio, K. Poutanen, Effect of pH on viscosity of oat beta-glucan. *Proc. 7th Int. Oat Conf.*, 138 (2004).
36. C. Lancelot, E. Hannon, S. Becquevort, C. Veth, H. J. W. De Baar, Modeling phytoplankton blooms and carbon export production in the Southern Ocean: Dominant controls by light and iron in the Atlantic sector in Austral spring 1992. *Deep. Res. Part I Oceanogr. Res. Pap.* **47**, 1621–1662 (2000).
37. I. Salter, R. S. Lampitt, R. Sanders, A. Poulton, A. E. S. Kemp, B. Boorman, K. Saw, R. Pearce, Estimating carbon, silica and diatom export from a naturally fertilised phytoplankton bloom in the Southern Ocean using PELAGRA: A novel drifting sediment trap. *Deep. Res. Part II Top. Stud. Oceanogr.* **54**, 2233–2259 (2007).
38. K. H. Coale, K. S. Johnson, F. P. Chavez, K. O. Buesseler, R. T. Barber, M. A. Brzezinski, W. P. Cochlan, F. J. Millero, P. G. Falkowski, J. E. Bauer, R. H. Wanninkhof, R. M. Kudela, M. A. Altabet, B. E. Hales, T. Takahashi, M. R. Landry, R. R. Bidigare, X. Wang, Z. Chase, P. G. Stratton, G. E. Friederich, M. Y. Gorbunov, V. P. Lance, A. K. Hilting, M. R. Hiscock,

- M. Demarest, W. T. Hiscock, K. F. Sullivan, S. J. Tanner, R. M. Gordon, C. N. Hunter, V. A. Elrod, S. E. Fitzwater, J. L. Jones, S. Tozzi, M. Koblizek, A. E. Roberts, J. Herndon, J. Brewster, N. Ladizinsky, G. Smith, D. Cooper, D. Timothy, S. L. Brown, K. E. Selph, C. C. Sheridan, B. S. Twining, Z. I. Johnson, Southern Ocean Iron Enrichment Experiment: Carbon Cycling in High- and Low-Si Waters. *Science* (80-.). **304**, 408–414 (2004).
39. S. Iwade, K. Kuma, Y. Isoda, M. Yoshida, I. Kudo, J. Nishioka, K. Suzuki, Effect of high iron concentrations on iron uptake and growth of a coastal diatom *Chaetoceros sociale*. *Aquat. Microb. Ecol.* **43**, 177–191 (2006).
 40. A. Marchetti, M. S. Parker, L. P. Moccia, E. O. Lin, A. L. Arrieta, F. Ribalet, M. E. P. Murphy, M. T. Maldonado, E. V. Armbrust, Ferritin is used for iron storage in bloom-forming marine pennate diatoms. *Nature*. **457**, 467–470 (2009).
 41. A. B. Kustka, A. E. Allen, Sequence analysis and transcriptional regulation of iron acquisition genes in two marine diatoms. **729**, 715–729 (2007).
 42. H. Gunshin, B. Mackenzie, U. V Berger, Cloning and characterization of a mammalian proton-coupled metal-ion transporter. *Nature*. **388**, 6264–6268 (1997).
 43. V. Lanquar, F. Lelievre, S. Bolte, C. Hames, C. Alcon, D. Neumann, G. Vansuyt, C. Curie, A. Schroder, U. Kramer, H. Barbier-Brygoo, S. Thomine, Mobilization of vacuolar iron by AtNRAMP3 and AtNRAMP4 is essential for seed germination on low iron. *EMBO J.* **24**, 4041–4051 (2005).
 44. J. Nuester, S. Vogt, B. S. Twining, Localization of iron within centric diatoms of the genus *Thalassiosira*. *J. Phycol.* **48**, 626–634 (2012).
 45. J. K. Egge, Are diatoms poor competitors at low phosphate concentrations? *J. Mar. Syst.* **16**, 191–198 (1998).
 46. S. T. Dyhrman, B. D. Jenkins, T. A. Ryneerson, M. A. Saito, M. L. Mercier, H. Alexander, L. P. Whitney, A. Drzewianowski, V. V Bulygin, E. M. Bertrand, Z. Wu, C. Benitez-nelson, A. Heithoff, The Transcriptome and Proteome of the Diatom *Thalassiosira pseudonana* Reveal a Diverse Phosphorus Stress Response. *PLoS One.* **7** (2012), doi:10.1371/journal.pone.0033768.
 47. L. Alipanah, P. Winge, J. Rohloff, J. Najafi, T. Brembu, A. M. Bones, Molecular adaptations to phosphorus deprivation and comparison with nitrogen deprivation responses in the diatom *Phaeodactylum tricorutum*. *PLoS One.* **13**, 1–24 (2018).
 48. G. D. Aquila, S. Zauner, T. Heimerl, J. Kahnt, V. Samel-gondesens, S. Runge, F. Hempel, U. G. Maier, Mobilization and Cellular Distribution of Phosphate in the Diatom *Phaeodactylum tricorutum*. *Front. Plant Sci.* **11**, 1–14 (2020).
 49. M. Hothorn, H. Neumann, E. D. Lenherr, M. Wehner, V. Rybin, P. O. Hassa, A. Uttenweiler, M. Reinhardt, A. Schmidt, J. Seiler, A. G. Ladurner, C. Herrmann, K. Scheffzek, A. Mayer, Catalytic Core of a Membrane-Associated Eukaryotic Polyphosphate

- Polymerase. **324** (2009).
50. J. Liu, L. Yang, M. Luan, Y. Wang, C. Zhang, B. Zhang, J. Shi, F. Zhao, W. Lan, A vacuolar phosphate transporter essential for phosphate homeostasis in *Arabidopsis*. *Proc. Natl. Acad. Sci.*, 6571–6578 (2015).
 51. C. Wang, W. Yue, Y. Ying, S. Wang, D. Secco, Y. Liu, J. Whelan, S. D. Tyerman, H. Shou, Rice SPX-Major Facility Superfamily3 , a Vacuolar Phosphate Efflux Transporter , Is Involved in Maintaining Phosphate. *Plant Physiol.* **169**, 2822–2831 (2015).
 52. J. Diaz, E. Ingall, C. Benitez-nelson, D. Paterson, M. D. De Jonge, I. McNulty, J. A. Brandes, polyphosphate: A key player in geologic phosphorus sequestration. *Science (80-)*. **13193**, 652–656 (2008).
 53. S. A. Henson, R. Sanders, E. Madsen, Global patterns in efficiency of particulate organic carbon export and transfer to the deep ocean. *Global Biogeochem. Cycles.* **26**, 1–14 (2012).
 54. A. Yool, T. Tyrrell, Role of diatoms in regulating the ocean’s silicon cycle. *Global Biogeochem. Cycles.* **17**, 1–21 (2003).
 55. E. J. Villareal, T. A. and Carpenter, Chemical composition and photosynthetic characteristics of *Ethmodiscus rex* (Bacillariophyceae): evidence for vertical migration. *J. Phycol.* **30**, 1–8 (1994).
 56. C. M. Boyd, D. Gradmann, Impact of osmolytes on buoyancy of marine phytoplankton. *Mar. Biol.* **141**, 605–618 (2002).
 57. V. A. Chepurnov, D. G. Mann, K. Sabbe, W. Vyverman, Experimental studies on sexual reproduction in diatoms. *Int. Rev. Cytol.* **237**, 91–154 (2004).
 58. V. A. Chepurnov, D. G. Mann, P. Von Dassow, E. V. Armbrust, K. Sabbe, R. Dasseville, W. Vyverman, Oogamous reproduction, with two-step auxosporulation, in the centric diatom *Thalassiosira punctigera* (Bacillariophyta). *J. Phycol.* **42**, 845–858 (2006).
 59. N. A. Davidovich, S. S. Bates, Sexual reproduction in the pennate diatoms. *J. Phycol.* **137**, 126–137 (1998).
 60. D. Sarno, A. Zingone, M. Montresor, A massive and simultaneous sex event of two *Pseudonitzschia* species. *Deep. Res. Part II Top. Stud. Oceanogr.* **57**, 248–255 (2010).
 61. P. Assmy, J. Henjes, V. Smetacek, M. Montresor, Auxospore formation by the silica-sinking, oceanic diatom *Fragilariopsis kerguelensis* (Bacillariophyceae). *J. Phycol.* **42**, 1002–1006 (2006).
 62. H. J. Hoops, G. L. Floyd, Ultrastructure of the centric diatom, *Cyclotella meneghiniana*: vegetative cell and auxospore development. *Phycologia.* **18**, 424–435 (1979).
 63. A. Waite, P. Harrison, Role of sinking and ascent during sexual reproduction in the marine

- diatom *Ditylum brightwellii*. *Mar. Ecol. Prog. Ser.* **87**, 113–122 (2009).
64. N. Poulsen, P. M. Chesley, N. Kröger, Molecular genetic manipulation of the diatom *Thalassiosira pseudonana* (Bacillariophyceae). *J. Phycol.* **42**, 1059–1065 (2006).

Chapter 4 Figures

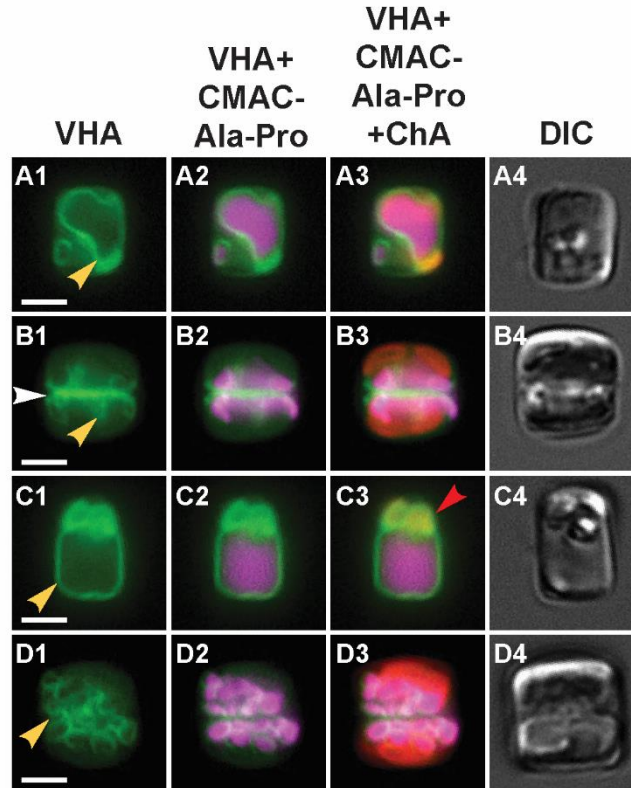


Fig. 4.1 Localization of VHA in vacuole tonoplasts of *T. pseudonana* expressing VHA_B-eGFP. The VHA is present in the tonoplasts (yellow arrows) of various sized vacuoles marked by CMAC-Ala-Pro. It is also present the SDV silicalemma (B; white arrow)) and chloroplast (C; red arrow), highlighting the multiple roles VHA is known to function in diatoms. Green: VHA_B-eGFP; red: chlorophyll; magenta: CMAC-Ala-Pro; white: co-localization of VHA and CMAC-Ala-Pro. Scale bar: 5 μ m.

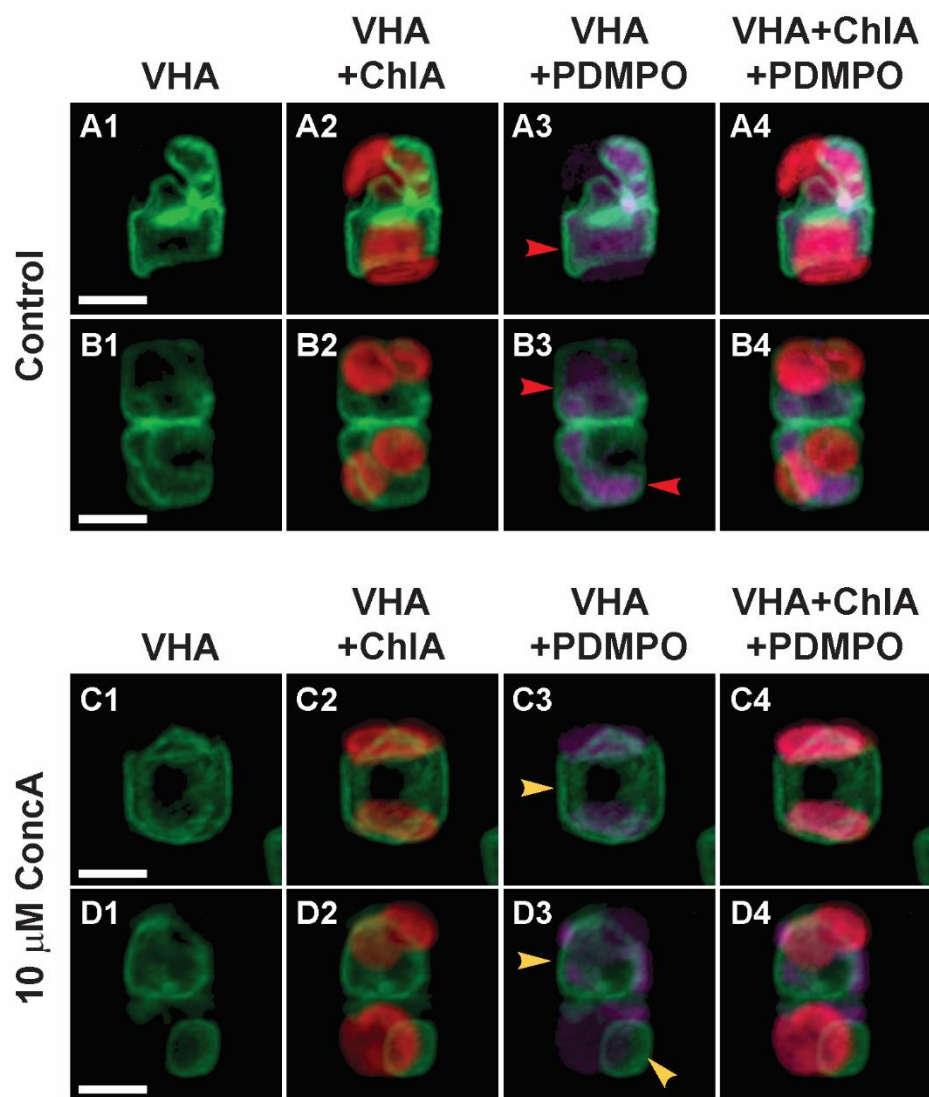


Fig. 4.2 Super-resolution confocal 3-D projections of *T. pseudonana* expressing VHA_B tagged with eGFP. The presence of VHA is detected in the vacuole tonoplast, accumulation of PDMPO within the vacuole suggest an acidification of $\text{pH} \leq 5.5$ (red arrows) on control cell (A-B), however a lack of PDMPO in the vacuoles (yellow arrows) in concanamycin A treated cells (C-D) suggest an inactivation of proton pumping into the vacuoles. Green: VHA_B-eGFP; red: chlorophyll; magenta: PDMPO; pink: co-localization of chlorophyll and PDMPO; white: co-localization of VHA and PDMPO. Scale bar: 5 μm .

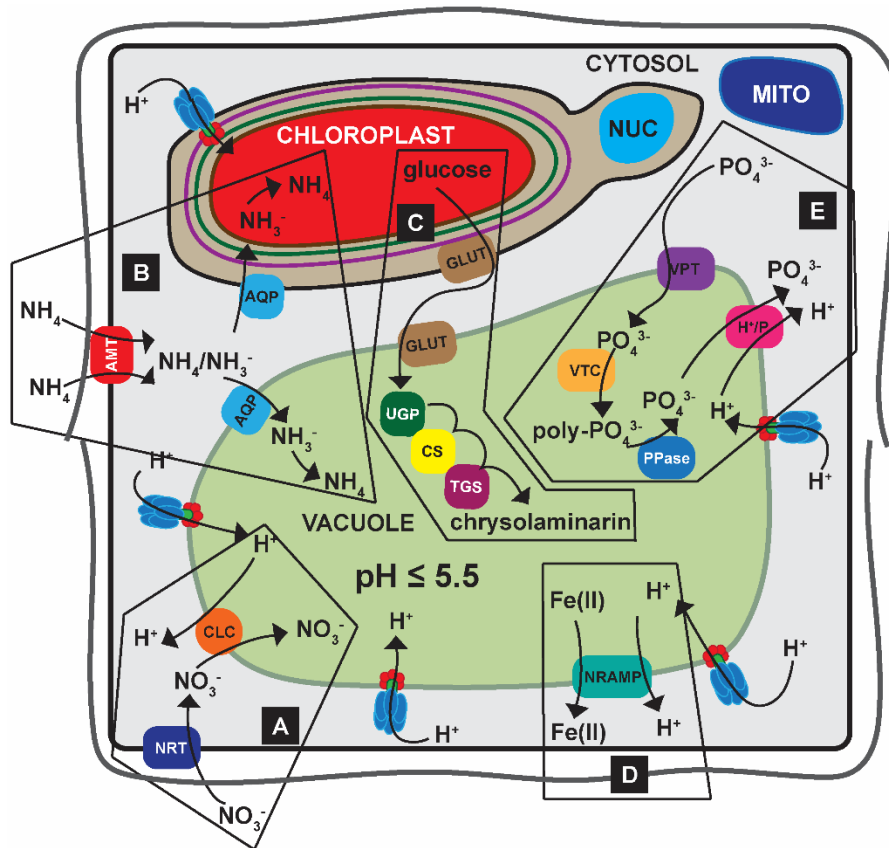


Fig. 4.3 Diagram of a hypothetical model for a VHA mediated solute transport in diatom vacuoles. (A) NO_3^- is imported to the cytosol by plasmalemma NRT then shuttled into the vacuole by secondary active transport by VHA through tonoplast CLC NO_3^-/H^+ exchangers. (B) NH_4 is imported to the cytosol through plasmalemma AMT where some of it equilibrates to NH_3^- and diffuses into vacuoles or chloroplasts through AQPs where it equilibrates to NH_4 under acidic conditions and gets trapped. (C) Glucose is transported from the chloroplast and into the vacuole through GLUTs and gets synthesized into chrysolaminarin by the UGP-CS-TGS cascade, chrysolaminarin is stabilized and condensed for storage by the acidic environment of the vacuole. (D) Fe(II) that has been accumulated in the vacuole by an unknown mechanism is redistributed back to the cell by H^+ -coupled transport through tonoplast NRAMP. (This mechanism is exclusive to centric diatoms) (E) PO_4^{3-} in the cytosol enters the vacuole by facilitated diffusion through tonoplast VPT and is synthesized into polyphosphate by VTC for storage. Afterwards, an unidentified PPase breaks down polyphosphate into PO_4^{3-} which is shuttled back to the cytosol by proton coupled transport via tonoplast H^+/P . The compartmental abbreviations are: V-type H^+ -ATPase (VHA), nitrate transporter (NRT), chloride channel NO_3^-/H^+ exchanger (CLC), ammonium transporter (AMT), $\text{CO}_2/\text{NH}_3^-$ aquaporin channel (AQP), glucose transporter (GLUT), UDP-glucose pyrophosphorylase (UGP), chrysolaminarin synthase (CS), 1,6-b-transglycosylases (TGS), natural resistance-associated macrophage protein (NRAMP), vacuolar phosphate transporter (VPT), vacuolar transporter chaperone (VTC), generic phosphatase (PPase), H^+/P cotransporter (H^+/P), mitochondria (MITO), and nucleus (NUC).

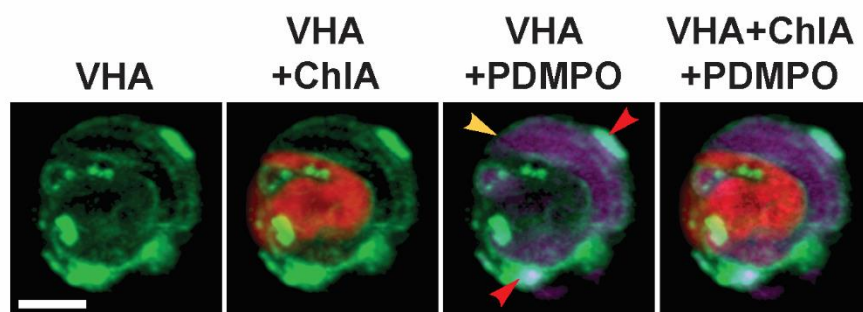


Fig. 4.4 Super-resolution confocal 3-D projections of a *T. pseudonana* auxospore expressing VHA_B tagged with eGFP. The presence of VHA is detected in the vacuole tonoplast, accumulation of PDMPO within the vacuole suggest an acidification of $\text{pH} \leq 5.5$ (yellow arrow), PDMPO is also strongly co-localized with VHA in the SDVs of biomineralizing siliceous scales (red arrows). Green: VHA_B-eGFP; red: chlorophyll; magenta: PDMPO; white: co-localization of VHA and PDMPO. Scale bar: 5 μm .

CHAPTER 5

Conclusion

5.1 Dissertation synopsis

Studying the breadth of molecular mechanisms carried out in diatoms is key to understanding the ecology and biogeochemistry of earth's oceans and atmospheres. Due to their rapid growth and ability to form dense blooms, diatoms play a significant role in primary production and turnover of various nutrients in the oceans. Therefore, studying the mechanisms that enable their productivity may allow us to predict how diatoms will respond to climate change and influence the health of the planet. Advances in diatom genomic tools over the past two decades have given researchers an unprecedented view into the molecular life of diatoms, but we are just beginning to understand their biological origins spanning over 250 million years of evolution. This dissertation aims to bridge some of the gaps in molecular knowledge by linking genotype to phenotype of several defining diatom physiologies including silica biomineralization, photosynthesis, and nutrient storage. Specifically, this work focused on the functional characterization of V-type H⁺-ATPase (VHA), an evolutionarily conserved proton pump and pH regulation enzyme in the marine diatom, *Thalassiosira pseudonana*.

In Chapter 2, VHA was functionally characterized in the role of acidifying the silica deposition vesicle (SDV) to promote the biosynthesis of silica frustules (*I*). The use of advanced microscopy techniques including epifluorescence and super-resolution confocal microscopy were crucial for studying fluorescently tagged proteins through space and time. Culture manipulation by silicon starvation and VHA inhibition with concanamycin A was used to study the dynamics of VHA and its influence on SAP1, and valve morphology in synchronized cells. The VHA proton pump was observed to dynamically translocate from vacuole tonoplasts to the silicalemma in order to acidify the SDV. Acidification of the SDV was found to coincide with peak silica biomineralization in the cell cycle, and also involved in trafficking SAP1 containing vesicles from

the cytosol to the SDV. Electron micrographs of diatom valves showed a reduction in valve development and deformities in structure when VHA was partially inhibited. Overall, this chapter addressed long-standing questions within the field of diatom silicification such as the origins of the SDV membrane and how the SDV becomes acidified. We also identified that VHA, either by pH regulation or its localization to the silicalemma plays a role in trafficking other silica biomineralizing proteins to the SDV.

In Chapter 3, VHA was shown to participate in the CCM for photosynthesis. Protein localization in *T. pseudonana* expressing VHA_B-eGFP showed VHA surrounding chloroplasts also marked with the acidotropic pH stain PDMPO, indicating an acidification of the organelle. Physiological characterization of VHA's role in photosynthesis was carried out by measuring oxygen production and carbon fixation under various biotic and abiotic conditions with the VHA inhibitor concanamycin A. Enhancement of photosynthesis by VHA was measured over a range of environmentally relevant conditions and was shown to respond to changes in DIC and irradiance. Similar mechanisms for VHA enhanced photosynthesis were observed in another diatom and coccolithophore but not a chlorophyte, suggesting this is a conserved mechanism of secondary endosymbiosis of red algal symbionts. Furthermore, analogous mechanisms involving VHA in coral and giant clam photosymbioses suggest a convergent evolutionary utilization of VHA in aquatic photosynthesis. Given the widespread distribution of blooming diatoms and coccolithophores, and the importance of tropical coral reef ecosystems, the impact of VHA on global primary production is bound to be immense.

In Chapter 4, I explored the role of proton pumping and acidification by VHA in the diverse functions of the diatom vacuole. Localization of VHA to the tonoplast vacuole was reported in Chapter 2 and 3, and observed throughout various stages of the cell cycle including

auxosporulation. A functional observation for VHA was made where incubation of cells with concanamycin A blocked the accumulation of PDMPO and reduced acidification in the vacuole. An in-depth review of literature covering biological and ecological theories for vacuolization, solute transporters in plant, yeast, and diatom models resulted in generating an up-to-date hypothetical model for how diatoms may utilize the proton pump to store and move molecules through their vacuoles. While the link between VHA acidification and the operation of these various mechanisms remain to be proven, these hypotheses provide a launching point for many studies of the vacuole to follow. Because the vacuole is hypothesized to carry out such diverse functions it will be important to test the effect of VHA inhibition in these roles under physiologically relevant conditions. For example, whether diatoms store nitrate or ammonium in the vacuole could depend on nitrogen status of the media and metabolic activity in exponentially growing versus stationary cells.

In this dissertation, I was able to identify VHA in three distinct organelle membranes of the diatom cell and describe a mechanism for its action in the SDV and chloroplasts. However, the question remains of how the cell regulates the activity of VHA to serve in multiple functions? Is there a single pool of VHA shared across the various organelles, or are there membrane specific isoforms that target the protein in different locations? It has been shown that VHA isoforms are differentially targeted in plants (2) and led to the hypothesis that assembly of the proteolipid ring with different combinations of the c subunit may influence where VHA is localized (3). Of the seven c/c' subunit isoforms found in the genome of *T. pseudonana* (4), I was able to clone and express one c and one c' subunit tagged with eGFP. A preliminary look at the protein localizations appear to show both proteins in the chloroplast ER, while VHA-c also looks to be distributed within the chloroplast (Fig. 5.1). The signal in the ER, however, may be an artifact of the tagged

protein getting trapped in the membrane since eGFP is more than twice the size of the c subunit. While these results support the role of VHA in photosynthesis described in Chapter 3, the hypothesis that c subunit isoforms differentially target VHA remains unconfirmed. Further work to answer this question will require localization of the remaining c subunits.

There is no single reason that explains the success and dominance of diatoms over other phytoplankton. However, by leveraging advances in genomics and high-throughput sequencing with multiscale cellular imaging, work carried out here establishes VHA as a major pH regulating enzyme in diatoms, and addresses many questions regarding the role of pH regulation in diatom biology. Collectively, the mechanisms described in this dissertation highlight how a single enzyme can operate in multiple physiologies of the cell. Physiologies that help diatoms build a protective shell out of silica, concentrate CO₂ to enhance photosynthetic efficiency and production, and store nutrients and provide buoyancy for the cell. The work to functionally characterize the proteins encoded in diatom genomes remains an enormous task for biologists. However, insights gained will help us understand how diatoms impact the environment and predict how different phytoplankton populations will respond to a changing climate.

5.2 Methods and Materials

Transgenic diatoms expressing fluorescently labeled VHA

VHA subunit c and c' labelled with eGFP was expressed under the control of the fcp promoter. For Thaps3_261500 (VHA_c) and Thaps3_264807 (VHA_{c'}) the full-length coding sequence of the gene was amplified from *T. pseudonana* genomic DNA, and cloned into Gateway destination vector pMHL_79 with eGFP at the end of the coding sequence. The final vector was co-transformed with a pMHL_09 expressing the *nat1* gene which confers nourseothricin resistance by biolistic gene gun method (5). Liquid cultures grown in ASW medium containing

100 µg/ml nourseothricin were enriched for cells expressing eGFP using several rounds of fluorescence-activated cell sorting on a BD Influx Cell Sorter (BD Biosciences), from which single colonies expressing eGFP were selected for on ASW agar plates containing nourseothricin.

Fluorescence microscopy

Super-resolution confocal microscopy was used for *T. pseudonana* expressing VHA_c-eGFP and VHA_c^Δ-eGFP. Cells were then transferred to a 35 mm poly-d-lysine coated glass bottom petri dish and mounted on a Warner Instruments QE-1HC Quick Exchange Heated/Cooled stage chamber controlled by CL-200 Dual Channel Temperature Controller maintained at 18 °C. Cells were imaged with a Zeiss LSM800 inverted confocal microscope equipped with a Zeiss Plan-Apochromat 63× (1.4) Oil DIC M27 objective, and Zeiss Airyscan super-resolution detector. Z-stacks of three channels were acquired to monitor eGFP (Ex 488 nm with 0.3% laser power, Em 509 nm, detection 490-535 nm), and chlorophyll (Ex 488 nm with 0.2% laser power, Em 667 nm, detection 450-700 nm) fluorescence.

5.3 References

1. D. P. Yee, M. Hildebrand, M. Tresguerres, Dynamic subcellular translocation of V-type H⁺ -ATPase is essential for biomineralization of the diatom silica cell wall. *New Phytol.* **225**, 2411–2422 (2019).
2. C. Kluge, T. Seidel, S. Bolte, S. S. Sharma, M. Hanitzsch, B. Satiat-Jeunemaitre, J. Ross, M. Sauer, D. Gollmack, K.-J. Dietz, Subcellular distribution of the V-ATPase complex in plant cells, and in vivo localisation of the 100 kDa subunit VHA-a within the complex. *BMC Cell Biol.* **5**, 29 (2004).
3. T. Seidel, C. Kluge, M. Hanitzsch, J. Roß, M. Sauer, K. Dietz, D. Gollmack, Colocalization and FRET-analysis of subunits c and a of the vacuolar H⁺ -ATPase in living plant cells. **112**, 165–175 (2004).
4. A. Bussard, P. J. Lopez, Evolution of vacuolar pyrophosphatases and vacuolar H⁺-ATPases in diatoms. *J. Mar. Sci. Technol.* **22**, 50–59 (2014).
5. N. Poulsen, P. M. Chesley, N. Kröger, Molecular genetic manipulation of the diatom *Thalassiosira pseudonana* (Bacillariophyceae). *J. Phycol.* **42**, 1059–1065 (2006).

Chapter 5 Figures

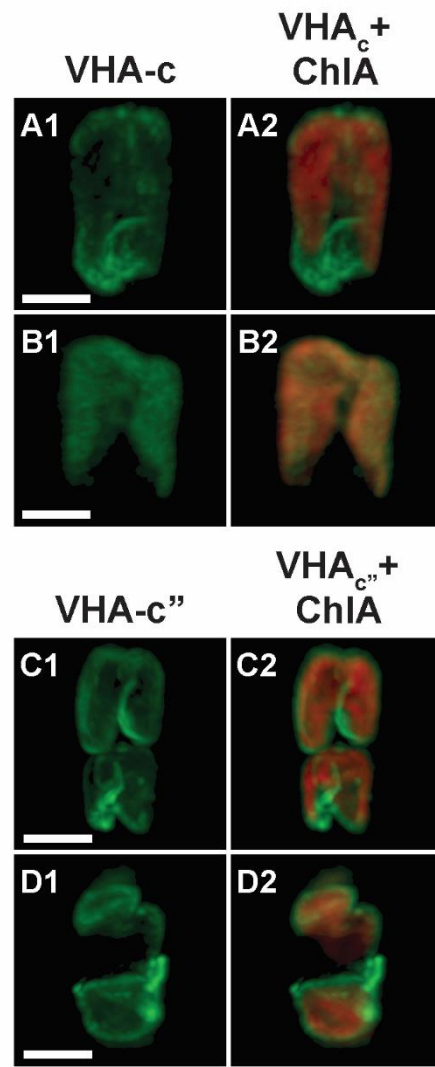


Fig 5.1 Super-resolution confocal 3-D projections of *T. pseudonana* expressing (A-B) VHA subunit c tagged with eGFP, and (C-D) VHA subunit c'' tagged with eGFP. Green: VHA_B-eGFP; red: chlorophyll. Scale bar: 5 μ m.